UNIVERSITÉ DU QUÉBEC À CHICOUTIMI

THESIS PRESENTED TO THE

UNIVERSITY OF QUEBEC AT CHICOUTIMI

IN PARTIAL FULFILMENT OF

THE REQUIREMENT FOR THE DEGREE OF

DOCTOR OF PHYLOSOPHY IN ENGINEERING

BY

REHAM MAHMOUD HEFNY

NUMERICAL AND EXPERIMENTAL INVESTIGATION OF THE INFLUENCE OF DYNAMIC LOADS ON WET SNOW SHEDDING FROM OVERHEAD CABLES

June 2013

UNIVERSITÉ DU QUÉBEC À CHICOUTIMI

THÈSE PRÉSENTÉE À

L'UNIVERSITÉ DU QUÉBEC À CHICOUTIMI

COMME EXIGENCE PARTIELLE

DU DOCTORAT EN INGÉNIERIE

PAR

REHAM MAHMOUD HEFNY

ÉTUDE NUMÉRIQUE ET EXPÉRIMENTALE DE L'INFLUENCE DE CHARGES DYNAMIQUES SUR LE DÉLESTAGE DE LA NEIGE COLLANTE DE CÂBLES AÉRIENS

Juin 2013

Dedicated to my parents, ADEL

and my kids

Many people think they want things, but they don't really have the strength, the discipline. They are weak. I believe that you get what you want if you want it badly enough.

Quote

RESUMÉ

Plusieurs types de givrages atmosphériques peuvent se déposer sur les lignes aériennes de transport d'énergie électrique incluant la neige collante lourde et adhérente, le givre dur, le givre mou et la glace à haute densité. Des dépôts de neige sur les structures exposées peuvent avoir un impact sur le fonctionnement, la sécurité et la fiabilité mécanique. Plus spécifiquement sur les lignes aériennes de transport d'énergie électrique, les charges de gravité résultant de l'accrétion de la neige lourde combinée aux charges du vent sur la neige peuvent causer des dommages structuraux, une rupture ou même en cascade des pylônes. La chute des dépôts de neige peut appliquer une charge dynamique sur la ligne de transport par les vibrations induites sur le câble et provoquer un effet déstabilisant entre les portées adjacentes couvertes et non couvertes. Ainsi pour protéger les lignes de transport contre les charges résultantes de l'accrétion de la neige sur la ligne et pour assurer la fiabilité des réseaux de distribution électriques, les processus du délestage de la neige doivent être compris et des techniques de prévention comme des méthodes d'antigivrage et de dégivrage doivent être utilisées.

Cette étude porte sur l'analyse dynamique des lignes aériennes de transport d'énergie couvertes de neige et soumises à des charges périodiques. De telles charges peuvent être le résultat de l'effet d'une charge périodique externe appliquée pour enlever la neige accumulée sur les lignes ou le résultat d'effets naturels comme le vent ou des charges en déséquilibre conséquentes d'une chute de neige soudaine ou propagé d'une portée adjacente . L'objectif est de comprendre le phénomène du délestage de neige induite mécaniquement sur les portées des câbles aériens et de simuler les effets des charges périodiques sur la chute de la neige collante. Lors d'études précédentes, les réponses de la ligne de transmission aux chutes instantanées ont été modélisées alors que dans cette étude, on étudie la propagation de le délestage de la neige le long de la portée en réponse à une charge périodique. Plus particulièrement, la réponse dynamique des câbles couverts de neige aux charges périodiques est examinée par modélisation mathématique en utilisant une analyse d'éléments finis non linéaires et des études expérimentales en chambre froide.

Le modèle numérique peut servir de base à l'étude de critères différents de rupture de la neige collante en ce qui concerne l'adhésion. Pour atteindre cet objectif, on a d'abord étudié expérimentalement l'adhésion en tension et en cisaillement à la surface des câbles. Ceci est essentiel pour mettre en corrélation la chute et la force d'adhésion entre la neige et le câble, puisque le délestage survient lorsque l'adhésion disparaît. Les mesures ont été obtenues en utilisant une machine à essayer le matériel et une centrifugeuse. Puis un critère de rupture de la neige collante a été déterminé et appliqué dans le modèle numérique. Ce modèle simule les vibrations du câble couvert de neige mouillée, par l'application d'une excitation périodique, celui que provoque du processus de chute de neige. L'excitation périodique est modélisée en utilisant une fonction temporelle de déplacement initial à une extrémité du câble, rendant la variation de la fréquence d'excitation possible. Le défi est de prédire si le dépôt va demeurer fixé au conducteur ou s'il va tomber suite à la vibration provoquée. Le modèle considère le délestage de la neige en retirant les éléments de la neige le long du câble, lorsque le critère de rupture est satisfait.

Dans l'étude expérimentale, les manchons de neige collante ont été reproduits à échelle réduite en utilisant une technique développée précédemment. Les charges de neige de différentes épaisseurs ont été utilisées sur la portée et les charges périodiques ont été

appliquées au point de suspension de façon à initier une vibration du câble et observer le mécanisme du délestage. La similitude des résultats du modèle numérique et ceux des simulations expérimentales à échelle réduite valide le modèle et assure sa fiabilité. Finalement le modèle de neige développé, avec un critère de rupture, est appliqué aux simulations numériques subséquentes des portées simples à échelle réelle soumis à des impacts périodiques.

ABSTRACT

Several types of atmospheric icing deposits may load overhead cables including heavy adherent wet snow, hard rime, large but lightweight soft rime and high-density glaze ice. Snow deposits on exposed structures can be the source of several serviceability, safety and mechanical reliability issues. On overhead power lines in particular, the gravity loads due to heavy snow accretion, coupled with wind-on-snow loads, may lead to structural damages, or failure and even cascading collapse of towers. The shedding of the snow deposit can apply dynamic loads on the line by the initiated cable vibration and results in unbalanced tension between shed and unshed adjacent spans. Therefore, in order to protect the line against loads resulting as a consequence of accreted snow on the line and to ensure the reliability of electrical power delivery networks, the processes of snow shedding have to be profoundly understood and countermeasures have to be taken, e.g., by applying anti-icing and de-icing methods.

This study focuses on the dynamic analysis of snow-covered overhead transmission lines subjected to periodic loads. Such loads may result from the effect of an external periodic load intended to remove accreted snow from the cable, or from such natural effects as wind or load imbalances due to sudden or propagating snow shedding from an adjacent span. The objective is to understand the phenomenon of mechanically-induced snow shedding on overhead cable spans and to simulate the effects of periodic loads on wet snow shedding. In previous studies, the response of the line to instantaneous shedding was modeled, whereas in this research, the propagation of snow shedding along the span as response to a periodic load is studied. In particular, the dynamic response of snow-covered cables to periodic loads is examined by numerical modeling using nonlinear finite element analysis as well as experimentally in a cold chamber.

The numerical model can serve as a basis to study various failure criteria of wet snow in terms of adhesion. In order to achieve this goal, first the tensile and shear adhesion of snow to cable surfaces were experimentally studied, which are essential to correlate shedding and the adhesive strength between cable and snow, since shedding occurs after adhesion vanishes. These measurements were carried out using material test machine and centrifuge machine. Then, a criterion of wet-snow failure was determined and applied in the numerical model, which simulates vibrations of the cable covered by wet snow due to application of periodic excitation resulting snow shedding process. The periodic excitation is modeled by an input displacement time function at one cable end, making the variation of excitation frequency possible. The challenge is to predict whether the deposit will remain attached to the conductor or fall off during the resulting vibration. The model considers snow shedding by removing snow elements along the cable where the failure criterion is satisfied.

In the experimental study, wet snow sleeves were reproduced on a small-scale span by using a formerly developed technique. Snow loads of different thickness were thus created on this span and periodic loads were applied at the suspension point in order to initiate cable vibration and observe the resulting shedding mechanism. The coincidence of results of numerical model and those of small-scale experimental simulations validates the model and assures its reliability. Finally, the developed snow model with failure criterion is applied in further numerical simulations for real-scale single spans subjected to periodic impact.

ACKNOWLEDGMENTS

First of all, I am thankful to **God**, who helped me too much during this study. I would like to express my deepest gratitude to my supervisor, Professor **Masoud Farzaneh** who is Chair holder of the NSERC/Hydro-Québec/UQAC Chair on Atmospheric Icing of Power Network Equipment (CIGELE), as well as the Canada Research Chair, Tier 1, on the Engineering of Power Network Atmospheric Icing (INGIVRE). He granted me the invaluable opportunity to pursue my Master's then my Ph.D. studies. I will forever be indebted to him for his encouragement, guidance, support, patience, supervision and motivation from the initial to the final level thereby enabling me to develop a thorough understanding of the subject; really it is a signal honour for me to work with him.

I would like to express particular appreciation to Dr. **Laszlo Kollar,** the co-director of the project. His ideas and the discussions was the light during my study. He has helped me immensely with this study for his insight, understanding and valuable advice. His field experience was also a great advantage to proceeding of this work. I am particularly grateful for all of his time and help during my PhD study, for his patience, guidance, advice, suggestions, his tolerance with my thesis writing, scientific criticisms and constant encouragement. His truly scientific intuition exceptionally inspired and helped me grow as a student and as a researcher.

I would like to thank the CIGELE partners (Hydro-Québec, Hydro One, Réseau Transport d'Électricité (RTE) and Électricité de France (EDF), Alcan Cable, K-Line Insulators, Tyco Electronics, Dual-ADE, CQRDA and FUQAC) whose financial support made this research possible.

I am grateful to my committee members, Prof. **Mohamed Bouazara and** Prof. **Gholamreza Aryanpour** for their time and efforts to read this thesis and give me useful advice, encouragement and the opportunity to present this work.

I am very grateful to Prof. **Mohamed Bouazara** and Prof. **Guy Simard** for accepting to be members of the doctoral examination committee during all their research and academic activities. A special great "thank you" goes to Dr. **Majid Kermani** for his help during my work using MTS machine.

I am grateful to the researchers, professionals and technicians at CIGELE, who provided me with their technical support and valuable suggestions in the fulfillment of this study. These people include **Pierre Camirand, Claude Damours, Denis Masson, Xavier Bouchard** and **Francis Deschênes**. I appreciatively thank Mr. **Pierre Camirand**, who helped me with his smart solutions to technical problems, he was a friend and a counsellor at all times. I can never forget him advising me to release the problems.

An acknowledgement is specifically extended to Dr. **Raafat Mustafa,** for his patience and kindness in editing my thesis. I would like to thank him too much for all his great efforts and his useful comments.

My profound gratitude goes to my parents, for their substantial contribution and sacrifice throughout the duration of my PhD studies. My **Mom** and my **Dad** are greatly deserving of

PUBLICATIONS

Seven research articles have been prepared from this work for publication. Of these, three conferences have been attended, three journal papers have been published and one journal paper will be submitted. Further, there are four colloquium oral presentations have been attended. The details are provided below.

Journals

1. Reham M. H. Hefny, László E. Kollár, Masoud Farzaneh , " Modelling the influence of periodic loads on snow detachment from suspended cables," Cold Regions Science and Technology, accepted and in press for June 2013.

2. Reham M. H. Hefny, L. Kollar & M. Farzaneh, « Simulation of Snow Adhesion on Real-Scale Lines ». International Journal of Mechanical Engineering and Mechatronics, Vol. 1, Issue 1, 2012, pp. 102-108.

3. Reham M. H. Hefny, L. Kollar & M. Farzaneh, « Experimental Investigation of Dynamic Force on the Performance of Wet Snow Shedding ». International Journal of Mechanical Engineering and Mechatronics, Vol. 1, Issue 1, 2012, pp. 72-79.

4. Reham M. H. Hefny, László E.Kollar, Masoud Farzaneh, "The effect of periodic loads on real-scale cable", will be submitted to Cold Regions Science and Technology.

Conferences

5. R. Hefny, M. Farzaneh, L. Kollar « Simulation of snow adhesion on power transmission cables ». Proceedings of the International Conference on Mechanical Engineering and Mechatronics, Ottawa, Canada, Paper 79, August 2012.

6. R. Hefny, L. Kollar & M. Farzaneh, « Influence of Dynamic Forces on Wet Snow Shedding from Overhead Cables ». Proceedings of the International Conference on Mechanical Engineering and Mechatronics, Ottawa, Canada, Paper 208, August 2012.

7. R. Hefny, L. Kollar, M. Farzaneh, C. Peyrard, « Adhesion of Wet Snow to Different Cable Surfaces ». Proceedings of the 13th International Workshop on Atmospheric Icing of Structures, IWAIS 2009, Andermatt, Suisse, Poster Session, September 2009, 7p.

Colloquium

8. R. Hefny, L. Kollar & M. Farzaneh, « Modeling snow shedding from a cable ». 14e Colloque annuel de la CIGELE/INGIVRE, Université du Québec à Chicoutimi, 30-31 May, 2012.

9. R. Hefny, M. Farzaneh & L. Kollar, «Investigating the effects of variable loads on the snow shedding process». 13e Colloque annuel de la CIGELE/INGIVRE, Université du Québec à Chicoutimi, 22-23 June, 2011.

10. R. Hefny, M. Farzaneh, L. Kollar, « Effect of galloping on snow shedding from cables ». 12e Colloque annuel de la CIGELE/INGIVRE, Université du Québec à Chicoutimi, 2010 June.

11. R. Hefny, M. Farzaneh, L. Kollar, « Experimental study of wet-snow adhesion to cable surfaces ». 11e Colloque annuel de la CIGELE/INGIVRE, Université du Québec à Chicoutimi, June 2009.

TABLE OF CONTENTS

LIST OF FIGURES

LIST OF TABLES

APPENDIX

CHAPTER 1
INTRODUCTION

CHAPTER 1

INTRODUCTION

1.1 Overview

It is common knowledge that in cold regions snow layers may accumulate on cables and conductors. This accumulation can produce major problems such as overloading the conductors and towers, galloping of cables in high wind-speed conditions, snow shedding, short-circuit due to wire sag. This in turn affects the human life security, material damage and reliability of electrical transmission lines. Some towers collapsed due to early failure and cascade collapse. Impulse loads due to sudden snow shedding can be considered as another source of trouble in power networks. Each year, numerous failures due to ice/snow storms are reported from Canada, the United States, the United Kingdom, Russia, France, Germany, Norway, Iceland and Japan, in which affect the related over-head transmission networks.(C1-Gholamreza). The damage caused by a single wet snowstorm can necessitate the expenditure of sums on the order of 100 million dollars. In Québec, which relies heavily on electric power, electric outages lasting even a few days in harsh cold conditions have serious public safety and economic consequences (e.g., lack of heating, water supply and paralysis of several industrial and public service activities). A major snow storm in 2007 has hit eastern Canada and north-eastern areas of the US, killing many people and causing major disruption to air travel. Furthermore, transportation networks erupted into in China 2008 and USA 2011, where these snow storms caused extensive damage to a vast number of low-rise buildings, causing several deaths. The unforgiving storms had detrimental economic effects (Figures 1.1, 1.2, 1.3).

The natural forces exerted on snow deposit can be divided into: (a) static loads (snow weight, torsion loads from cable twist, thermal stresses resulting from temperature gradients in snow sleeve; (b) the quasi-static classification comprises mainly the effects of steady wind, snow accumulation and maintenance; (c) several cyclic effects derive from wind-induced vibrations, while natural snow shedding and forces, due to flashovers or mechanical de-icing processes, must be treated as transient dynamic loads. Exceptional events, such as conductor breakage or drop of conductor suspension assembly may also cause severe dynamic loads

(Kollar and Farzaneh, 2005, Lapointe, 2003; McClure and Tinawi, 1987; McClure and Lapointe, 2003). Power transmission lines comprise four major components that are interconnected: towers, foundations, cables and interfaces such as insulators and other items of line hardware. Although most line design procedures are based on static analysis, more advanced dynamic analysis is essential to understand and predict the line transient response to complex dynamic loads.

Figure 1.1 Snow storm in China 2008 (Knowledge allianz web site).

Figure 1.2 Snow accumulations on transmission lines during New Jersey storm 2011 (Snow Murray web site).

Snow shedding from ground wires differs from ice shedding, because the process and structure of ice and snow accretion are different. The principal condition of snow growth is that, adhesive forces between the snow and ground wire surface, as well as cohesive forces between the snowflakes, are high enough to keep the snowflakes together on the ground wire. Wet snow sleeves shed naturally in some hours after their accumulation. Heating effects like Joule heating and solar radiation increase Liquid water content (LWC) of snow accretions. When snow sleeve loses its cohesion, it sheds naturally under the effect of gravity and wind, or artificially by the effect of Joule heating.

Wet snow shedding involves several feedback mechanisms and non-linear relationships between various factors, including forced, natural air convection, the shape of the snow sleeve and its surface roughness. Snow-grain morphology, the arrangement of snow grain and liquid water, are the most important parameters for predicting snow failure, or shedding. Shedding tends to cause power outages to the power network structures, thereby leading to a number of serviceability, safety and mechanical reliability issues. All these factors cause high amplitude movement of cables, increasing the possibility of little or no clearance between the adjacent cables or between cables and towers. Consideration of snow shedding problems is very important in determining the alignment of the conductors, the type of towers and the configurations of spans. The shedding involves some danger, because it causes unbalanced load on adjacent spans of the line. Thus, from the point of view of line design it is essential to know the duration of snow persistence on the cable and understanding the snow-shedding propagation phenomena.

Figure 1.3 The snow storm in New Jersey (USA) (Snow Murray web site).

The dynamic effect of snow shedding on transmission lines creates two major categories of concern: electrical and mechanical. A lack of clearance between adjacent cables, cables and towers and cables and the ground are the main electrical concerns. Mechanical concerns include the impact of suspension strings on towers, which may result in broken insulators. Snow shedding may also cause mechanical problems with excessive tensions generated in the cables and eventually, large unbalanced loads on towers. In addition, shedding generates strong conductor motion, which causes conductor swing toward each other. These dynamic forces can cause cascading of the towers, resulting in heavy damage to the line (Roberge, 2006). Anti-icing and de-icing methods should be investigated to reduce the line damage and to improve the mechanical characteristics of line components.

Flashover may occur between phases or between shield wire and phase conductor, due to unequal sag increase between spans and phases of line (Sakamoto, 2000). A more frequent problem arises when the load is suddenly released. The conductor springs upwards and if the horizontal spacing between phase conductors is small, flashover between conductors may happen (Morgan and Swift, 1964). For conductor of two phases, where heavy snow load remains on the top-phase conductor, while the bottom-phase conductor snow load has shed, it is possible that flashover occurs between these two conductors particularly in windy conditions, since the horizontal separation is very small. Another hazard is conductor jump arising from the sudden release of ice or snow from conductors; this may cause them to rise to heights that exceed the normal spacing between both conductors (Morgan and Swift, 1964).

1.2. Problem Definition

The consequences of atmospheric icing of overhead power lines are extremely important in terms of human life security, material damage and reliability of electrical transmission lines. This often creates many serious electrical and mechanical problems in the transmission network due to the high adherence of snow to substrates. The major results are overloading the conductors and towers; short circuits due to unequal sag; and galloping of cables in high-wind conditions. Galloping and other dynamic loads result in line components fatigue and damage. The impulse loads due to sudden snow shedding are another source of troubles in power networks.

This study focuses on the dynamic analysis of snow overhead transmission lines subjected to periodic loads. The periodic loads are those that result from the effect of an external load intended to remove accreted snow from the cable, or from load imbalances due to sudden snow shedding. The interest of numerical modelling of the effects of snow-shedding phenomena is to assess the possible dynamic amplifications of cable tensions in the line, which are eventually transferred to supports and to check whether the amplitude of the induced motion is within the design limits of electrical clearances with the ground or with other conductors.

1.3. Objectives

The main goal of this research is to better understand the phenomenon of periodic-load induced snow shedding by performing experimental observations and by developing a numerical model, which includes a new snow failure criterion. The new failure criterion is applied to various shedding examples of a single span small-scale line for validation and also a real scale transmission line.

The specific objectives stated as follows:

To investigate the effects of periodic loads on wet-snow shedding from overhead cables, the following steps should be realized:

(1) Studying the tensile and shear adhesion strength in order to correlate shedding to the adhesive strength between cable and snow.

(2) Simulation of vibrations of the cable covered by wet snow due to application of periodic-excitation experimentally and observing the resulting snow shedding process.

(3) Developing a model where simulating snow adhesion failure propagation is possible.

(4) Validation of the numerical model by comparing the dynamic response of snow-covered cable subjected to periodic impact obtained from numerical modeling using Automatic Dynamic Nonlinear Analysis (ADINA) to those observed in small scale experiments.

(5) Investigating how variables including snow thickness and impact load characteristics affect the dynamic response of snow-covered cables subjected to periodic loads.

(6) Implementing the new failure adhesion criterion to study snow shedding on line sections of EDF (Électricité de France) and Hydro-Quebec.

1.4. Methodology

In order to achieve the above-mentioned objectives, knowledge of snow adhesion and dynamic characteristics of the shedding process is essential, and lack of information and data in this field leads to do some experimental work to obtain the tensile and shear adhesion properties, as well as the cable response to the periodic impact.

This research is carried out mainly in three stages:

(1) Mechanical tests using MTS machine and centrifuge machine for measuring shear and tensile adhesion of snow.

(2) Physical simulations using reduced-scale laboratory experiments of a suspended snow cable subjected to periodic loads for simulating snow shedding.

(3) Numerical simulations of overhead snow cables subjected to periodic impacts used for proposing a snow model and simulating snow shedding and then applied the suggested model to real scale cables. The methodology is summarized in the flowchart shown in Figure 4.1.

Figure 1.4 Flowchart of the project.

1.4.1. Laboratory Experiments

1.4.1.1. Adhesion Test Description

The laboratory experiments applied on snow samples subjected to shear or tension were carried out in the cold room in CIGELE (more details will be explained in Chapter 3), two adhesion strengths were measured as follows:

(1) The shear adhesion strength was measured by the centrifuge machine.

(2) The tensile strength was measured using the Material test machine (MTS) machine.

The experimental considerations are as follows:

(1) The dry snow was stored in a cold room at temperature above 0°C for a certain time, in order to obtain wet snow with LWC between 10% and 45%.

(2) Experiments were carried out in the 0°C to 1°C temperature range, which most likely exists when structures are exposed to snow events.

(3) Snow sample for the centrifuge machine was prepared on the extremity of a beam by inserting the beam inside a small mold, while the sample was prepared in MTS machine by a semi-spherical casserole with a flattened top (Figures 3.2, 3.7c).

(4) For shear tests, the beam with the snow sample was rotated in the centrifuge machine with increasing angular velocity, until snow sample was detached from the beam (Figure 3.4).

(5) In the tensile tests, the semi-spherical snow sample was slowly compressed from the top by a plate, moving downward at a constant speed, the compression stopped at specific instant and then tensile load was applied until snow is detached from the grip (Figures 3.7d, 3.8a).

1.4.1.2. Dynamic Test Description

The reduced-scale laboratory experiments on a suspended snow-covered cable subjected to periodic impact are carried out as follows:

Description of the experimental setup:

(1) The experimental setup is installed at the CIGELE icing precipitation simulation laboratory. It consists of a rigid support mounting a flexible stainless-steel cable pin-ended to a load cell.

(2) The periodic-load (impact) is provided by a setup installed at the cable suspension- point.

(3) Voltage excitation and signal conditioning are provided by a channel signal conditioner for the accelerometer and by strain gauge signal conditioner for the load cell. Data acquisition is controlled by the DT Measure Foundry DAQ software (DT Measure Foundry, 2005).

(4) Snow formation on the cable is provided using a wooden mold of around 2.5 m and a small semi-spherical tool to compact wet snow with suitable LWC (10 % to 40%) around the cable.

Experimental considerations:

(1) Horizontal component of cable end-tensions in both the static and dynamic analyses are measured by the load cell.

(2) Time histories of the vertical displacement of the cable at mid-span and end point are monitored using two digital high-speed cameras. One of these cameras also recorded the shedding process. Images are processed to yield some quantitative time history responses.

(3) Experiments are carried out in the 0°C to 1°C temperature range that most likely exists when structures are exposed to snow events.

(4) Several snow shedding scenarios were studied with variables including snow sleeve diameter and periodic load functions defined by amplitude and frequency. The initial cable sag and cable length are always constant.

1.4.2. Finite Element Modeling

As in previous numerical studies (Jameleddine et al, 1993; Roshan Fekr, 1995; Roshan Fekr and McClure, 1998) of ice shedding from line conductors, the commercial finite element software package ADINA (ADINA, 2004) is used in the current study to simulate the dynamic effects of snow shedding induced by a periodic excitation applied directly on a cable of a level single-span section.

Model Assumptions:

(1) Several different snow-cable modeling scenarios are mentioned in order to model snow failure propagation along the span. The cable is modeled with a uniform mesh of pre-stressed tension-only isoparametric truss elements relying on successful previous studies (Jameleddine et al, 1993; Lapointe, 2003; McClure and Tinawi, 1987; McClure and Lapointe, 2003; Roshan Fekr, 1995; Roshan Fekr and McClure, 1998).

(2) Snow is modeled using point-load springs with mass only to simulate its load at each point, whereas the adhesion properties are modeled using the vertical springs with only stiffness and neither mass nor damping properties.

(3) The snow failure is modeled using the failure condition depending on adhesion properties, as it will be explained later in Chapter 4.

(4) The flexibility of the towers and their foundations is not modeled and the cable right end is assumed to be rigidly fixed, while the left end is assumed to be movable in the vertical direction.

(5) The periodic-load is simply defined by displacement profile at the suspension-point obtained from videos captured by a digital camera. Different periodic load characteristics are represented by the variation of displacement amplitude and excitation duration.

(6) Aerodynamic damping is neglected and only structural damping of the cable is considered in the numerical models. Therefore, damping is modeled by using nonlinear axial dashpot elements parallel to each cable element, relying on previous studies (Lapointe, 2003; McClure and Tinawi, 1987; Jameleddine et al, 1993; Roshan Fekr, 1995; Roshan Fekr and McClure, 1998; McClure and Lapointe, 2003).

(7) Before starting the transient dynamic analyses, mode shape analyses are conducted on a single-span cable model. The calculated mode shapes and corresponding natural frequencies are compared to those obtained from Irvine's theory (Irvine, 1981).

(8) The time step and the mesh size are selected so as to provide adequate sampling of the excitation function and the wave, as it travels through the cable finite element mesh.

(9) Dynamic analyses start from the initial static equilibrium of the snow-covered cable. In order to avoid the stiffening effect of the flexural rigidity of the snow element on the initial static profile, the deformed cable profile is calculated beforehand using concentrated loads which simulate snow load.

1.5. Originality and Contributions to Knowledge

The present research has original contributions that will be stated as follows:

(1) A novel numerical modeling technique is developed using ADINA software, which is capable of simulating propagating and partial snow shedding on overhead cables subjected to periodic loads. This modeling approach integrates the failure criteria of snow detachment from cable depending on adhesion properties, which is investigated experimentally in CIGELE laboratory.

(2) This study is the first to use the centrifuge machine for investigating the shear adhesive strength of wet snow. Moreover, it is the first time to examine the tensile adhesion strength using this specific procedure comparable to previous researchers. In addition, this project provides a good reference concerning the relation between wet snow strengths and its physical properties (e.g., LWC), also it highlights the effect of cable surface roughness on the wet snow strengths.

(3) The numerical model is validated on a level single-span reduced-scale experimental model, where it is the first time the snow-covered cable is investigated dynamically using the proposed setup in CIGELE laboratory.

(4) The numerical model is successfully applied for simulations of level single-span real scale overhead line: a classical stranded-steel ground wire, which is the first dynamic investigation in this research area.

(5) Effects of several parameters on snow-shedding are studied, including snow thickness, amplitude, frequency of excitation and LWC for reduced scale cable experimentally and numerically. Concerning the real scale model, some other parameters are investigated such as span length, load position and damping ratio.

1.6. Thesis structure

This thesis consists of six chapters which may be itemized as follows:

Chapter 1 is the basic introduction to the thesis, which provides a summary of the background to the research, including the issues and problems involved in the effects of the severe atmospheric icing on transmission lines damage. Moreover, the statement of the problem, the objectives and the methodology applied are mentioned in detail. The necessity of the research and original contributions are also discussed.

In Chapter 2, a survey of related literature will be presented and reviewed, pertaining to the topics of this research. Snow shedding, snow metamorphism, the mechanical problems associated with atmospheric icing of power lines, recent de-icing methods are discussed. Furthermore, the numerical model developments of the snow-shedding phenomenon and a brief review of current knowledge on the mechanical properties of snow. It is essential to know the principles and processes required, together with the results obtained. These reviews will contribute to help the reader understanding the phenomena.

Chapter 3 describes the experimental procedure for performing the experiments in laboratory. Additionally, this chapter covers the details of the facilities, the techniques and the instruments used in the study. Besides, the experimental results obtained are examined.

Chapters 4 and 5 present the numerical results. Chapter 4 presents the newly developed finite element model that explicitly considers the snow shedding by integrating the adhesion properties of snow into the model. Limitations of the numerical model are highlighted in this chapter. A comparison of numerical and experimental results of the reduced-scale model is presented also in Chapter 4. The results of several snow-shedding scenarios are discussed in Chapter 5. Conclusions are given at the end of each chapter as relevant.

In Chapter 6, the general conclusions derived from the results and discussions covered in the previous chapters will be presented. It will also include the areas of research that we recommend exploring for continuity and progress following the research described herein. The conclusions emerging from this thesis make it possible to illustrate the assessment of our contribution to the progress of this field.

The references cited in this thesis are presented at the end, after the final chapter. Detailed diagrams for the signal conditioner and the accelerometer used in the experimental study, as well as the calibration instruments are presented in Appendix A. Appendix B summarizes the wind induced vibrations properties, the cable properties, the main cable equations, damping properties, boundary conditions, cable and spring geometries and description of the devices.

In Appendix C, program code written in MATLAB is provided to calculate the static profile of a level single-span axially rigid catenary under its self-weight.

1.7. Conclusion

The general objective of this research work, as a part of general snow shedding problem, is to model the behavior of wet snow on the cable affected by period loads. The need for this research work comes from the fact that snow shedding creates many serious problems in the power transmission line industry, thereby; this study provides the fundamentals for modeling the behavior of wet snow. The model is developed based on the existing models for the mechanical behavior of ice and snow. The methodology of the problem is based on the application of both experimental and numerical simulation approaches. The results are to be used to explain the mechanism of snow shedding and also to improve mechanical de-icing techniques. The commercial finite element software ADINA is used to simulate the snow shedding as a result of dynamic loads acting at one cable end. To do this, the adhesion properties of wet snow, should be known. The results of this model are validated by the experimental results obtained in the CIGELE laboratories.

CHAPTER 2

LITERATURE REVIEW

CHAPTER 2
LITERATURE REVIEW

2.1 Introduction

Mainly five types of icing may deposit on structures: glaze, soft rime, hard rime, wet snow, dry snow and hoar frost (Poots, 1996). Typical temperature during wet snow events is slightly above freezing point of water (0°C). The occurrence, severity and type of snow depend largely on temperature, wind speed and water droplet size. Snow shedding from the conductors, which is classified as a type of mass reduction, could be a source of structural damages, failure or even cascading collapse of towers. This mass reduction can be caused by some physical mechanisms: snow melting and mechanical snow breaking. In this chapter, the snow shedding phenomenon and factors influencing it will be discussed in more detail. The first part of this chapter reviews the essential results obtained relating to the snow structure, metamorphism, water saturation and thermodynamic aspects. In the second section, the snow accretion studies are investigated. Adhesion properties of wet snow will review the icing adhesion and cohesion tests. Finally, the last section will focus on the mechanical properties of snow. The main objective of this chapter is to introduce the properties of wet snow, to learn what causes snow shedding and to understand the adhesion properties.

2.2. Wet Snow Metamorphism and Thermodynamic Balance
2.2.1. Snow Structure

Snow is a cellular form of ice in which the individual ice crystals of snow are bonded together. Gibson *et al.* (1997) reported the mechanical properties of cellular solids in details. Cellular solids can be either closed-cell form or open-cell form such as Sponge. Snow is considered as an open-cell polyhedral type (Petrovic, 2003).

2.2.2. Snow Metamorphism

Colbeck and Denoth (1973, 1979, 1982, 1997) are the most important contributors in understanding the microstructure of snow. Denoth (1982) investigated the role of snow LWC in details. Colbeck (1973) mentioned that water exists in wet snow in three forms determined by the amount of water it contains as follows:

a- Capillary area: The water content is small and exists between ice particle constrictions (Figure 2.1), which corresponds to low LWC.

b- Catenary area: Water appears around ice particles.

c- Reticulation area: When water reaches to 14% by volume, the ice particles are completely covered with water and the gap is distributed in the water as isolated bubbles (Denoth, 1986, Colbeck ,1982).

The rapid metamorphosis of snow at positive air temperature was published by Wakahama *et al.* (1977) and theorized by Colbeck (1973). The first photos of such grain clusters were presented by Colbeck and Ackley (1982). Wet snow is the result of the rapid metamorphosis of dry snow formed at negative temperature into super-cooled clouds. When the snowflakes penetrate an air layer at positive temperature, the dry snowflakes consisting of millimetric hexagonal ice crystals that were collected under weak mechanical bonding, begin their metamorphosis by rounding their crystalline shape. Once the snow is fully exposed to air-snow thermal exchanges, the metamorphosis is rather rapid.

The metamorphosis proceeds as follows: a liquid phase occurs over the ice, where at that moment the hexagonal crystals round out, shorten and turned into agglomerates of ice granules, then weltering in their own melting water, surrounding by trapped air bubbles (Dalle, 2011). This metamorphosis transforms the weak mechanical bonding of dry snowflakes into strong capillary bonding of wet snow granules, as described by (Wakahama, 1965) and theorized by (Colbeck, 1973, 1979). The temperature of metamorphosis is generally located between 0°C and 2.5°C (Grenier and Admirat, 1984; Dalle, 1984). Once the air temperature exceeds 3°C, the wet snow turns into water droplets. When the heat exchanges are restricted (low wind speed <1 m/s, air temperature close to 0.1°C and snowfall intensity >10 mm/h), the wet snow presents half-transformed snow with density < 100 kg/m^3, low LWC < 5% and many air bubbles. Conversely, if the heat exchanges are very active (wind speed = 10 m/s, air temperature = 2°C and low snow fall < 2 mm/h), the wet snow material considered as a fully transformed-snow (density 500 kg/m^3, LWC > 40% and few air bubbles) (Dalle, 2011).

Figure 2.1: (a) Ice crystals gathered into tightly packed grain clusters in wet snow at low liquid contents (Colbeck ,1982), (b) Well-rounded ice crystals in wet snow with high liquid contents (Colbeck, 1982).

2.2.3. Liquid Water Content Concept

The variables used to describe wet snow accretions are snow thickness, density, overload and liquid water content (LWC) (Roberge, 2006). Thus, LWC is a main factor in wet snow studies. Measurements of liquid water content are expressed by volume (water volume, ice volume and porosity, which usually requires a separate measurement of density (Colbeck *et al.*, 1990). Several methods are used today for field measurements to determine liquid water content, e.g., hot (melting) and cold (freezing) calorimetry, dilution and dielectric measurements.

Denoth (1982) defines the amount of water saturation as the extent (%) to which liquid water fills the available pore space in the snow matrix. Wakahama (1977, 1979), Poots (1996), Admirat (1986, 1988, 1990) and Sakamoto (2000, 2005) all express the LWC as the mass percentage of liquid water in a total mass of wet snow, as a percentage (%LWC by mass).

Accreted snow can melt by a raise in air temperature, by solar radiation or energizing the wire. The liquid water flows down to the bottom (this happened for density less than 0.6 kg/m^3); once the bottom becomes saturated with liquid water and appears to be transparent, snow shedding then occurs. When snow accretion forms in a cylindrical sleeve, it hardly drops off the wire (Sakamoto, 2005).

Liquid water content determines the surface tension forces and plays an important part in the cohesive strength of the material. High LWC values prevent the growth of large sleeves

by forcing them to break up, it flows like viscous fluid. However, low LWC corresponds to the maximum cohesion of the material and allows the growth of heavy sleeves without breaking them (Grenier, 1986).

When LWC increases, the internal cohesive forces (capillary forces and ice bonding) decrease. Once the external aerodynamic and gravitational force overcome the internal forces, the snow sleeve breaks up or separates from conductor (Admirat *et al.*, 1988). The transient snow loading on the conductor takes a saw-tooth form (Poots, 1996). The sleeve diameter is around 10 cm at shedding and a maximum cohesion is found between 10-15% of LWC (Sakamoto *et al.*, 1988).

Admirat (1986) presented a thermodynamic model to calculate the mean LWC of a snow sleeve as a function of sleeve growth, air temperature, differential vapour pressure (defined from the relative humidity of air), wind velocity, vertical snowflake velocity, precipitation intensity and initial snow water content (Eshiemogie, 2011).

An alternate model was developed by Poots and Skelton to calculate LWC during axial growth of wet snow on a fixed cylinder. This model considered more parameters than those listed above and the authors provided a critical precipitation rate which corresponded to the cohesive limit. The critical cohesion value depends on air temperature and wind velocity and if the precipitation rate is higher than this critical value, then LWC will exceed 40 % resulting in snow deposit shedding (Eshiemogie, 2011).

2.2.4. Heat Balance

Grenier *et al.* (1986) studied the heat balance of wet snow sleeve during 1980's and established a model of cylindrical accretion process, which includes precipitation rate, collection efficiency (the fraction of droplets approaching a surface), the influence of wind speed and air temperature. This model was validated using wind tunnel experiments and field observations. The model was used to predict accretion diameter, snow density and LWC. The cooling and heating effects are identified as follows:

1- Q_a: heat supplied or removed by forced convection during accretion. When air temperature is above freezing, heat is supplied to snow. Whereas after the accretion, air temperature drops below the freezing point, heat is being removed.

2- Q_{evap}: heat removed by source of evaporation at the accretion surface (neglected).

3- Q_{cond}: heat supplied to the surface by the condensation.

4- Q_{melt}: heat removed by the melting process of accreted snow.

5- Q_{joule}: heat supplied by Joule effect if cable carries an electric current.

Grenier *et al.* (1986) suggested that Joule heating can be used to promote shedding and increase LWC. Heating and cooling are balanced by melting and freezing of water inside snow mass. The instantaneous energy balance of snow sleeve is determined using Equation 2.1 (Grenier *et al.*, 1986, Farzaneh, 2008)

$$Q_a^+ + Q_{c/e}^\pm + Q_{melt}^- + Q_{joule}^+ = 0 \qquad \text{Equation (2.1)}$$

Wakahama *et al.* (1979) indicated that the thermodynamic balance can estimate the LWC of the accretion. If the LWC of the accretion is greater than the range between 20% and 40% by mass, then it will have insufficient cohesive strength and it is likely to be blown off a transmission line (Sakamoto, 1988).

The intergranular cohesion is due to capillary forces at the ice-water interface, which originated from surface tension between ice grains and water and/or bonding forces at the ice-ice interface. The thermodynamic balance ensures that the sum of supplied and removed heat is nil at any time. Equilibrium modifications due to climate or Joule effects are compensated by changes in the melting ratio (Sakamoto, 1988).

2.2.5. Regimes of Water Saturation
2.2.5.1 Wet Snow in the Pendular Regime

There are two regimes of water saturation in wet snow: pendular and funicular. In the pendular regime, air is continuous as shown in Figure 2.2(a,b). Large grains grow and connecting surfaces extend, thus snow strength increases. Field measurements for the LWC in this unsaturated regime range were found between 3% and 5% by volume (Colbeck, 1979). Concerning capillary forces, the LWC in the snow matrix facilitates contact between individual grains and promotes heat transfer (Colbeck and Ackley, 1982).

The metamorphism is driven by the conductive heat flow, as a result of small temperature differences between individual grains. Grain clusters in Figure 2.2 develop naturally trying to minimize the surface free energy. Large grain boundaries are more stable

thermodynamically but they tend to melt if subjected to large normal compressive loads. "In the snow cover on the ground, the high densities take months to achieve unless many meters of wet snow accumulation occur. On power lines, in the presence of high wind, the forces are sufficient to cause high-accretion densities and large specific grain boundary areas. Thus only few hours is required to develop high strength simultaneously with grain growth and grain rounding, in wet snow on power lines" (Colbeck and Ackley, 1982).

<div align="center">(a)   (b)</div>

Figure 2.2: (a) Snow matrix in pendular regime (Colbeck, 1973), (b) Grain cluster in the pendular regime (Colbeck, 1997).

Liquid water is contained in the menisci held by individual particles, in internal veins and external fillets (Colbeck, 1997). Veins and fillets are frozen if the temperature drops below 0°C, this explains the increase in the strength of wet snow sleeves subjected to overnight freezing (Sakamoto, 2000).

Ice grains are joined in groups of two or more and are held by ice-to-ice and capillary bonds. Capillary forces are strong in tension but weak in shear. However, snow sleeves exhibit considerable shear strength by resisting gravity and wind. Colbeck and Ackley (1982) reveal that not only capillary forces explain strong cohesive forces but also ice bonding.

2.2.5.2. Wet Snow in the Funicular Regime

In the funicular regime, water becomes continuous in the inter particle space and air appears in the form of bubbles. This type of snow is called slushy and resembles fluid as indicated in Figure 2.3(a,b). Bonding stress is low because particles are fewer and weakly held together. Snow sheds naturally in this regime by the effects of wind load and gravitational force (Poots, 1996; Grenier *et al.*, 1986).

Figure 2.3: (a) Snow matrix in funicular regime (Colbeck, 1973), (b) Grain cluster in the funicular regime (Colbeck, 1997).

Colbeck (1973) mentioned that the transition between the pendular and funicular regimes occurred at a liquid saturation of about 14% by volume. Denoth (1982) observed that this transition varies for different types of snow. For new fine-grained snow, the transition was observed between 13% and 18% by volume, which corresponds to 27% by mass. For funicular regime, once the snow particles are stressed, they melt away by pressure melting. Whereas for pendular regime, the ice-to-ice bonds are stable against pressure melting (Colbeck, 1979). There is a basic difference between pendular and funicular regimes, where the pendular regime has higher strength compared with funicular regime.

2.3. Snow Accretion

Wet snow accretion usually occurs in France, United Kingdom, Alaska in USA, Norway, Iceland and Japan. Icing can be classified to precipitation icing consisting wet snow or dry snow accretion and in-cloud icing includes glaze, hard rime or soft rime (Meteorological report, 2004). Wet snow accretion was examined in Japan (Wakahama et al., 1977), in France (Admirat et Lapeyre, 1986; Admirat et al., 1990) and in Iceland (Eliasson and Theorsteins, 2000). Eliasson and Theorsteins (2000) studied fallen snow samples. Admirat et al. (1990) constructed a model of wet snow accretion including a condition for shedding. They proposed that snow sleeves broke up when the LWC reached 40%. The failure condition was applied also in wet snow accretion models developed by Poots (1996) and Skelton (1994).

All countries have noticed the severity of the snowfall experienced in New England and United States in 1717. The year 1888 was a brutal year for snow, as many school children were victims of the blizzard. This monster blizzard was called 'The Great White Hurricane''.

The financial losses amounted to a staggering $25 million. Moreover, in 1940, a devastating snow storm swept through the Midwest of the United States causing several disasters. The Storm of the Century of 1993 in United States can be considered also as one of the worst storms. Furthermore, a Snow Storm of 2011 in United Kingdom may be classified under this group of snow accretion events.

2.3.1. Experimental Observations

Wet snow accretion on a stranded conductor has been studied in wind tunnel in Japan since 1970s. The artificial wet snow used in wind tunnels was obtained either by heating natural dry snow or by injecting a water spray along with crushed ice or dry snow. Wakahama (1977) studied the growth accretion, texture and trajectories of wet snow. Admirat (2008) mentioned that there is no snow accretion on the conductor when the test is carried out at negative air temperature and wind speed above 2 m/s. The opinion of French wet snow specialists was that the equivalence between field observations and wind tunnel annotations was difficult to achieve due to the poor design of the wind tunnel itself, which could not provide flow uniformity at the test section (Admirat *et al.*, 2006).

2.3.1.1. Types of Snow Accretion

Dry snow accretion occurs at sub-zero air temperature and wind speed less than 2 m/s. Its density is too low; not much more than 0.1 g/cm^3. Furthermore, dry snow adhesive force is small; it rarely gives rise to extreme loads. However, dry snow cylindrical sleeve can form and shed spontaneously, giving dynamic vibration (Sakamoto, 2000). Whereas wet snow accretion occurs at temperature above freezing point, its density spans a range from 0.1 to 0.95 g/cm^3. Wet snow accretion may form a cylindrical sleeve which cannot shed easily by wind because it has greater adhesive strength (Sakamoto, 2000).

Wet snowflakes look like ice crystals suspended in a liquid water matrix at temperature just above the freezing point, usually between 0.5 and 2°C. At LWC between 15 and 40%, the flakes adhere readily to objects. At LWCs levels below 15%, the snow fails to accrete on structures, whereas at high LWC above 40% the accretion falls off objects. Wet snow accretion is greatly affected by wind speed, air temperature, precipitation flow, LWC of snowflakes and snowflake size (Meteorological report, 2004).

Regarding the growth on the conductor, the axial growth occurs on the windward side of cables, when the cable rotation is prevented like close to the towers and also on the bundled conductors (Sakamoto, 2000), as shown in Figure 2.4(a,b). On the other hand, for cables which have finite torsion rigidity, they may have eccentric snow load. Moreover at mid-span, the cable rotates more than one revolution leading to cylindrical sleeve (Sakamoto, 2000) as shown in Figure 2.5(a,b). For cables with low torsion rigidity, like single phase conductor or overhead ground wire, a cylindrical sleeve may cover the entire span (Poots, 1996). Cylindrical wet snow sleeve formation was observed in the field on cables with a diameter <12 cm, with snow density between 250 and 350 kg/m³ and LWC from 25 to 35% (Gland *et al.*, 1986). Wakahama *et al.* (1977) were the first researchers who studied the effect of wind on snow rotation, (Figure 2.5 (a, b)).

The snow piled on thin wires drops off spontaneously due to eccentric weight of accreted snow caused by wire twisting, while snow piled on thick wires does not drop off but creeps in a way to wrap the wire (Sakamoto, 2005). The torsion rigidity of the wire has a great effect on snow growth. The results of experiments mentioned by Poots *et al.* (1996) demonstrate that, in the case of cable span of 350 m, snow accretion developed a cylindrical snow sleeve. However, in the case of 125 m snow accretion did not form a cylindrical shape, even with an extension of time during the experiments (Sakamoto, 2005). Wet snow is easily compressible: wind has a considerable effect on its compaction, especially at high LWC (Colbeck and Ackley, 1982). The wind plays an essential role in the heat exchanges between a wet snow sleeve and its environment. The wind can have a heating or cooling effect by bringing forced convection to the accretion (Roberge, 2006).

(a)   (b)

Figure 2.4: (a) Axial growth in wind tunnel, (b) Schematic of axial growth (Dalle and Admirat, 2010; Sakamoto, 2000).

(a)

(b)

Figure 2.5: (a) Cylindrical snow sleeve on stranded cable, (b) Cylindrical snow sleeve in wind tunnel (Sakamoto, 2000; Dalle and Admirat, 2010).

2.3.2. Field Observations

Concerning the measurements and observations in natural snowfalls in France during 1983-1990 (Figure 2.6), it was mentioned that damage occurred when the threshold of snow overload equal or over 3 kg/m. However, it reaches its maximum for snow load higher than 10 kg/m. Wet snow is described in terms of their thickness and their weight per cable length. Values found in the literature range are around 5 cm for radial accretions and 10 kg/m for snow loads. Severe storms generate accretion up to 15 cm and snow overload up to 20 kg/m (Roberge, 2006). Sliding of wet snow is observed at the end of events when two conditions are met: a warming temperature is predominated; a great slopping of the conductor higher than 30° is obtained as well.

Generally wet snow densities in the field ranged between 100 to 220 kg/m³. Liquid water content was found in the range of 0% to 14% by volume. These LWC values are less than the laboratory results recorded (Admirat *et al.*, 2006). A comparison of wet snow data reported by monitoring programs in France, Japan and Iceland over the 20 years is presented in Table 2.1.

The research results displayed by Japan and France reflect the fact that these countries are vulnerable to wet snow accumulation on overhead cables and structures. Sakamoto (2000) reported that dry snow accretions are easily blown off from cables at wind speed exceeding 2 m/s and density less than 0.1 g/cm^3. Admirat *et al.* (1990) reported that a succession of dry and wet snowflakes was observed at temperature close to 0°C. Under low wind speeds, the densities of dry and wet snow accretions were observed between 0.1 g/cm^3 and 0.22 g/cm^3. Wakahama (1977) mentioned that monsoon-induced snow accretions occur at low-wind speeds producing low-density accretion; however, cyclone-induced snow accretions severely occur at high-wind speeds resulting high-density accretions.

Figure 2.6 Field measurements (Cigre, 2006).

Table 2.1 Field results in France, Japan and Iceland during 20 years.

	France (1983-1990) (Admirat *et al.*, 1990)	Japan (1965-1985) (Wakahama *et al.*, 1977)		Iceland (1977-2000) (Elisson & Thorsteins, 1996)
		Monsoon	Cyclone	
Wind speed (m/s)	0 ~ 5	0 ~ 3	> 10	10 ~ 25
Density (g/cm^3)	0.1 ~ 0.22 0.5 (single event)	0.2	0.2 ~ 0.87	0.3 ~ 0.95
Snow overload (kg/m^3)	0 ~ 10	0 ~ 5	0 ~15	0 ~ 20

2.3.2.1. Mechanisms of Accretion

a- Self - limiting axial accretion mechanism on fixed conductor

The fixed conductor which has high rigidity can resist torque. The snow deposit may only grow in the axial wind direction and snow accretion rate decreases as a function of time (Figure 2.7(a , c)).

b- Unlimited cylindrical accretion mechanism on a free rotation conductor

The conductor does not resist torque and rotational motion is generated. For the reason of low rigidity, this mechanism is unlimited and continues as long as the meteorological conditions are present, limited by conditions that cohesion is less than gravity (Figure 2.7(b,c)).

c- Unlimited cylindrical accretion on a smooth conductor

Wet snow accretion on smooth conductor is always cylindrical; this formation is a result of rapid sliding of snow on the smooth conductor-snow interface. The conductor rigidity has no effect and this type is always theoretical unlimited (Farzaneh, 2008, Wakahama, 1977).

Figure 2.7: (a) Axial and cylindrical accretion for 150 kV, (b) axial and cylindrical 500 kV and (c) Schematic of accretions on cable (Dalle and Admirat, 2010; Sakamoto, 2000).

2.3.3. Wet Snow Accretion Models

Models have been based on either the thermodynamics or the mechanics of the accretion process. The model introduced by Admirat *et al.* (1986) is a thermodynamic model; it treats the accretion as radically symmetric at all times. This model separates the accretion process into 3 stages, formation, growth and collapse, described as follows:

a- Formation stage:

The formation stage begins with the impact of the snowflakes on the conductor at positive temperature. The snow then melts and cools the conductor to as low as 0°C.

b- Permanent growth stage

Snow accumulation keeps on as long as the ambient thermodynamic conditions remain appropriate. Except the Joule effect, all the heat exchanges are permanent at the air/snow interface.

c- Gradual breaking up stage (collapse)

A gradual breaking of snow occurs for thermodynamic reasons such as interruption of snowfall, warming, sublimation of ice and excess LWC. Generally, all the factors which cause reduction of cohesive forces may cause snow collapse.

2.4. Wet Snow Shedding

The study of wet snow shedding from structures is essential, since snow shedding from one span causes imbalance between adjacent spans and may damage transmission line elements. Snow shedding may occur naturally or following the application of an external force leading to forced shedding. Natural snow shedding can occur as a result of dynamic effects like galloping. Galloping usually occurs when a moderately strong and steady wind (above 7 m/s) acts upon an asymmetrically iced conductor. Melting due to temperature increase, or effect of solar radiation (Olqma, 2009) has also a significant effect on shedding. Shedding may be achieved by de-icing methods like the thermal methods, *i.e.*, Joule heating or by short circuiting the conductor (Laforte *et al.*, 1998). Moreover, the mechanical methods, as the adhoc and the rolling methods may affect snow shedding to high extent (Laforte *et al.*, 1998).

2.4.1. Shedding Modes

Roberge (2006) reported Guilbeault's observations that snow sheds in a random and partial manner on phase conductor; however, on overhead ground wires, snow sheds in an unzipping manner, which causes large oscillations. The modes of shedding are mentioned as follows:

a- Unzipping shedding mode

A realistic explanation of unzipping shedding is that partial shedding on an adjacent span can generate a transverse wave travelling along the ground wire span by a constant speed. To achieve this, LWC should be high enough to reduce the cohesive strength of snow. In addition, the vertical acceleration should be enough to trigger shedding (Roberge, 2006). It may be remarked that the unzipping is observed only on overhead ground wires, because it is more likely to arise on cables with smaller diameter. Snow unzipping is simulated by removing the snow elements from the model at the rate of 111 m/s (Roberge, 2006, Roberge et al., 2007).

b- Partial snow shedding mode

Roberge (2006) reported that during the experiments, wet snow on a short cable was observed to shed naturally at speeds up to 14 m/s. There were no recorded field observations on the length of partial snow shedding. It was generally described as being anywhere from few meters to ten meters.

c- Mixed shedding mode

Snow sleeve has neither uniform density nor LWC along the entire span and consequently, the unzipping mode is limited to a fraction of a span. Thus, the remaining accretion can shed in random segments if there is no mean of generating another transverse wave. When partial and unzipping modes occur together, this mode is known as the mixed mode (Roberge, 2006).

2.4.2. Forced Shedding

Poots (1996) suggested that wet snow can shed by forced shedding similarly to glaze and rime ice. A sudden twist is given to rime ice accretion, but an axial traction, or bending moment to glaze ice (*e.g.*, from a propagating axial or transverse wave) can lead to fracture and shedding. There are no field observations to confirm that this is applicable to wet snow. Poots (1996) mentioned that snow can be subjected to large transverse acceleration, *i.e.*, a combination of wind, gravity and inertia effects, once the resultant load exceed the adhesion strength, snow shedding may occur. Since snow is a highly plastic material, thus applying static deformation cannot trigger its shedding.

In general, methods used after an ice storm when the line is covered with a significant sheet of ice are termed as de-icing techniques. They essentially aim at limiting the time it takes to restore the lines to service after a storm and to limit the extent of damages. De-icing techniques can be classified according to various criteria (Volat *et al.*, 2005) based on the physical principle used in the method to remove the ice from the structure (Laforte *et al.*, 1998).

The de-icing techniques have been classified to the following four categories:

1- Thermal methods based on the melting of ice

2- Mechanical methods based on breaking up of ice

3- Passive methods based on natural forces

4- Diverse methods based on fundamentals

The thermal methods are techniques related to heating the conductor by means of Joule heating or by short circuiting the conductor (Laforte *et al.*, 1998). Relating to the mechanical methods, there are eight main techniques, three developed for conductors, *e.g.*, adhoc, rolling and forced vibrations methods. The rolling method is the only mechanical method which is operational for de-icing of conductors. In addition, there are three other techniques like the ultrasonic vibrating, electromagnetic impulse and pneumatic impulse techniques. The electromagnetic seems to be the most adaptable method for conductors (Laforte *et al.*, 1998).

The mechanical methods, which are based on the breaking of ice deposits, have been studied by Kalman (Kalman T., 2007). These methods use mechanical shocks to de-ice the ground wire taking advantage of the brittle behavior of ice at high strain rates (Kalman *et al.*, 2007). The present research can be considered as a way of mechanical de-icing, but by using periodic load at the excited end. It can be indicated that mechanical shocks require low energy for breaking ice comparing to other methods. They require 30 to 40 times less energy than thermal methods, thus it is considered as the best type of de-icing techniques (Laforte *et al.*, 1998).

Another classification is investigated to illustrate the permanent or temporary character of the method. There are thirty seven potential methods which can be divided into inline (9), punctual (9) and permanent (19). Inline methods refer to those using Joule effect to melt the ice, whereas punctual methods regroup all methods that are not installed permanently

on the line. The mechanical methods can be considered as punctual methods (Volat *et al.*, 2005).

2.4.3. In-Situ Observations of Wet Snow Shedding

Observations of natural wet snow shedding from a cable are rare and not well-documented. Shedding occurs following an increase in LWC governed by its thermal equilibrium. The exact LWC value, at which shedding occurs is difficult to predict as it depends on the density of snow and external factors. The range of LWC by mass for high adhesion was reported between 20% and 40% in some studies (Farzaneh, 2008; Admirat *et al.*, 1988), whereas it was observed between 35% and 50% in others (Roberge, 2006; Olqma, 2009).

It was observed that snow begins to shed at first at the axial growth area, which is close to towers where cable rotation is prevented. The axial growth area is found to be ranged from 20 to 30 m from the tower (Admirat and Lapeyre, 1986). In case of a cylindrical sleeve, snow sheds partially, where this partial shedding occurs in 5 to 10 min (Roberge, 2006) (Figure 2.8).

Figure 2.8 Wet snow load on a river crossing cable in Iceland 2005 (Cigre, 2006).

Shedding may be preceded by two types of creep, the first type being caused by the effect of gravity, wind, temperature, solar radiation and liquid precipitation (Roberge, 2006); however the other type, by the inclination of the cable if it is more than 30-40°, causing the snow sleeve to lose its adhesion from the cable and slides along it. Observations in Nova

Scotia were reported and showed that sleeve diameter increased from 7.5 to 50 cm following creep (Admirat and MacCagnan, 1985) (Figure 2.9).

Admirat *et al.* (1988) also suggested that LWC reaches a maximal value when dripping starts and leads to shedding; this value was found to depend on the initial value of snow density. Increase in LWC is mainly due to the convective exchanges which control melting, such as wind speed, air temperature, or the electric current. Conversely, LWC decreases due to the increase in snowfall intensity and the increase of the collection coefficient while wind speed decreases (Farzaneh, 2008).

During wet snow events, there are successive cycles of accretion and shedding (saw-tooth loading). The frequency of these cycles is increased by using Joule heating, which also limits the maximum snow load and delays the start of the accretion phase (Admirat *et al.*, 1986). Poots (1996) suggested that snow might shed suddenly from a whole span, but this has never been observed in the field; it is very unlikely that all snow sheds at the same time.

Figure 2.9 Creep of wet snow sleeve on a steep cable (Admirat and MacCagnan, 1985).

Snow may shed naturally after overnight freezing; this phenomenon depends on the weather conditions during and after the accretion. Wet snow may be shed by sublimation or melting when temperature is above freezing, as occurs for rime ice and glaze ice. However, it can also stay on the cable for many weeks (Elisson and Thorsteins, 2000).

2.4.4. Experimental Observations of Wet Snow Shedding

Wind tunnel experiments have shown that snow shedding is a random process. On short cable, wet snow sheds suddenly or in partial random segments (Sakamoto, 2005). It is observed in wind tunnel tests that at high wind speed, accretion holds well even if the eccentric weight and cable twist are large. Moreover, accretions tend to shed more easily from cables with high torsion rigidity and a complete snow sleeve is difficult to shed by wind and gravity loads alone (Sakamoto, 2005).

Previous wind tunnel tests and field observations indicated that snow sleeves exhibit creep prior to shedding. When LWC reached a critical value, the initial cross section became elongated and a cavity was formed as the snow migrated (Figure 2.10).

Shedding was observed in the cold room of CIGELE laboratories. It was initiated at one end along the cable and progressed at a measurable speed (Roberge, 2006). Wet snow with high initial density sheds later than wet snow with low density, since the cohesion force is stronger. Whereas, wet snow with high initial LWC sheds rapidly because shedding is reached earlier.

Figure 2.10 Snow creeps prior to shedding (Roberge, 2006).

Roberge's experiments (2006) did not exhibit any sudden shedding behavior. In his observations, shedding progressed rather very slowly from the cable ends. Even if temperature was high, no snow sleeve was observed to shed spontaneously along its entire length. Time for shedding was longer for eccentric sleeves than for centered one.

It was observed in the cold chamber in CIGELE that when the bottom of the accretion was saturated with water, thus snow becomes transparent, which causes liquid water dripping on the floor (Roberge, 2006) (Sakamoto, 2000; Wakahama, 1977). In the wind tunnel, the LWC migrates into the lower regions of the snow sleeve by the effect of gravity; as a result, the snow considers in the funicular regime in the bottom, while the top of the sleeve persists on the cable. Sakamoto (2005) found the following tendencies of snow shedding in relation to different parameters (e.g., density, wind speed, temperature and torsion rigidity):

1- Accreted snow of small density tends to drop off more easily than that of large density (for a non-complete cylindrical sleeve).

2- When wind speed is high, the external force exerts on the accreted snow with the eccentric weight is greater, thus the accreted snow does not tend to drop off easily.

3- A wire with strong torsion rigidity promotes snow shedding higher than the wire with small torsion rigidity.

4- Once snow wraps around a wire, it is unlikely to drop off in a relatively short time (Sakamoto, 2005).

2.4.5. Previous Shedding Models

The first attempts to estimate rebound heights of conductors due to sudden ice release were made decades ago (Morgan and Swift, 1964). Matsuura *et al.* (1995) carried out real scale observations and analyses of ice shedding, which are fully exposed to heavy atmospheric icing (6 kg/m). They measured the meteorological conditions, weight of ice and the tension of insulator strings. In addition, they monitored the motion of conductors. Matsuura *et al.* (1995) performed the dynamic effects of sudden ice shedding by the finite element method using Automatic Dynamic Incremental Nonlinear Analysis (ADINA) software. It may be noticed that a detailed description of their numerical model is lacking, but they concluded that the numerical and experimental results of the maximum cable jump were in a good agreement. Thus, the numerical analysis of the ice shedding phenomena by the finite element method could be useful for the design of transmission lines prone to severe atmospheric icing.

The improvement of computer software has led to the finite element modeling of both static and dynamic effects of instantaneous ice shedding on overhead lines (Jamaleddine *et al.*, 1993; Matsuura *et al.*, 1995; Roshan and McClure, 1998; Kalman *et al.*, 2007). Jamaleddine *et al.* (1993) studied the effect of ice shedding on overhead lines using ADINA

(ADINA, 2004), a commercial software package. In their study, reduced-scale ice shedding simulations were carried out experimentally by the sudden drop of dead weights. A comparison between the experimental and numerical model results confirmed the good performance of the numerical models for both static and transient dynamic analyses.

Jamleddine and Roshan Fekr (1995, 1998) explored many ice-shedding scenarios on single and multiple spans of overhead cables with different parameters; including ice thickness, span length and difference in support elevation. These scenarios were 2-D simplifications of actual overhead lines and they did not consider the flexibility of the support towers. The models consisted of cable pinned at the ends and hinged suspension strings. Roshan Fekr (1995, 1998) studied a two-span line section response to instantaneous shedding. He considered several ice-shedding scenarios with variables like ice thickness, span length, difference in elevation between extremes and suspension points, number of spans per line section, presence of unequal spans and partial ice shedding on sub-spans. The general modeling approach has been summarized in McClure and Lapointe (McClure and Lapointe, 2003) explaining the transient response following a cable rupture.

Kalman's study (Kalman et al., 2005, 2007) is an advanced application to ice shedding. He studied the application of a mechanical shock on the cable, which created a propagating wave causing ice rupture. Ice deposits are modeled as a beam finite element connected in parallel to cable elements using ADINA software. Ice beam elements are prone to failure criteria based on axial and bending stresses. When the stresses exceed this failure criterion, the ice elements are removed from the model (element death upon rupture). This model was a powerful tool to estimate the amount of ice that may be shed following the application of a shock load.

Roberge (2006) simulated the dynamic effects following snow shedding from a cable. He proposed a finite element model for snow using non-linear horizontal spring elements with zero stiffness and damping properties. Snow elements with mass are modeled as vertical loads acting on the nodes. The propagation of snow shedding is modeled by removing mass of adjacent elements at time intervals corresponding to the speed of shedding. Roberge et al. (2007) reported that the lowest cohesive forces of wet snow sleeves occurred at the instant prior to natural shedding. Failure criteria should be added to the model based on an upward acceleration not on mechanical stresses. They concluded that the effects of partial shedding

are proportional to the amount of snow removed; where the mid-span displacement and the cable tension amplitudes were doubled when snow shedding percentage was doubled. It was found that snow does not shed suddenly from the cable: it will either shed completely by unzipping manner or partially. Roberge performed simulations on a 470-m ground wire model and he observed two speeds to evaluate the effects of snow shedding. The speed at which total unzipping may progress is 111m/s; whereas 14 m/s is the speed at which partial snow shedding is observed. Roberge (2006) performed his tests in the cold room in CIGELE on 2.5 m cable section.

Olqma (2009) and Fonyo (2008) studied the thermodynamics of snow shedding and observed the shedding mechanism from a cable with negligible and significant sag, respectively. Olqma (2009) observed that shedding began at the ends of a snow sleeve using negligible sag. He developed a two-dimensional thermodynamic model that considered the effects of electric current, wind speed, air temperature and solar radiation on snow shedding. Fonyo (2008) observed that for sagged cables, shedding started at the end of the short sleeve, whereas it started at mid-span for the long sleeve. In addition, Zhang (2009) proposed a model in which he investigated the characteristics of forced convection from a snow sleeve in a cross flow of air. He found that snow roughness has a significant effect on heat transfer rate, while, the sleeve shape effect on snow shedding is negligible.

2.5. Adhesion for Wet Snow

Adhesion causes problems for many industries, especially power networks. In the case of overhead electrical lines, the combination of wind and icing could cause damage, leading to power outages. The adhesive forces are significantly larger for wet snow accretion above 0.5°C. Wet snow may not shed even if exposed to high wind speed, thus promoting the growth of heavy loads. If ambient conditions change during snow accretion such that the air temperature drops below freezing point, the wet snow will freeze in place, thus causing the adhesive forces to increase and leading to further snow growth. Adhesive forces during snow accretion have different sources depending if the process is dry (at low air temperature) or wet (when air temperature is high). The liquid water content (LWC) of snow was especially scrutinized in related research studies as it proved to be the main variable which determines whether wet snow accretes on conductors and whether it sheds (Eshiemogie, 2011).

Increasing the LWC of the snow matrix weakens the internal cohesive forces which keep snow particles together. Above a specific diameter of snow deposit, aerodynamic and gravitational forces overcome the cohesive forces, thus the snow sleeve breaks up and the snow deposit drops off. This maximum diameter decreases rapidly with LWC increase. Eshiemogie (2011) proposed an empirical relationship between initial snow water content and air temperature. He concluded that it was not possible to obtain a clear relationship between the snow sleeve water content and the cohesion of the sleeve. Eshiemogie proposed the critical LWC value of 40% when the maximum snow sleeve diameter is around 5 cm. Above this LWC level, the snow sleeve breaks up before its diameter reaches 5 cm. At this moment, wet snow accretion continues if the ambient conditions remain favourable; however, wet snow always sheds, at least partially, before the sleeve diameter reaches 5 cm. In France and Japan, snow sleeves of large diameter may grow when LWC approaches the lower limit of the ranges observed, therefore the resulting overload may be significant and causes damage to transmission lines (Eshiemogie, 2011).

2.5.1. Cohesion and Adhesion Definitions

Cohesion is the intermolecular attraction between 'like-molecules' usually referred to the strength with which the particles of an object or fluid attract to each other (Adhesion Database Web Site). Adhesion is the intermolecular attraction between 'unlike-molecules', usually referred to the attraction, or joining of two different objects or fluids to each other (Sakamoto, 2000). In addition, adhesion strength is defined as the energy per unit surface required to separate ice from its substrate in an adhesive failure (Javan - Mashmool, 2005).

Wet snow is an adhesive material, because it contains free water. There is a negative pressure, which is induced in water existing at the interface between snow samples and a contacting material and that is the reason of adhesion. The pressure, P, is given by the equation 2.2.

$$P = - (\sigma / r) \hspace{4cm} \text{Equation (2.2)}$$

where σ is the surface tension, r is the radius of curvature of a concave water surface at the interface. The radius of curvature depends on many factors which include free water content, grain size and density of snow (Wakahama and Mizuno, 1977). The snow adhesion strength has the maximum value for a water content of about 15% and this value is close to the critical

water content from the catenary to reticulation area (Section 2.1.2) as described by Colbeck (1973) and Denoth (1982). The main types of intergranular forces in snow are as follows:

1. Friction and interlocking of grain without sintering at cold temperature.

2. Adhesion force due to water-like-film of grain surface without sintering at high temperature (semi-bonded snow) (Colbeck, 1973; Denoth, 1982).

2.5.2. Adhesion Mechanisms

Adhesion mechanisms can be described as follows:

1- Freezing

2- Bonding through freezing of super-cooled water droplets existing on the surface of snowflakes

3- Sintering

4- Condensation and freezing of vapour in air

5- Mechanical intertwining of snowflakes

6- Capillary action due to liquid water included

7- Coherent force between ice particles formed through metamorphism of snowflakes

Wet snow adhesion may be explained by mechanisms 6 and 7, while dry snow adhesion can be described through mechanisms from 1 to 5 (Sakamoto, 2000).

2.5.3. The Main Adhesive Forces

The attractive bond forces between molecules include three types: Dipole-Dipole forces, London dispersion forces and Hydrogen bonding. Dipole-Dipole forces act between polar molecules. London dispersion forces are one component of the intermolecular Van der Waals forces, while Hydrogen bonding is a very strong attraction that occurs among molecules (Rimai et al., 1995).

2.5.4. Previous Icing Adhesion and Cohesion Tests

2.5.4.1 Cohesion Tests

Snow bottom in Roberge's experiments stayed on the cable by tensile capillary forces, which are weaker than the cohesive forces involved in top half (LWC < 28%). The snow sleeve maintains on the cable demonstrates good cohesion where the snow grains were frozen onto the metal strands. As soon as the grains were exposed to warm air, the internal bonds disappeared because of melting and a water film formed between the cable and snow causing the accretion to twist to the bottom in a corkscrew manner (Roberge, 2006).

2.5.4.2. Adhesion Tests

Some methods to determine ice adhesion strength were reviewed (Javan-Mashmool, 2005). The basis of an adhesive test involves a load applied to the adhesive material/substrate system until failure occurs. Shear mode tests like lap shear or torsion shear tests are the most widespread. Aside these shear tests, all the ice adhesion tests before the centrifuge test present problems and shortcomings like instantaneous increasing rate of applied load, direct application of load onto ice, or unclear adhesive failure determination (Archer and Gubta, 1998; Javan-Mashmool, 2005).

The centrifuge adhesion test can be used for measuring the force capable of separating ice from the substrate. There were a lot of methods in literature for measuring ice adhesion as previously mentioned; they gave highly variable results (Laforte and Beisswenger, 2005). Accordingly, the centrifuge adhesion test was selected for its excellent capability at measuring shear adhesion force between snow and a substrate. Adhesion stress of wet snow examined during wind tunnel experiments was 19 ± 1 kPa, where this was the case for LWC of snow around 20% or greater (Wakahama et al., 1977).

2.6. Mechanical Properties of Snow

Shapiro et al. (1997) wrote a recent review on the state of knowledge of dry snow mechanics in relation to engineering applications. Mechanical properties of snow were measured during avalanche studies in Switzerland and were gathered by Bader et al. (1939). In the 1950's and 1960's, several experimental observations were made in Hanover, New Hampshire (USA). At the same time, Canada, Switzerland and Japan also conducted laboratory and in-situ experiments on snow mechanics (Shapiro et al., 1997).

Langham (1981) reported that snow may be deformed elastically when subjected to a small load for a short period of time. Under these conditions, the strains are small enough and recoverable once the stress is removed. Snow deforms continuously and permanently if a sustained load is applied, this is referred to as creep or viscous plastic flow. Plastic flow requires a threshold stress to be reached before flow can start; however, for snow this stress is so small that it cannot be measured and so snow is referred to as a viscoelastic material.

2.6.1. Compressive Strength

The loading rate affects the failure mode in such way that it is ductile at low-deformation rates and brittle at high deformation rates. Grain metamorphism is found in dry snow with increase in cohesive strength. The rate of metamorphism is slower in dry snow than in wet snow, in which it happens over a period of days and even months. Figure 2.11 indicates that six days old or three days old snow samples have compressive strength around 10 times of the compressive strength of fresh snow. how calculated or measured

Figure 2.11 Unconfined compressive strength versus deformation rate for snow samples of various ages (Fukue, 1977).

Concerning the relation between compressive stress and strain, there is a linear increase up to a certain point (strain of 0.4%), as shown in Figure 2.12. Since, the relationship is nonlinear; thus the compressive stress exhibits a slow increase with strain afterwards. In addition, when comparing with tensile stress, there is an increase around 30% from tensile to compressive stress (McClung, 1981).

Figure 2.12 Compressive stress versus strain (McClung, 1981).

2.6.2. Tensile Strength

The tensile strength is one of the important parameters for assessing the failure of snow. Snow is an elastic-visco-plastic highly temperature dependant complex material showing a wide variation in its strength. Many parameters affect the strength of snow, like density, snow temperature and micro-structural parameters. A theoretical porosity-dependant expression for the tensile strength of fully age-hardened snow was developed by Ballard and Feldt (1965).

Keller and Weeks (1968) conducted centrifugal tensile experiments on fine-grained snow and compared their data with a theoretical relation given by Ballard and Feldt (1965). It was found that there was less scatter in centrifugal tensile strength of snow and much simple relation with density in comparison to the earlier data. The effect of sintering time on tensile strength was determined. It was observed that below 10 days of sintering time, tensile strength was <10 kPa, while at 100 days sintering time, tensile strength reaches to 100 kPa.

Sommerfeld (1973) reported that density of snow represents an important measurable parameter to study the tensile strength of snow. Comparison of McClung data (1979) and the non-in-situ data from centrifugal test (Keller and Weeks, 1968; Sommerfeld, 1974) leads to the conclusion that increased sample size results in lower-mean values of strength and less

scatter as a function of density. It can be seen that there is an increase in failure stress with density. For density above 300 kg/m^3, failure stress of majority of snow samples is found to be above 20 kPa. Few data have values of failure stress below 20 kPa for densities below 300 kg/m^3, as depicted in Figure 2.13 (McClung, 1979).

For measuring the tensile strength, a semi-spherically-shaped snow sample was slowly compressed from the top, using a plate moving downward at constant speed. The compressive force increased with time and the motor was stopped, and then followed by a relaxation of stress. When the force reduced to a quarter of the initially given compressive force, the pulling up of the plate was started by the motor and the tensile force linearly increased with time until detachment (Wakahama and Mizuno, 1979). The maximum adhesive strength values were found between 12 to 16% of free LWC. Moreover, it was found that the adhesive strength increases by increasing the initial applied compressive strength. The adhesive force itself remained constant for each material when the free water content of snow was larger than 7-8%. This finalizes that the adhesive strength of wet snow depends not only on the wettability of contacting materials but also on its flexibility (Wakahama, 1977).

Seasonal snow in mountains is a bonded granular material for which failure depends on deformation rate and strain conditions. It is also characterized with its high porosity. Figure 2.14 shows a schematic of a failure diagram for Narita's data (Narita, 1980). The strain rate at which the transition from fast to slow rates occurs, is in the order of 10^{-6}/sec. This strain rate depends on snow characteristics such as density, temperature and test conditions. In the area of fast strain rate, the tensile stress increases with increasing strain, although in the slow strain area, the inverse happened. Once density increases, the tensile stress decreases for the same strain (McClung, 1981).

Figure 2.13 Tensile strength versus snow density (McClung, 1979).

Figure 2.14 Tensile failure stress versus failure strain (McClung, 1981).

The tensile strength of snow as a function of density is shown in Figure 2.15. It can be indicated that the tensile strength of snow is much lower than that of ice. The tensile strength of snow decreases substantially with decreasing snow density. The snow strength is dependent primarily on the bonding contact of the individual ice particles, the number of particles and

their shape (Petrovic, 2003). Tensile strength of snow is determined by using a centrifugal testing device, where a snow sample is held in place by U-shaped clips made of copper tubes onto a sample holder. When the sample holder is rotated, the speed of rotation is progressively increased up to a point where the developed centrifugal force exceeds the adhesion strength of the snow sample, causing it to fail. It was found that for low densities, failure occurred in the stress range of 10-20 kPa (Upadyay *et al.*, 2007). The compressive strength of snow is very high compared with the snow tensile strength, which is about 0.2% of the compression strength (Kovacs, 1977).

Figure 2.15 Tensile strength versus density (Petrovic, 2003).

2.6.3. Shear Strength

Figure 2.16 shows that increasing normal stress augments shear stress causing strain failure (McClung, 1981). In addition, the relation between horizontal displacement versus shear stress increases up to a certain limit, then it decreases with further strain increase. Figure 2.17 demonstrates results for similar samples of low density, where snow subjected to shear at different rates under the same normal load. It provides a graphic illustration of the dependency of shear stress on strain rate. For lower strain rate, there is a proportional relation between strain and shear stress. However, by increasing strain rate there is a relative relation only up to a certain limit. Then, there is an inverse proportional between strain versus shear stress (McClung, 1981).

Figure 2.16 Shear stress versus horizontal displacement for different normal stresses (McClung, 1981).

Figure 2.17 Shear stress versus horizontal displacement for different strain rates (McClung, 1981).

2.6.4. The Relation between Density and Other Material Properties of Snow

Mellor (1975) stated that snow has very complex properties, exhibiting visco-elastic and undergoing large strains. As snow normally exists at temperatures above 0°C, its basic structure is thermally unstable. Mellor (1975) also mentioned that coherent deposited snow may be regarded as a quasi-homogenous sintered compact of ice grains. Snow possesses most of the mechanical properties of solid ice. Ice can be considered as temperature-sensitive nonlinear visco-elastic material under typical loading conditions, but rupture may occur by

visco-elastic yielding (by brittle fracture). However, snow is highly porous material and it has high and largely irreversible compressibility that distinguishes it from ice and most engineering materials.

Figure 2.18 gives a general expression of elastic modulus as a function of density for dry snow. It demonstrates the relation between density and Young's modulus for dry coherent snow for different cases of temperature and strain rate (Figure 2.18)(Mellor, 1975).

In Figure 2.19 dynamic and static viscosity are plotted against density showing a rapid increase of viscosity with increasing density. The dynamic viscosity is higher than the static one. Generally, it is not sufficient to characterize the mechanical behavior of snow only in terms of the original physical state like density and the state of stress. It is also necessary to account for the stress or strain history (Mellor, 1975).

Figure 2.18 Young's modulus versus density for dry snow: (A) Pulse propagation or flexural vibration at high frequencies, -10° to -25°C. (B) Uniaxial compression, strain rate approximately 3×10^{-3} to 2×10^{-2} s^{-1}, temperature -25°C. (C$_1$) Uniaxial compression and tension, strain rate approximately 8×10^{-6} to 4×10^{-4} s^{-1}, temperature -12°C to -25°C. (C$_2$) Static creep test, -6.5 ° to -19 °C (Mellor, 1975).

Figure 2.19 Viscosity versus density (Mellor, 1975).

2.7 Conclusion

A brief review of the recent developments in wet snow studies is given in this chapter to determine whether the existing approaches are sufficiently appropriate. If not, what are the shortcomings of those researches in predicting of the mechanical behavior of wet snow?

There are many drawbacks in previous studies, such as the tensile and shear strengths of wet snow had not been related to snow microstructure and LWC. However, this relation should be considered since the component of any material will extremely affect its response to load. Many researchers investigated the compressive strength of wet snow, indicating that snow compressive strength is higher than the tensile strength. Therefore, these previous observations motivate the author to study the tensile strength of wet snow precisely. Numerical analysis studies of snow shedding on real lines are scarce. Moreover, there is no modeling study associated with forced snow shedding. These shortcoming aspects prompt the need of wet snow shedding modeling resulting from dynamic loads. Furthermore, there were some studies concerning snow shedding in the wind tunnel and the climate room; though, there is nothing correlated to snow-composite cable affected by a load. Therefore, further analysis of this phenomenon is still required to determine the extreme motions and damages

that have resulted due to the snow shedding process. This study may be considered as a follow-up work to the snow modeling research done before.

In order to model the propagation of snow shedding along the span and therefore to integrate the failure criteria of snow into the model; knowledge of the adhesion properties of snow is essential. Experimental analysis of snow shedding problems on a full-scale is difficult and costly to achieve. Therefore, it is envisioned that finite element models will provide a powerful simulation tool to assist in the management of mitigation for wet snow shedding effects on power lines.

CHAPTER 3
EXPERIMENTAL STUDY

CHAPTER 3
EXPERIMENTAL STUDY

3.1. Introduction

The experimental work was carried out to determine the adhesion of wet snow to transmission line cables and consequently, to achieve the simulation of vibrations of the cable covered by wet snow due to the application of periodic excitation, as well as investigating the resulting snow shedding process. While shedding occurs when adhesion vanishes, studying the tensile and shear adhesion is essential to correlate shedding to the adhesive strength between cable and snow.

3.2. Adhesion Experiments

Snow adhesion to cable is the source of significant danger, since it causes snow shedding once it fades away, thereby it is essential to measure such adhesion forces. This chapter will describe the shear and tensile adhesion tests, which these results will be the main input to the numerical model, where it will be studied later in Chapter 4. Two sets of adhesion experiments were carried out in this chapter including: (a) shear experiments using the centrifugal machine and (b) tensile experiments using the material test machine.

3.2.1. Shear Adhesion Tests

3.2.1.1. Cold Room Laboratory

The snow samples were tested using the centrifuge machine for shear adhesion tests, in a cold room of CIGELE laboratories. All the tests were conducted under constant temperature conditions, where the temperature can be adjusted to values as low as $0 \pm 2°C$.

3.2.1.2. Equipments

The shear adhesive strength of wet snow was determined by centrifuge machine test, which it was first investigated by Stallabrass (1962).

The advantages of the centrifuge adhesion test (CAT) are that wet snow can be prepared in a cold room under simulated atmospheric conditions. This centrifuge test among various techniques has gained popularity recently because it is simple, low cost and can be

performed timely. Furthermore, it is a repeatable method including small standard deviation and the snow samples that examined are homogenous, since they have small size (Hefny et al., 2009).

There are many types of equipment used in shear adhesion tests as follows:

a- Beams and Surfaces

The test proceeds by artificially icing the extremity of a beam, then, spinning them in a centrifuge machine to determine the speed and force at which the snow detached. The tests were conducted on a 31 mm wide, 0.6 mm thick, aluminium flat beam which was cut to a 340 mm length, as shown in Figure 3.1(a, b). A counter weight was fixed a distance away from the other extremity of the beam with about the same weight as the snow, to balance the beam. The centrifugal force resulting from the rotation tends to detach the snow layer. When this force reaches that of the adherence of the snow, the snow detaches (Hefny et al., 2009).

In the current shear experiments, four types of surfaces (140 x 32 x 1.5 mm) were used in order to study the effects of surface roughness on adhesion. These surfaces are smooth surfaces, rough surfaces (prepared by sandpaper No. 100, 50) and a stranded cable surface. Figure 3.2 shows bar surfaces, which were used in shear tests. The rough and smooth surfaces may be described as follows (CAMI Web Data base reference):

CAMI Grit designation: No. 50 (coarse surface) = average particle diameter 348 μm.

CAMI Grit designation: No. 100 (fine surface) = average particle diameter 140 μm.

CAMI Grit designation: No. 400 (smooth surface) = average particle diameter 23 μm

Stranded-cable surface was prepared using a milling machine resulting in a rough height, which simulates the fiber radius of the stranded surface of 0.066 inch (1.68 mm) (Oberg *et al.*, 1976). A semi-spherical wet snow mold (45 cm- long) was used, which can be considered as a method to compact wet snow sample upon the extremity of aluminium small bars(Hefny et al., 2009).

(a)

(b)

Figure 3.1: (a) The centrifuge beam plan, (b) Detailed schematic of the centrifuge beam.

Figure 3.2 Bars with different surface roughness.

(Hefny et al., 2009).

b- Devices for measuring LWC/Density

LWC and density were measured in the shear and tensile adhesion experiments. The LWC was obtained by using a Decagon model EC-5 moisture sensor (Figure 3.3). This sensor

was connected to a voltmeter, which provides a reading in voltage based on the dielectric constant of the medium. This voltage is converted into volumetric water content using a calibration curve (Eq. 3.1). The LWC (% by mass) is obtained by dividing the volumetric water content by the snow density. The density is calculated by dividing snow mass per snow volume, where the mass is measured using a digital balance; however, the volume is deliberated by using a cylinder of a known volume.

$$VWC = (v * 0.06) - 23 \hspace{3cm} \text{Equation (3.1)}$$

Where v is the voltage, VWC is the volumetric water content.

Figure 3.3 EC-5 sensor and voltmeter.

c- Measuring Devices and Data Acquisition System

Analog to digital conversion is provided by a drive module. The module was installed outside of the refrigerated room and connected to a computer. Once any piece of snow touched the vat wall causing vibrations, thereby there is a rare cohesive break occurred and the test automatically stopped. The test is then rejected and repeated.

3.2.1.3. Shear Test Procedure

The dry snow was stored in a cold room at temperature above 0°C for around 30 min or longer, in order to obtain wet snow with LWC between 10% and 45%. The obtained wet snow was laid in a semi-cylindrical mold (45 cm-long) and compacted evenly. Once the bottom half of the sleeve was formed, two small bars were inserted at both sides of the mold. The aluminium bars were separated with accreted snow on their surfaces after 20 minutes later. The snow mass on each beam was as low as 10 g ±10%. The LWC of the snow in the

mold was measured immediately after the end of the test. The snow in the mold was assumed to obtain the same LWC as the snow samples on the small bars, which were tested in the centrifuge machine.

The snow beams were tested using the centrifuge machine in a cold room, as depicted in Figures 3.4(a,b). The beam was then rotated at increasing speeds resulting in a controlled ramp of the centrifuge force. When this force reached the adhesion force of snow, the snow detached from the sample surface. The exact rotation speed at the time of snow detachment was determined from the computer software developed in-house (Hefny et al., 2009). The shear force was obtained from the angular speed of rotation when the snow detached from the beam as follows:

$$F = m \, r \, \omega^2$$
<div align="right">Equation (3.2)</div>

where F is centrifugal force [N], m is snow mass[kg], r is radius of the bar [m], ω is speed of rotation [rad/s]. Using the centrifugal force, the shear stress is determined as follows:

$$\tau = \frac{F}{A}$$
<div align="right">Equation (3.3)</div>

where τ is the shear stress [N/m^2], A is the snow area [m^2].

<div align="center">(a)   (b)</div>

Figure 3.4: (a) Centrifuge machine, (b) Detailed plan of the centrifuge beam
(Hefny et al., 2009).

3.2.1.4. Shear Test Results

The shear adhesion test results illustrate the relation between shear adhesive strength and snow properties, as well as between shear adhesive strength and surface roughness. More

than 180 tests were conducted in order to obtain reliable results. Standard deviation of average values in each 5% interval for LWC is presented in the strength-LWC graphs, where percentage of error of results is around 1.85 as maximum. Figure 3.5 explains the relation between the shear adhesive strength and LWC. When the LWC augments, shear strength increases as well, reaching its maximum value at 20 to 27% of LWC for all surfaces. For higher values of LWC, the shear strength decreases with LWC. It can be observed that there is a rather scatter in the measurement points. As shown the correlation factor (R) is close to 1, thus these curves can be used as the best fit for approximating the relation between shear strength and LWC, Figure 3.5. It may be concluded that, snow containing a low amount of liquid water has poor adhesion to aluminium beams, where snow slid off the cable surface easily. When free water begins to increase, snow at this stage is wet and adheres more strongly. Then snow starts to be transparent and slushy, wherever at this stage it has low-adhesion strength. Using a moderate value of LWC, the cylindrical snow sleeve develops and can not be broken easily by vibrations. However, with a very high value of LWC, the snow sleeve flows like a viscous fluid and then breaks under gravity effect. The surface roughness has a very significant effect on adhesive shear strength. The greater the roughness is, the higher the adhesion will be(Hefny et al., 2009).

Figure 3.6 shows the proportional relation between LWC and snow density for different surface roughness. It may be observed that snow samples with LWC in the range from 20 to 27% correspond to densities between 0.4 to 0.5 g/cm^3. The shear strength increases with density up to a density value ranging from 0.4 to 0.5 g/cm^3. After that, the shear strength decreases at high values of density. Furthermore, it may be illustrated that the shear adhesive strength of snow is greater on stranded beams than on rough surfaces prepared with sandpaper No. 100 or 50; where these rough surfaces give results very close to each other, as illustrated in Figure 3.5.

Figure 3.5 Relation between LWC and shear adhesive strength for wet snow.

Figure 3.6 Relation between LWC and density for wet snow samples.

3.2.2. The Tensile Adhesion Tests

3.2.2.1. Equipments

The main equipments used in tensile tests are as follows:

a- Surfaces and Plates

Smooth, rough (50) and stranded surfaces were used to study the tensile properties of snow. These square plates were illustrated in Figure 3.7(a, b). A semi-spherical mold with a flattened top (D_{small} = 70mm, D_{big} =165 mm) was used for preparing the tensile samples, as shown in Figure 3.7(c). The snow shape obtained using the semi-spherical plate, could be seen in Figure 3.7(d).

b- Measuring Devices and Data Acquisition System

The material testing system (MTS), as depicted in Figure 3.8(a), was used for conducting material tests (tension and compression), which is equipped with the following:

(a) Hydraulic closed loop to perform a controlled low to high strain rate creep test.

(b) Multi-channel data acquisition system to record the output data.

(c) Confining hydrostatic pressure chamber up to 20 MPa.

(d) Cooling chamber with a temperature as low as -25°C.

Analog to digital conversion was provided by using two drivers, which were installed outside the refrigerated room and connected to a computer, as shown in Figure 3.8(d) (Hefny et al., 2009).

(a)   (b)

(c)   (d)

Figure 3.7: (a) Plates with different roughness surfaces, (b) Stranded surface, (c) Semi-spherical surface mold and (d) Elevation view of MTS and snow sample(Hefny et al., 2009).

(a)   (b)

Figure 3.8: (a) Material testing machine (MTS), (b) Drivers for MTS machine.

3.2.2.2. Tensile Test Procedure

The dry snow was stored at room temperature for at least 30 min until it became wet. The LWC of snow varied between 10% and 45%. In the meantime, the cold room where the MTS machine exists was cooled to a temperature as low as $0 \pm 3°C$. The tensile test procedure is based on the recommendations of Wakahama (Wakahama, 1979). The semi-spherical snow sample was slowly compressed from the top by a plate, moving downward at a constant speed of 1mm/min. The compressive force was increased with time and the motor was stopped at the instance when the force reached 80 N. However, as mentioned by Wakahama, compression was stopped at certain stress equals 16 kN/m^2 (Hefny et al., 2009).

The diameter of the snow contact area with the plate was increased from 70 mm (original) to 75-80 mm during compression; thus, the resultant compressive stress was found to be between 16 and 18 KN/m^2. After compression was stopped, a period of stress relaxation started, whose duration is selected to be 2:20 min; nevertheless, Wakahama suggested that

relaxation is around quarter of the optimum stress. Afterwards, an upward motion of the plate was started at the same speed of 1 mm/min. The force was changed from compression to tensile; at that moment the tensile force increased with time until the plate and the snow sample were separated from each other (Hefny et al., 2009). The tensile force was recorded at snow-plate separation. The tensile adhesive strength S was calculated according to the following equation:

$$S = F_t / A \hspace{4cm} \text{Equation (3.4)}$$

where S is the tensile adhesive strength [N/m^2], F_t is the tensile force [N] and A is the contact area between snow sample and plate [m^2].

3.2.2.3. Tensile Test Results

Similar to shear adhesion tests, average values in each 5% interval of LWC were examined using standard deviation. This standard deviation shows how much variation deviates from the average. Figure 3.9 describes the relation between tensile adhesive strength and LWC. It may be observed that tensile adhesive strength is high compared to shear strength; it is about 10 to 40 times greater depending on the surface roughness (Hefny et al., 2009).

The tensile strength increases with LWC up to a certain range, followed by a decrease with any further increase. The maximum strength is found between 25 and 30% of LWC. This tendency may be explained by the smaller contact area between snow particles and plate surface for middle values of LWC and the higher adhesive force as well, as shown in Figures 3.9,3.11. When the LWC increases, the adhesive force and strength decrease correspondingly. From the point of view of the physical description; the snow grains near the interface are compressed by the initial compression. Once, the snow grains are locally densified, the radius of curvature of the concave water between snow and plate surface becomes small and consequently the strength increases with decreasing curvature (Wakahama and Mizuno, 1977).

However, when snow contains large amount of water, most of air voids are saturated, which decreases the snow strength (Wakahama, 1979). Figure 3.9 stated that tensile strength for smooth surfaces is greater by a factor of about 1.9 than stranded surfaces, but it is close to

rough surfaces prepared with sandpaper No. 50. This result is obtained due to the fact that the snow particles are compressed greatly on the stranded plates. In that case, some snow particles can remain in the plate grooves even after the detachment as shown in Figure 3.10. Thereby, the real contact area between the plate and the detached snow may be reduced significantly because there are some loses through the stranded plate, which results in high tensile strength for the smooth surface. The tensile adhesion force for the smooth surface is higher than the force for the stranded surface since it is easier for the stranded surface to be detached along the plate grooves (Figure 3.10). Adhesion Force is found around 32N average for smooth cable but 8.7N average for stranded surface, as depicted in Figure 3.11. The contact area is assumed constant during the same type of surface roughness; however, it changes by changing surface roughness.It may be observed that the density of snow increases with its LWC. Density values between 0.5 to 0.8 g/cm^3 result in the maximum adhesive force. It may be stated that these density values correspond to LWC ranges between 25 to 30%(Hefny et al., 2009).

Since tensile strength is higher than the shear strength, tensile strength will be determined when shedding occurs. If the load is so high that it exceeds the shear strength, but it is not high enough to exceed the tensile strength, then the tensile adhesion will still keep the snow on the cable. When the load also goes above the tensile strength, then snow sheds. If the load exceeds tensile strength and the snow is still on the cable, then it is the cohesion that keeps the snow sleeve together (but this is not considered in the author's model) (Chapter 4).

Figure 3.9 Relation between LWC and tensile adhesive strength.

Figure 3.10 Snow accumulation on the aluminium plate grooves.

(Case of stranded surface) (Hefny et al., 2009).

Figure 3.11 Relation between LWC and tensile adhesion force.

3.2.2.4. Comparison with the previous tensile strength investigation

Relation between tensile strength and LWC are in a good agreement with those of other investigators (Wakahama, 1979). In the sense that, the tensile strength for both previous and present results increases with LWC until a maximum value, followed by decreasing with higher values of LWC, as illustrated in Figure 3.12. However, the maximum values of tensile strength have been obtained for different LWCs comparing both cases.

Figure 3.12 Relation between LWC and tensile adhesive strength for smooth surface.
(Hefny et al., 2009).

In previous results, the maximum tensile strength was reached at a range from 12 to 16% of LWC, corresponding to LWC range from 25 to 30% for these present experimental results. The reason behind this discrepancy may be that the test procedures are not identical in the two studies. The maximum compression force in the current experimental procedure is chosen to be 80 N, which is greater than the force in the procedure of Wakahama (1979). Furthermore, the sample size in the present study is greater than Wakahama study (Wakahama used sample size of 5.5 cm diameter); although, the compressive stresses in the two studies are approximately the same (Hefny et al., 2009). It is noteworthy that high force was used in order to obtain the same stress using large snow area, which is 7.5cm. Additionally, Wakahama (1979) started the process of pulling up after the compression force decreased to its quarter, while in the present study the application of tension begins at a constant time (2:20min) after the compression is stopped. The time when the compressive load is reduced to its quarter is quite changeable; this is why choosing a constant time is found to be more pertinent considering the loading conditions.

3.3. Dynamic Experiments to Simulate Snow Shedding

3.3.1. Introduction

The experimental results measured on a level single-span reduced scale cable, will be presented in this section and then be validated using the numerical model in Chapter 4. Several icing scenarios were studied that comprised snow cable models with equivalent radial snow thickness of 47 mm. Furthermore, some cases with equivalent radial snow thickness of 23.5 mm were investigated using the same stainless steel cable. A stainless steel cable with a diameter of 4.1 mm was used throughout the analyses. The span length was set to be 4.14 m and the initial sag-to-span ratio ranged from 6.5 to 9% depending on each case. It is supposed that the reduced-scale model may serve to analyze and better understand the problem. It may be stated that the numerical results of the level single-span reduced-scale model are in a good agreement with those obtained experimentally, then the numerical model would be used for simulations of real-scale lines. The reduced-scale model is considered as the only way to validate the experimental study.

3.3.2. Icing Laboratory

The experimental setup was installed at the CIGELE icing precipitation simulation laboratory. This laboratory is held in a refrigerated room, where the air temperature is controlled and may reach -30 °C. In the present experiments, the room temperature was set at 1°C ± 0.2, which is typical of wet snow accumulation on overhead cables.

3.3.3. LWC and Density Measurements

LWC was measured using a Decagon model EC-5 moisture sensor. This sensor was connected to Em5b device, which provided a reading in a voltage (v), based on the dielectric constant of the medium. This voltage was converted into volumetric water content using a calibration curve. The LWC (by mass) was obtained by dividing the volumetric water content by the snow density. The volumetric water content (VWC) was calculated by Eq. (3.1) (Sec. 3.2.1.2). Em5b is a data collection system, which is a reliable way for measuring different readings of LWC and it has five different ports, as depicted in Figure 3.13(b). By fixing the probes inside these ports, the device may save the data, which can be read using the concerned software. In the dynamic test, four probes were used. Each two of them were placed at each end of the snow sleeve and the LWC was obtained by calculating the average of these voltages. The average error in these measurements was evaluated around ± 4%. The

snow density was determined by dividing the snow mass by the volume of a container, where a snow sample was collected.

(a)   (b)

Figure 3.13 Devices for measuring LWC (a) Em5b device, (b) Ec-5 moisture sensor connected to Em5b device.

3.3.4. The Level Single-Span Reduced-Scale Conductor Model

The experimental setup consisted of one fixed support and another movable one, mounting a flexible stainless steel cable (RR-W-410D301/302, 4.14-m long and 4.1-mm diameter). The cable was raised over the ground around 1 m. Its length was defined to provide an initial sag-to-span ratio from 6.5 to 9 % by keeping the span length at 4.14-m. The stainless steel cable was pin-ended to the load cell, as illustrated in Figure 3.14. The periodic impact was provided by a system, which will be explained in next sections. This system had a main-rotated bar connected to a gear box, which in turn, connected to an electric motor. An accelerometer mounted close to the cable suspension-point, was used to measure the acceleration. Two high speed digital cameras were used to capture the cable mid-span displacement and suspension-point displacement respectively. The data acquisition system was also connected to the setup. The snow sleeve length was selected to be around 2m for all the tests (Hefny et al., 2012 a,b).

Figure 3.14 Schematic diagram of the physical setup.

3.3.4.1. Periodic Impact Generator

The periodic impact was applied by using a setup as depicted in Figure 3.15. The setup consists of a Reliance electric Dc motor of variable speeds, with 1725 rpm, 1/2 hp, Figure 3.15(a-A). This motor was connected to a gear box (David Brown gear industries) with ratio 1 to 7.5, Figure 3.15(a-B). The gear box and the motor were fixed on a rectangular plate (Figure 3.15(a-C)) connected by a belt (Figure 3.15(a-D)) and then the gear box was attached to a circular disk (Figure 3.15(a-E)). This circular disk was connected to a bar with two disks (Figure 3.15(a, b, c-F)), where this bar was moving in a circular trajectory. At each cycle, it raised the horizontal bar (H), which was connected to the cable and then let it fall until it reached another bar (G), causing a mechanical impact (Figure 3.15(a, c, H-G)) (Hefny et al., 2012 a,b).

The distance between the disks, Figure 3.15(b-I) and the rotational axis of the bar varied between 15.5 and 18.5 cm. The motor rotated the bar with the two disks which touched alternately another bar, Figure 3.15(a, c-H), connected to the cable. Once the disk was detached from the bar falling on a fixed bar, a periodic movement of the cable suspension point with an impact occurred, Figure 3.15(a, c-G). Depending on the position of the two disks on the bar, as well as on the adjustable speed of the motor, the impact and the whole movement may be varied, Figure 3.15(c). By increasing the frequency of the excitation, the horizontal bar (H) falls more quickly, thereby causing greater acceleration at the moment of impact and resulting in shedding over a longer section of the cable(Hefny et al., 2012 a,b).

3.3.4.2. Measuring Devices and Data Acquisition System

Horizontal component of the stainless steel cable end-tension was measured using universal pancake-load cell manufactured by FUTEK (model: LCF 450), as shown in Figure 3.16. This model used metal foil strain gauge technology (Asch, 1999). The load cell is designed for both tension and compression applications and has a capacity of 2224 N (500 lbf). The bridge excitation for the load cell was provided by a signal conditioner amplifier manufactured also by FUTEK (model: CSG110), Figures 3.17(a, b)(Appendix A).

The periodic impact acceleration was measured by an ICP low-impedance quartz accelerometer manufactured by PCB Piezotronics Inc. (model: W352C04), as shown in Figure 3.18(a,b), where it was mounted almost at the movable cable end. The accelerometer is mounted to a flat aluminium stud fixed to the cable surface. Power to operate the accelerometer is 18 to 30 VDC, 2 to 20 mA constant current supply, which is provided by a signal conditioner. This signal conditioner is manufactured by PCB Piezotronics Inc. (model: 482A212), Figure 3.19 Appendix A) (Hefny et al., 2012 a,b).

The acceleration results obtained by the accelerometer were calibrated to validate their reliability, also to check if the accelerometer works rather well. The system used to calibrate the accelerometer accuracy is illustrated in Appendix A. The acceleration measured by the software is in a good agreement with the theoretical equations for the piston system, which enhances the perfect quality of the accelerometer (Appendix A).

(a)   (b)

(c)

(d)

Figure 3.15 Periodic impact generator (a)Side-view section of periodic impact generator(Hefny et al., 2012 a,b), (b) Principal bar, (c) Elevation of bars, (d) Dc-drive changeable speeds.

Figure 3.16 Load cell%(Hefny et al., 2012 a.b).

(a)

(b)

Figure 3.17: (a) Signal conditioner for load cell, (b) Voltage output of a signal conditioner versus load.

Figure 3.18: (a) Accelerometer, (b) Accelerometer connection to suspension-point.
(Hefny et al., 2012 a,b)

The choice of the mounting method of the accelerometer to the cable depends on the effect the mounting technique on the high frequency performance of the accelerometer. Adhesive mount is selected from six mounting techniques for the current experimental study. This adhesive mount is often used for temporary installation, or when the test object surface cannot be prepared for stud mounting. Direct adhesives like two-part epoxies or quick bonding gels may provide a more permanent installation.

The adhesive mount can be classified into two methods; the adhesive mounting base or the direct adhesive mount. The adhesive mounting base was used in the current study, where it involves attaching a base to the cable structure, then securing the sensor to the base. The importance of this base is that it manufactured of hard coated aluminium, which provides an electrical isolation to eliminate ground loops and reduce electrical interference that may propagate from the surface of the cable, as illustrated in Figure 3.20.

Analog to digital conversion is provided by a USB function module manufactured by Data Translation Inc. (model: DT9804). The module is installed outside of the refrigerated room and connected to a computer through a Universal Serial Bus (USB) port (Kalman, 2007). The five analog input signals are connected to the module using differential configuration (Asch, 1999), Figure 3.21(b). A measurement application is built using commercial software called DT Measure Foundry (DT Measure Foundry, 2005)(Appendix A). Two high speed digital cameras manufactured by Panasonic (model 3CCD/055475) and Sony (model DCRSX63/SC) were used to capture the jump of the suspension-point and the cable mid-point, respectively. The frame rate of a camera is the number of frames recorded

per second. The maximum frame rate of the Panasonic and Sony cameras are of 30 fps (frame rate per second) allowing sufficient seconds of recording time. The videos were extracted from cameras and presented by Media player classic. The cable jump was investigated using MnS-Utility v-1.3 (software used to capture the coordinates of each point in the frame (Hefny et al., 2012 a,b).

Figure 3.19 Signal conditioner for the accelerometer.

Figure 3.20 Adhesive mount installation.

| (a) | (b) |

Figure 3.21 Analog to digital conversion: (a) USB Function Module DT9804, (b) Electrical circuit connections.

3.3.5. Dynamic Test Procedure

A typical test sequence comprises three major steps: (1) Creating wet snow deposit on the suspended stainless steel cable; (2) Applying a periodic impact to the cable by actuating the motor setup; (3) Measuring and recording the characteristics of the periodic impact, the cable end-tension and the cable displacement at mid-span and at the suspension-point.

3.3.5.1. Wet Snow Sleeve Moulding

Fresh dry snow was used to prepare the wet snow in the climate room. The dry snow was collected from the top layer of snow banks outside the campus. The LWC of the snow approached that of precipitating wet snow after being exposed to warm air for a period ranging from 1 to 3 hrs. This method produced wet snow with homogenous LWC based on the recommendations of Sakamoto (2000; 2005) and on the experiments of (Roberge, 2006).

The wet snow was laid in a semi-cylindrical mold and compacted evenly in layers. Once the bottom half of the sleeve was formed below the cable, as depicted in Figure 3.22(a), the top half of the sleeve was then prepared of compacted layers using a semi-cylindrical tool, forming a snow sleeve of 2 m long, Figure 3.22(c). Since, two moulds of different diameters were used; the fabricated snow sleeve had a uniform diameter of 9.8 or 5.1 cm after mold removal. Figure 3.22(a,c) illustrated the steps of preparing snow sleeve(Hefny et al., 2012 a,b).

(a)   (b)   (c)

Figure 3.22: (a) Snow sleeve below the cable, (b) Compacting tool, (c) Complete Snow sleeve inside the mold. (Hefny et al., 2012 a,b)

The acceleration and the cable end-tension were recorded by using the measurement application software. Concerning the cable mid-span and suspension displacement, they were observed by the high speed digital cameras, which were started right before actuating the periodic-impact generator. The periodic impact generator was actuated by the push button

found on its control drive (Figure 3.15(d)). Finally, the results were documented and the entire system was turned off.

3.3.6. Dynamic Test Results

In this section, the characteristics of the measured parameters such as the periodic acceleration, the horizontal component of cable end-tension and the cable mid-span displacement are presented and analyzed. The following graphs serve to interpret the characteristics of measured parameters in some details.

Four parameters were varied during the experiments, namely, (i) LWC with values ranging from 10 to 40%; (ii) sleeve with two outer diameters: 51 mm (small sleeve) and 98 mm (large sleeve); (iii) excitation amplitude with 155, 170 and 185 mm, which called low, middle and high amplitude, respectively, (iv) motor speed at levels ranging from 2 to 8 (*i.e.,* 20% to 80% of the motor base speed; 1725 rpm (Table 3.5)) controlling the period of excitation corresponding to the time between two impacts. It is not worthy that; the excitation amplitude is the distance between the main bar center and small disk, as shown in Figure 3.15(b) (Hefny et al., 2012 a,b). It should be mentioned that there are two pullies connect between the motor and the gear box (Figure3.15a)could transfer the movement (1 inch connected to 3.5inch). This composition means that the input motor speed increases by a ratio of 1 : 1.75, resulting in an increase of the output motor speed (Table 3.5).

3.3.6.1. Suspension-Point Displacement

The movement of the suspension-point (where the accelerometer was fixed) was tracked using the videos. These videos were recorded during the entire tests using the Panasonic camera (Section 3.3.4.2). At the beginning, the videos were run using Media player classic program. Afterwards, by using MnS-Utility software, the movement of the required suspension-point was tracked, which moved in approximately an ellipse-shape. By calculating the coordinates of the point in each frame vertically and horizontally, these coordinates might be converted from pixel to meter, in order to find the final displacement. Figure 3.23 shows the results at the suspension-point for the middle excitation amplitude, where it is around 11 cm peak. This peak increases to around 15.5 cm for high-amplitude excitation; however, it decreases to 5.5 cm peak for low-amplitude. The displacement results are considered as the input to the numerical model, which will be investigated in detail in Chapter 4(Hefny et al., 2012 a,b).

Figure 3.23 Time history of displacement at suspension-point (Hefny et al., 2012 a,b,c,d).

3.3.6.2. Periodic Impact Characteristics

This section shows a typical dynamic acceleration characteristics measured by the ICP accelerometer sensor during a test. Recording of data was started at t = 0 s; however, the periodic impact generator was actuated only after some seconds later. The full spectrum of the acceleration measurement shows a periodic high impact, which is repeated for around 10 cycles. Between each impact and the successive one there are a couple of low oscillations peaks. In the dynamic tests, the periodic impact was applied as an input, where the snow-shedding process, the cable jump at mid-span and the cable tension were investigated.

The presented figures were selected from the results of more than 120 tests carried out to observe and verify the characteristics of the measured parameters. Ranges for the excitation period, for motor speed level 2 are provided in Table 3.1. Table 3.1 shows that the period of excitation increases with increasing LWC and sleeve diameter. Once these parameters increase the weight of snow increases as well, thereby it is more difficult for the setup to raise a cable with a heavy sleeve. Moreover, once a section of the snow sleeve sheds, the load becomes lighter and the period is further decreases. It would be difficult to compare different cases for higher motor speed levels as the rate of shedding affects the results(Hefny et al., 2012 a,b).

Table 3.1 Ranges for period of vibration for different LWCs and sleeve diameter
(Hefny et al., 2012 a,b).

Sleeve diameter	Large sleeve		Small sleeve	
LWC	Low	High	Low	High
Time (s)	1.74-2.9	2.16-3.29	0.98-1.74	1.34-2.37

Many different cases were studied, either by changing sleeve diameter or excitation amplitude, it may be listed as follows:

a. Large Snow Sleeve and Middle-Excitation Amplitude

Snow shedding at low (less than 15%) or high (more than 35%) LWC usually propagated in an unzipping way from the excited end towards the fixed end of the cable, which is followed by partial way (in small sections at distinct locations). Some parts of snow shed at low-motor speed (level 2) in pieces of about 35 cm, then after waiting around 60 cycles with no more shedding, the motor speed was increased to speed level 3 resulting in a complete shedding. The highest acceleration peak is found at range from 200 to 300 m/s^2, Figure 3.24(a), at level-2 motor speed, in addition, from 300 to 400 m/s^2 at level-3 motor speed, Figure 3.24(b). The time between two impacts decreases from 2.9 s to 1.2 s. As snow shed, the acceleration and tension change even at the same motor speed level because the cable becomes unloaded. The acceleration peak at shedding is around 380 m/s^2; however, after shedding, it decreases to about 200 m/s^2 at level-3 motor speed, Figure 3.24(b). The circle in the figures refers to which impact shedding happened at, but the arrow demonstrates the decrease of acceleration after shedding, as illustrated in Figure 3.24(a, b) (Hefny et al., 2012 a,b).

(a)

(b)

Figure 3.24 Time history of acceleration: (a) Low LWC – motor speed level-2, (b) Low LWC – motor speed level-3 (Large sleeve, middle amplitude). (Hefny et al., 2012 a,b)

The results are divided into different ranges of LWC, since different values of LWC give identical behavior for around 30 test in each LWC range. For the next sections the figures will be traced for a single LWC only, because it may represent the whole range of LWC. For LWC ranged between 15 to 20%, it may be observed that snow persists more time on the cable than the former case, as it can not shed easily at speeds 2 or 3. Some snow sections could stay until higher-motor speed like motor speed level-4, then they shed partially; however, at motor speed level 2 or 3 they shed by unzipping way. The acceleration peak at motor speed level-4 at shedding is 458 m/s^2. Snow blocks slid on the cable towards each other with no shedding indicating that cohesion still keeps snow particles together even if adhesion between the snow and the cable has vanished. Results for low LWC and middle LWC values show that shedding does not necessarily happen at first or second impact, since there is no exact time of shedding. There is a transverse wave caused by the periodic impact at the suspension-point, this wave moves along the cable, once the adhesion is as low as it can not resist the wave effect, snow chunks may shed (cf. Figs 3.24, 3.25) (Hefny et al., 2012 a,b).

Comparing time history of acceleration for motor speed level-2 for LWC 10% and 19% (cf.Figs 3.24(a), 3.25(a)) demonstrates that increasing LWC of wet snow augments the load that causes snow shedding. Generally, when the acceleration peak is lower than the critical value for any LWC, thus there is no shedding at that moment.

On the other hand, snow is most resistant when LWC is in the range of 20 to 30% (the highest snow adhesion). There is no shedding at the low motor-speed level although there are several cracks, as depicted in Figure 3.26. Afterwards, increasing motor speed to level-3 and 4 causes the snow to shed in a mixed way from the excitation side. Snow sections slid toward mid-span with no additional shedding, once motor speed increases to level-5, the remaining sections tend to shed suddenly. At that time, the acceleration peak at shedding is around 540 m/s^2.

(a)

(b)

(c)

Figure 3.25 Time history of acceleration: (a) LWC 19%– motor speed level-2, (b) LWC 19%– motor speed level-3, (c) LWC 19%– motor speed level-4 (Large sleeve, middle amplitude).

Figure 3.26 indicates that the acceleration peak at snow shedding increases with increasing LWC in the range from 20 to 30% (23% as an example), which reflects the increase of snow adherence to the cable. For LWC ranging from 10% to 15% snow shed at level-3 motor speed, with acceleration peak of 360 m/s² at shedding. While, for LWC between 15% and 20%, snow sleeve persists until speed level-4 is reached, as the average acceleration peak at shedding is 458 m/s². For LWC between 20% and 30%, snow stays until level speed-5 providing an acceleration peak of about 540 m/s² at shedding. Further increase in LWC weakens snow adhesion, as once LWC reaches 35%, snow shed for motor speed as low as level-3. Snow shed after the application of the severe excitation at LWC ranging from 20 to 30%, at which the highest adhesion strength is measured (Hefny *et al.*, 2009). Figure 3.27 shows the relation between LWC (horizontal axis) versus motor speed level and acceleration (vertical axis) at full shedding. The graph is a summary of what stated previously, as by increasing LWC snow persists on the cable up to motor speed level-5.

Furthermore, the acceleration increases with LWC up to range from 20 to 30%, followed by a decrease later on(Hefny et al., 2012 a,b).

Figure 3.26 Relation of acceleration peak versus motor speed level at different LWC values (Large sleeve, middle amplitude)(Hefny et al., 2012 a,b).

Figure 3.27 Relation between motor speed level, LWC and acceleration

(Large sleeve, middle amplitude). Acceleration values at full shedding

b. Large Snow Sleeve and Low-Excitation Amplitude

Snow stays long time on the cable at low-excitation amplitude (15.5 cm from bar's center) because the small amplitude causes low impact. Even at low or high LWC, snow persists on the cable until motor speed level-8. During the experimental tests, for the case of LWC ranged around 29%, the entire snow sleeve stays rigidly on the cable at motor speed levels 2 and 3. Then the major part of the sleeve shed by unzipping way at speed level-5. After further increase of the motor speed up to level-6, there is no shedding but snow blocks slide toward mid-span. Later, the rest of the sleeve shed at speed level-8 followed by a drop in the acceleration peak, as illustrated in Figure 3.28. For low excitation amplitude, the setup required low energy to raise the suspension-point, resulted in low acceleration. It may be stated that the acceleration peak increased by increasing the motor speed-level. Shedding happens at 380 m/s^2, which is assigned to speed level-8. It can be concluded that the impact at speed level-8 using low amplitude corresponds to the impact at speed level-3 for low LWC-middle amplitude (cf.Figs. 3.26, 3.29) (Hefny et al., 2012 a,b).

Figure 3.28 Time history of acceleration- LWC 32%-motor speed level-8

(Large sleeve, low amplitude).

c. Large snow sleeve and high excitation amplitude

When the excitation amplitude is high, snow sheds rapidly even for snow in the middle range of LWC. Some sections of 35 cm-length shed at speed level-2, but the rest shed at speed level-3. If level-4 motor speed is applied from the beginning of the test, wet snow may shed immediately. Acceleration peak at shedding is 350 m/s^2. A similar shedding scenario (continues up to motor speed level-3) happens at high LWC values (Figure 3.30), but with faster shedding at speed level-3 compared to the case aforementioned. Table 3.2 shows the relation between different excitation amplitudes and corresponding acceleration peaks for different LWC including cases (a, b and c) (Hefny et al., 2012 a,b).

Figure 3.29 Acceleration versus motor speed level for high LWC

(Large sleeve, low amplitude).

Figure 3.30 Relation between acceleration versus motor speed level
(Large sleeve, high amplitude) (Hefny et al., 2012 a,b).

Table 3.2 Relation between excitation amplitude and acceleration at shedding for different
LWC (Sleeve 98 mm).

Excitation amplitude (mm)	170			185		155
LWC (%)	10	19	23	24	35	32
Acceleration (m/s^2)	360	458	540	355	350	380

d. Small Snow Sleeve and Middle-Excitation Amplitude

Changing the snow diameter does not affect the snow shedding sequence. However, it influences significantly the acceleration amplitude and the time between two acceleration peaks. The acceleration peak values are lower for a small sleeve than for a large one, due to the fact that the small sleeve has a small weight, which moves easily. Changing the sleeve decreases the acceleration peak by 50% for speed level-2 (cf.Figs. 3.26, 3.33), but it decreases to a lower extent for level speed-3 (cf.Figs. 3.24(b), 3.32(b)). Snow persists for low LWC up to level-3 speed; however, for middle LWC it remains on the cable up to level-4 speed, where the acceleration peak at shedding is around 310 m/s^2. It should be mentioned that the cable

(a)

(b)

(b)

(c)

Figure 3.31 Time history of acceleration: (a) LWC 25% – motor speed level-2, (b) LWC 25% – motor speed level-3 and (c) LWC 25% – motor speed level-4 (Small sleeve, middle amplitude).

(a)

(b)

Figure 3.32 Time history of acceleration: (a) LWC 37% – motor speed level-2, (b) LWC 37%
– motor speed level-3 (Small sleeve, middle amplitude).

Figure 3.33 Acceleration versus motor speed level at different LWC values

(Small sleeve, middle amplitude) (Hefny et al., 2012 a,b).

e. Small Snow Sleeve and Low-Excitation Amplitude

In case of small snow sleeve, the shedding process is similar to that of a large sleeve and low-excitation amplitude, as depicted in Figure 3.34. However, lower acceleration peaks and lower tensions are obtained and the period of vibration is increased because snow load is small, *i.e.*, it is easier for the system to raise the sleeve efficiently in longer period of time. The acceleration peak at shedding is 300 m/s^2 at motor speed level-8 comparing to 380 m/s^2 for the large sleeve case (cf.Figs. 3.29 and 3.34).

f. Small Snow Sleeve and High-Excitation Amplitude

It is remarkable that for high and low LWC values, snow shed rapidly at low motor speed level. Whereas for high adhesion (middle range of LWC) snow may stay more above the cable, up to speed level-4. Sliding action becomes visible at speed levels-2 and-3, which enhances that adhesion can vanish early, while cohesion between snow particles is still high (even for the small sleeve and high LWC s). Acceleration peak at shedding is 340 m/s^2. Table

3.3 presents the relation between different excitation amplitudes and corresponding acceleration peaks at full shedding for different LWC including cases (d, e and f), as depicted in Figures 3.34 and 3.35(Hefny et al., 2012 a,b).

Figure 3.34 Relation of acceleration versus motor speed level
(Small sleeve, Low amplitude).

Figure 3.35 Relation of acceleration versus motor speed level
(Small sleeve, high amplitude).

Table 3.3 Relation between excitation amplitude and acceleration for different LWC

(Sleeve 51 mm). Acceleration at full shedding

Excitation amplitude (mm)	170		185	155
LWC (%)	25	37	35	32
Acceleration(m/s²)	310	255	380	300

3.3.6.3. Time History of Cable End-Tension

Horizontal component of the dynamic cable end tension depicted in Figure 3.36 was measured using the load cell as described in Section 3.3.4.2. The vertical component of cable end tension is small comparing to the horizontal, thereby it may be neglected. It can be observed that the tension slightly increases with increasing motor speed-level, but it decreases after snow shedding because of the load removal. The cable tension in the bare cable is 218.5 N, which increases to 250 N after adding the snow load. The LWC increase has no considerable effect on cable tension.

Figure 3.36 Time history of tension - motor speed level-3.

3.3.6.4. Mid-Span Jump and Rate of Shedding

The vertical mid-span displacement of the cable, which is a response to the periodic impact, was captured by the high speed digital camera mentioned in Section 3.3.4.2, as depicted in Tables 3.4-3.9.

Tables 3.4-3.6 show the rate of shedding and the corresponding cable jump for different excitation amplitude using large sleeve. Table 3.4 indicated that when rate of shedding increases, cable jump increases as well.

Table 3.4 Rate of shedding and cable jump for middle amplitude (Large sleeve).

Displacement peak at suspension- point is 11 cm.

LWC	10%		19%			23%			
Motor speed level	2	3	2	3	4	2	3	4	5
Shedding rate (%)	35	100	26	74.5	100	0	40	80	100
Cable jump mid-span (cm)	7	45	5	12	45	0	16	29.3	39

Figure 3.37 illustrates the sequence of shedding with time for middle LWC and middle amplitude. In addition the figure reveals that the snow shedding increases by increasing time. The numbers of impacts are also indicated for each case and at which motor speed level. The shedding parts are small for the small sleeve, i.e., they are 15 cm long compared with 35 cm for the large snow sleeve (Figures 3.37, 3.38).

(a) t= 00:00 min (0 impact)
Complete sleeve-Motor speed level 2

(b) t= 4:24 min (70 impact)
Unzipping shedding-Motor speed level 3

(c) t= 8:12 min (236 impact)
Partial shedding- Motor speed level 3

(d) t= 8:27 min (257 impact)
Partial shedding- Motor speed level 4

(e) t= 8:50 min (289 impact)
Partial shedding- Motor speed level 4

(f) t= 10:12 min(376 impact)
Sliding action- Motor speed level 4

(g) t= 10:31 min(381 impact)   (h) t= 10:43 min (402 impact)

Sliding action- Motor speed level 5   Complete shedding- Motor speed level 5

Figure 3.37 Sequence of snow-shedding process for middle LWC-middle amplitude-Large sleeve.

Table 3.5 Rate of shedding and cable jump for low amplitude (Large sleeve).

Displacement peak at suspension-point is 5.5 cm.

LWC (%)	32%						
Motor speed(rpm)	604	906	1208	1510	1725	2114	2415
Motor speed level	2	3	4	5	6	7	8
Shedding rate (%)	0	0	9.5	45.5	48	87	100
Cable Jump mid-span (cm)	0	0	4	20	23	39	45.5

Table 3.6 Rate of shedding and cable jump for high amplitude (Large sleeve).

Displacement peak at suspension- point is 15.5 cm.

LWC(%)	35%		24%		
Motor speed level	2	3	2	3	4
Shedding rate (%)	83.8	100	77.3	100	100
Cable jump mid-span (cm)	45.5	55.3	26	35.8	55

Tables 3.7 to 3.9 present the rate of shedding and cable jump for small sleeve. It can be illustrated clearly that LWC has no considerable effect on the cable jump for small sleeve. In addition, comparing the mid-span jump for small sleeve reveals that it is around 35% of cable jump for large sleeve. The reason behind that result is the small snow load for small

sleeve, in which it results in small sag and low tension. Figure 3.8 demonstrates the sequence of shedding for small sleeve with low amplitude.

Table 3.7 Rate of shedding and cable jump for middle amplitude (Small sleeve).

Displacement peak at suspension- point is 11 cm.

LWC (%)	25%			37%		
Motor speed level	2	3	4	2	3	4
Shedding rate (%)	35.8	87	100	29.5	92.7	100
Cable jump (cm)	5	9	16	4	13	14.6

(a) t= 00:00 s (0 impact)
Complete sleeve- Motor speed level 2

(b) t= 7:55 s (418 impact)
Unzipping shedding- Motor speed level 3

(c) t= 11:06 s (600 impact)
Unzipping shedding- Motor speed level 4

(d) t = 12:33 s (640 impact)
Partial shedding- Motor speed level 5

(e) t= 13:12 s (791 impact)
Partial shedding- Motor speed level 6

(f) t= 13:48 s (907 impact)
Partial shedding- Motor speed level 7

(g) t= 14:43 s (1029 impact)
Partial shedding- Motor speed level 8

(h) t= 15:46 s (1122 impact)
Complete shedding- Motor speed level 8

Figure 3.38 Sequence of snow shedding for middle LWC- low amplitude- and small sleeve.

Table 3.8 Rate of shedding and cable jump for low amplitude (Small sleeve).

Displacement peak at excitation point is 5.5 cm.

LWC (%)	29%						
Motor speed level	2	3	4	5	6	7	8
Shedding rate (%)	0	9.8	22.8	48.8	70.8	93.5	100
Cable jump (cm)	0	2	8	9.5	13	16	19.5

Table 3.9 Rate of shedding and cable jump for high amplitude (small sleeve).

Displacement peak at suspension-point is 15.5 cm.

LWC (%)	35%	
Motor speed level	2	3
Shedding rate (%)	80	100
Cable jump(cm)	9.5	11

3.4. Conclusion

3.4.1. Shear and Tensile Tests conclusions

Shear and tensile adhesion of snow to cable surfaces were studied experimentally. The adhesive strength was determined as a function of snow characteristics; particularly liquid water content, density and roughness of cable surface. The following conclusions can be drawn from the obtained results:

1. The shear strength increases as the LWC increases, reaching its maximum at 20 to 25% of LWC followed by decreasing at high values of LWC. The shear strength also increases as density augments up to density values ranging between 0.4 to 0.5 g/cm^3; after that the shear strength decreases at high values of density.

2. The tensile strength increases with LWC until a maximum limit occurring between 25% and 30% and then it decreases. The tensile strength on a smooth surface is about 1.9 times greater than that on a stranded surface and close to that on a rough surface. The tensile strength as well increases as density enlarges up to density values ranging between 0.5 to 0.8 g/cm^3, after that the tensile strength decreases at high values of density.

3. Tensile adhesive strength is about 10-40 times greater than shear strength, depending on surface roughness.

4. The greater the roughness is, the greater is the shear adhesion; however, the opposite is observed for tensile adhesion.

3.4.2. Dynamic Tests conclusions

Small scale experiments were performed to simulate snow shedding due to a periodic-load including an impact in each period. The following conclusions may be drawn from the obtained results:

5. Snow shedding happens in an unzipping way from the excited end toward the fixed end for low excitation frequencies, low motor speed levels or small impacts. However, it sheds partially or by mixed shedding at high frequencies. This sequence is generally the same for a large sleeve (D= 98 mm) and a small one (D= 51mm). Nevertheless, the size of the

shedding sections is different, in which found to be around 35 cm and 15 cm for large and small sleeve, respectively.

6. For middle values of LWC and for middle-excitation amplitude, snow sheds at high excitation frequencies. For low/ high LWC snow stays less time above the cable, for the case of middle-amplitude, compared with using low-excitation amplitude. Snow sheds easily for higher amplitude or higher excitation frequency because there is a greater impact in those cases and the resulting force exceeds the adhesion force.

7. At high-excitation amplitude, snow sheds easily with a very fast sequence, whereas at low amplitudes snow persists on the cable for a long time.

8. Changing snow sleeve diameter does not affect the sequence of snow shedding, but it rather changes the rate of shedding at each motor-speed level. Furthermore, the acceleration peaks decreases for the case of small sleeve.

9. Cohesion force within the snow is greater than its adhesion to the cable. At high-excitation frequencies, while snow shed partially snow sections are being observed sliding toward mid-span. It may be concluded that, adhesion can be vanished although cohesion maintains high.

CHAPTER 4

NUMERICAL MODELING AND VALIDATION

CHAPTER 4

NUMERICAL MODELING AND VALIDATION

4.1. Introduction

Wet snow shedding, as a result of wind loads, unequal sags, or any other external effect, poses a major inconvenience or even a significant danger. The dynamic effects induced by a periodic-type excitation on snow shedding were investigated herein in detail. In this chapter, the numerical results measured on the level single-span reduced scale model are compared to those obtained experimentally (Chapter 3). Several snow shedding scenarios are studied that comprise snow-cable models with 51 and 98 mm of snow diameter. A stainless steel cable with a diameter of 4.1 mm is used throughout the analyses. The span length is set to 4.14 m and the initial sag-to-span ratio is varied for different sleeve diameter. A numerical model using ADINA was developed to simulate snow shedding from cables due to dynamic effects. This chapter gives a detailed validation study of a numerical model by comparing it with the small-scale experiments, depending on the tensile adhesion criteria mentioned in experimental chapter.

4.2 Numerical model approach

4.2.1. Cable Modeling

The cable is assumed to be perfectly flexible in bending and torsion; hence it can be represented by 2-D two-node isoperimetric truss elements using the total Lagrangian formulation with large displacement kinematics and small strains (Bathe, 1996). The cable material is linear elastic tension-only; as a result it may allow slackening when the cable loses its pre-stressing force. The initial strain of the truss elements is specified from a preliminary static analysis by assuming a catenary profile under its self-weight, where the cable in-plane coordinates are calculated using MATLAB (Appendix C). Concentrated loads are added to that catenary model in order to simulate the snow load. In the model scenarios presented here, the initial sag-to-span ratio is chosen to be 6 to 9% according to snow sleeve diameter. The stress strain curve of a taut cable was preferentially chosen (Figure 4.1) for its reliable results comparing to the stress strain curve for flexible cable. The stress strain curve of sagged cable

is demonstrated in Appendix B. Figure 4.1 demonstrates a linear correlation between stress and strain providing a Young's modulus as high as 1.72 E11 N/m^2 (Hefny et al., 2013).

The two ends of the cable are considered as fixed end-points during the static analysis, but the vertical displacement of the left support is prescribed during the dynamic analysis which matches with the excitation. The nodes along the cable are assumed as free moving in the vertical plane in both static and dynamic analyses, as depicted in Figure 4.2.

Figure 4.1 Cable Stress-Strain relation in uniaxial test(Appendix B).

Z

Y

4.14 m

C
n_1

A
n_{415}

B
B
B
n_{207}
B
B
B
B

Master degrees-of-freedom

Y-translation (U_2)
Z-translation (U_3)
X-rotation (θ_1)

Boundary conditions

	U_2	U_3	θ_1
A	-	-	-
B	√	√	-
C	-	√	-

Figure 4.2 Boundary conditions for cable points.

4.2.2. Cable Damping

The aerodynamic damping, which arises from the motion of the cable relative to the air, is neglected. Internal damping, which is considered in the numerical study, defined as a combination of damping within the individual cable strands and sliding friction between the strands themselves. Numerical damping is used to filter out spurious high frequencies in the response due to finite element discretization. Damping is simulated for shield wires by using a viscous discrete dashpot applied in parallel to each cable element (in the axial direction of each element). To model damping properties of cables in such a way in ADINA, so-called "non-linear spring elements" are required for dashpots to be aligned with the cable element axis (Figure 4.3) (Hefny et al., 2013).

The damping constant is determined from the critical axial viscous damping of a Hookean rod given in Equation 4.1 (Lapointe, 2003), where C is the damping constant, ξ is the damping ratio, AE is the axial rigidity of the rod in N and m is snow mass per unit length in kg/m. In the present study, the damping constant is set to represent equivalent viscous damping ratio of 5% critical (Appendix B) for snow-composite cables. However, the damping ratio found for ice-cable composite studies was around 2% (Yu, 1952).

$$C = 2 \cdot \left(\xi \sqrt{AEm} \right)$$

Equation (4.1)

Spring element

i ⊓⊔ i+1

Cable element
i   i+1

Stiffness element (Adhesion)   **Stiffness element (Adhesion)**

j ◯   ◯ j+1

Mass element (Snow)   **Mass element (Snow)**

Figure 4.3 Spring stiffness and mass elements.

4.2.3. Accreted Snow Modeling

The snow sleeve length was around 2 m for the small scale cable (corresponding to the worst case of EDF snow load, which is around 4kg/m). The adhesive force is simulated in the finite element model using lumped elements (spring elements), whose stiffness is expressed by the spring adhesive force. The snow mass is simulated using spring point loads, *i.e.,* spring elements with mass only, as shown in Figures 4.3 and 4.4. The critical adhesive force, which used in the model was obtained from the experimental study (Figure 3.11). It should be stated that by using laboratory investigations, snow deposits can remain attached to the cable after the adhesion force diminishes as long as the cohesion force maintain the snow sleeve on the cable. However, this phenomenon is not considered and out of scope of this study (Hefny et al., 2013)..

Another approach was investigated concerning the simulation of wet snow, from the point of view of material properties failure criteria. Studies aforementioned in Chapter 2 depend on either stress or strain failure criteria (Chapter2). In the case of the static analysis, it is reasonable to use a plastic bilinear material for simulating wet snow, as snow includes the properties of elasticity and viscosity. The appropriate elements used for the static analysis are the shell four-node element, 2D solid element and the iso-beam two-node element. However, unfortunately this model provided less favourable results for the dynamic analysis. It is

noteworthy, that the reason behind this result is the failure adhesive criteria and its correlation to material properties. It needs further investigation in this research area.

Movable end (vl direction)

Fixed end

Stiffness spring element

Mass spring element

Figure 4.4 Simulation of adhesive force and snow using vertical and point load springs (Hefny et al., 2012 c,d, 2013).

4.2.4. Snow Failure Modeling

In this study, a comprehensive analysis was performed to observe the possibility of including a failure criterion for adhesion in the finite element model, to attain the following condition:

Snow mass × Acceleration of the corresponding element ≥ Critical adhesive force

Once the failure criterion is fulfilled at any integration point, the element simulating the corresponding snow chunk is assumed to be fully detached from the snow/cable interface.

Critical adhesion force is the maximum force defined by the force-displacement relationship, as seen in Figure 4.5. The spring stiffness is determined for adhesion in such a way that it increases linearly with displacement increase in both tension and compression. When it reaches the critical tensile adhesion limit for a small displacement, i.e., high stiffness, the stiffness of the corresponding element is reduced to zero, as illustrated in Figure 4.5. The detachment occurs in the tensile area since snow has higher compressive strength than tensile one (Keeler, 1968). For zero stiffness, i.e., zero adhesive force, the snow element is considered as dead, which simulates the snow when detached from the cable. The density, area and length of snow used are 600 kg/m^3, 0.00753 m^2 and 2 m, respectively. Since the

snow sleeve is modeled by 201 springs, the resultant mass for each spring is around 0.045 kg in order to obtain 9.036 kg as total (Appendix B) (Hefny et al., 2013).

Figure 4.5 Relation of force versus displacement for snow (ADINA input)
(Hefny et al., 2012c,d, 2013).

Snow failure or detachment is modeled using the adhesive force critical limit. Once the periodic load is applied to the cable at the movable end, a transverse wave moves along the cable and consequently, the nodes along the cable oscillate by the effect of this periodic-load. As soon as, the acceleration of a snow element reached the critical value, or in other words, once the force at any snow element exceeded the tensile adhesion force limit, the snow element underwent stepwise detachment.

4.2.5. Initial Static Equilibrium

In order to avoid the stiffening effect of the flexural rigidity of the snow element on the initial static profile, the deformed cable profile is calculated beforehand using concentrated loads to simulate snow load. The deflected static profile serves as the initial profile for the static snow-cable composite model, where the cable element is initially pre-

stressed by setting the initial strain to the value obtained from the catenary analysis (Appendix B).

4.2.6. Dynamic Analysis

Static analysis was completed in one load increment, thus dynamic implicit analysis is usually started at time t = 1 s. The load actuates at the suspension-point, where the displacement of the node is prescribed in the vertical direction, whereas, the horizontal movement is neglected. In order to investigate the effects of periodic-load characteristics on the dynamic response, the load is defined by different periodic functions. The time step and the mesh size are chosen so as to provide adequate sampling of the wave when it travels through the cable finite element mesh. There are two time functions, where the first time function "one" simulates the static analysis completing in 1s. Then, there is time function "two" which simulates the periodic load starting from 1s depending on the periodic functions for each case study (Figure 4.6).

Figure 4.6 Time functions for different analyses.

4.2.7. Numerical Considerations

Newmark integration method was frequently used in previous studies (Roberge, 2006; Kalman, 2007) demonstrating consistent results. It was found that Newmark integration method is not a suitable choice for this study due to the periodic-load excitation type and the small time step. Hence, the Bathe composite integration method (with parameter 0.5) is preferred because there are no numerical problems in the calculation resulting reliable results. For the calculation of all element matrices and vectors, Gauss integration is selected like previous studies. The convergence criterion is based on the energy tolerance; ETOL and displacement tolerance; DTOL, with ETOL $= 10^{-7}$ and DTOL $= 10^{-5}$. A lumped mass formulation is used throughout (Bathe, 1997). In the experimental setup, the cable and the centers of the attachment points at the end of the span were both aligned, consequently, the cable was in the same plane along its entire length. Furthermore, the periodic-load setup at the suspension point is aligned in the cable plane. Therefore, the numerical model can be well represented in the 2-D plane.

4.2.8. Modeling Limitations

4.2.8.1 Towers and Their Foundations

The response of a line section to periodic-load-induced snow shedding depends mainly on the interaction between transmission line components. In the present study, a simple 2-D level single-span numerical model is defined in the vertical plane w   ion structure nor the towers are considered. Therefore, the flexibility of the towers and their foundations is not modeled and the cable ends are assumed to be rigidly fixed. It was stated by Lapointe (2003) that the time of the response obtained by the 3-D models was notably delayed in comparison to the 2-D models. However, the 2-D models tended to overestimate the tensions in the conductors at the supports adjacent to the broken span compared to the more realistic detailed 3-D models of the suspension towers(Hefny et al., 2013)..

4.2.8.2. Damping

Many researches that are conducted on the damping of transmission line conductors are related to the study of wind-induced vibrations (Appendix B). It is evident that the aerodynamic damping plays an important role in the dynamic behavior of the cables (Loredo-Souza and Davenport, 1998; Momomura, 1997). However, the influence of aerodynamic damping on the transient response of a line section still needs to be quantified (McClure and Lapointe, 2003). Damping mostly affects the free vibration behavior of the cable by returning

to rest. Nevertheless, introduction of damping in the model is beneficial to filter out spurious high frequencies of the response generated by the finite element discretization.

4.2.9. Eigen-Value Analysis

It is essential to conduct eigen-value analysis on the line section prior to transient dynamic analysis since unrealistic natural frequencies or mode shapes are trouble-shooters. Therefore, several natural frequencies and mode shapes analyses were examined on cable span model to validate and adjust the parameters of the mesh. The frequency analysis is adjusted for the bare cable model only because the snow-covered cable has a large inertia, as well as it has different natural frequencies compared to the bare cable. Moreover, the snow-covered cable model using the spring elements does not have an exact catenary shape. The natural frequencies and mode shapes of the cable are examined using the model and compared to the analytical solution (Irvine, 1981), as shown in Table 4.1. Concerning the theoretical investigation, the asymmetric modes are calculated using a specified equation; however, the symmetric modes are solved numerically using Newton-Raphson method (Appendix C). The results demonstrated in Table 4.1; show that the model is compatible with the Irvine's theory with a maximum error of 4.3%. Asymmetric modes yield similar number of peaks and dips; however, the investigation of symmetric modes reveals that the number of peaks is higher than dips' number by one, as illustrated in Figure 4.7.

Table 4.1 Comparison between Irvine's theory and numerical model.

Mode	ADINA	Irvine's Theory (1981)
1st asymmetric	27.2	28.41
1st symmetric	38.7	39.5
2nd asymmetric	54.4	56.82
2nd symmetric	66.6	68.3
3rd asymmetric	81.6	85.23

(a) 1st asymmetric mode shape   (b) 1st symmetric mode shape

(c) 2nd asymmetric mode shape

(d) 2nd symmetric mode shape

(e) 3rd asymmetric mode shape

Figure 4.7 First five mode shapes for a small-scale bare cable.

4.3. Sensitivity Studies of the Small-Scale Numerical Model

4.3.1. Model Sensitivity to Finite Element Mesh Size

In order to study the sensitivity of the small-scale numerical model, a number of parametric studies were performed investigating different mesh size and also different damping ratio. The 415-element mesh which simulates a fine mesh is used to capture the successive snow-shedding process of snow chunks. Other coarser meshes (47 and 20 elements) than 415-element are also studied in this section to find out the reliable mesh size. The element size is about 0.009, 0.088 and 0.207 m for 415, 47 and 20-element mesh, respectively. When the number of elements increases, the convergence increases as well. It should be mentioned that the 200 or 300-element meshes gave identical results compared with the 415-element, consequently the 415-element mesh was selected, since it has smaller element size resulting accurate cable response.

The results of bare cable modeling revealed that the use of the 20-element yields to distorted time history graphs. The 415-element mesh demonstrates the better capabilities compared with the 20-element. Nevertheless, the high acceleration peaks are obtained for snow-cable composite model for the case of 415-element mesh, wherever there is a high rate

of shedding (cf. Figs.4.8, 4.11). At the mid-point, the cable jump for the bare cable using 415-element mesh is observed to be lower than the 47-element mesh. On the other hand, 415-element mesh for the snow-cable composite results in a high jump, presenting improved time history graphs, whereas the 20-element model underestimates the cable jump (cf. Figs.4.9, 4.11). The 415-element mesh for the snow-cable composite model demonstrates tension peaks lower than other meshes because of high rate of shedding.

It is evident that the cable jump increases and also the cable tension by comparing both bare and snow-cable composite cases. Cable jump is around 11 cm for bare cable versus 27 cm for the case of snow-cable composite model. Furthermore, cable tension has a value of around 650 N for bare cable, whereas it gives 1100 N for snow-cable composite model (cf. Figs. 4.9, 4.11 and cf. Figs. 4.10, 4.12). Comparing the two previous cases eventually for bare and snow-cable composite model reveals that the 415-element gives the accurate mesh. It is adequately refined to capture the dynamic response of the cable. Thus, the 415-element mesh is selected to be used for all next simulations.

Figure 4.8 Acceleration time history for different meshes at the suspension-point.

(Bare cable mesh study)

The initiation of the first peak of cable amplitude at the mid-span calculated by the numerical model is advanced in time compared to that obtained experimentally for the bare cable. However, for the case of snow-composite cable the inverse occurs. The 415-element mesh demonstrates the closest peaks to the experimental results (Figures 4.9, 4.11).

Figure 4.9 Cable jump time history for different meshes at the mid-point.
(Bare cable mesh study)

Figure 4.10 Tension time history for different meshes at the fixed end-point.
(Bare cable mesh study)

Figure 4.11 Cable jump time history for different meshes at the mid-point. (Snow- composite mesh

Figure 4.12 Tension time history for different meshes at the fixed end-point.
(Snow-cable composite mesh study)

4.3.2. Model Sensitivity to Damping

The dynamic response of a bare cable subjected to a periodic-load was examined using different damping ratios of 1%, 2% and 5%. The response obtained with the parallel dashpot spring elements (with 1%-damping or 2%-damping) has been superimposed over the 5%-damping and also Rayleigh damping (Figure 4.13). It may be concluded that 5%-damping gives the closest results to the experimental investigations, thus it can be considered as the reliable choice. The Rayleigh modeling technique does not appear to work well in this study, since the rate of shedding is not considerable comparing with previous researchers (Roberge, 2006). Rayleigh damping which used with the current model, are shown in Figure 4.13. Figure 4.14 shows how the acceleration peaks for 1%-damping are higher than the 5%-damping in which the acceleration for 1%-damping goes up to 350 m/s^2, whereas for 5%-damping, it does not exceed 200 m/s^2. Using Rayleigh damping results in less shedding compared to spring damping as indicated in Table 4.2.

Figure 4.13 Cable jump time history comparison for different damping at mid-point.

Figure 4.14 Acceleration time history for 1% and 5% damping at the mid-point.

Table 4.2 Rate of shedding for spring and Rayleigh damping

Damping type	Period of excitation(s)			
	1.039	0.9072	0.7812	0.6741
Spring damping (5%)	5.9%	35.8%	86%	100%
Rayleigh damping	0%	25%	72%	92%
Experiments	0%	40%	80%	100%

4.3.3. Sensitivity Conclusion

Sensitivity studies of the small-scale numerical model reveal that the more consistent results of the cable response including acceleration, cable jump and cable tension are obtained with the 415-element mesh model. The 415-element numerical model is used in the remaining analyses of snow-covered cables. In addition, the reliable results, which are close to experimental study are found by using 5%-damping. It is evident that 1%-damping gives high response and more severe shedding. On the other hand, Rayleigh damping provides lower unexpected rate of shedding than spring damping.

4.4 Comparison between Numerical and Experimental Results

4.4.1. Overview

There are many hypotheses are taken/not taken into consideration during the modeling analysis. According to the previous explanation, it may be concluded herein. The displacement time history is selected as an input to the numerical model, also the periodic load is affected at the excitation point. The cable damping provides a ratio of 5%, besides, Bathe composite analysis is selected for its reliable results. Further, the left end-point is prescribed to move in the vertical direction only. The consistent mesh of 415-element mesh is working better; as well the initial static strain is calculated from preliminary static analysis. It should be mentioned that a simplifying assumption of the cable axial rigidity is utilized. On the other hand, the cohesion forces may not be considered during the modeling analysis, the flexibility of the end-point as well. Moreover, the aerodynamic damping is neglected.

The periodic load generates a transverse wave (afore-mentioned) in the ground wire that propagates along the span. This transverse wave propagation causes significant bending of the snow deposit at high-deformation speed, which may break up the snow. In each snow-cable composite element, once the failure criterion of the snow in terms of adhesive tensile

strength is fulfilled at any integration point, the snow mass and stiffness contributions are removed from the model, *i.e.,* effective snow shedding is assumed to take place.

The time function of the periodic-load serves as an input to the numerical model, defined by a displacement time history. The shape of the displacement function is the same for all cases, as shown in Figure 3.23. When the period of excitation decreases, the length of time step, Δt, is changed correspondingly, but the number of time steps in one cycle is kept constant. The period varied from 1.039 s to 0.6741 s by setting Δt between 0.0165 s and 0.0107 s. The time step (or steps) during the calculation is set to be the same like the time step in the time function defining the cable displacement at the suspension-point. Time step should be small enough to capture the essential features of the wave propagation problem induced by the periodic-load. The periodic-load function (a displacement time history) serves as an input to the numerical model, which is obtained from the videos captured using cameras. This displacement input data results in acceleration peaks similar to the results measured by the accelerometer in the experimental study (Chapter 3) (Hefny *et al.*, 2013).

Simulation results indicate that the selection of the characteristics of the periodic load is an important issue since its energy content determines its capacity of removing the accreted snow from the ground wire. For a given load, the longer the duration (time–step) of the periodic-load, which is characterized by lower acceleration peaks, the lower is the initial amplitude of the transverse wave and consequently, the rate of snow shedding.

The experimental results presented in Chapter 3 for the small-scale cable will be compared to the numerical results obtained by ADINA software. Several snow shedding scenarios will be simulated including two snow sleeve diameters of 0.098 and 0.051 m. The span length is set to 4.14 m and the sag to span ratio is varied from 6 to 9%, depending on the snow load. The same parameters, which varied in the experiments, are examined in the numerical simulations. Experimental results revealed that snow shedding usually occurred during the first ten impacts, thus the ten impacts were chosen as an input for this modeling study, since snow shedding ceases to evolve further.

4.4.2. Rate of Shedding and Time Histories of Cable Response

4.4.2.1. Effect of Period of Excitation (Acceleration Peaks)

The parameters used for the main case study are LWC of 23%, snow sleeve diameter of 0.098 m, sag to span ratio of 7.5%, cable sag of 0.31 m, input displacement of 10 impacts, displacement input peak of 0.11 m and adhesion force of 8.7 N. Cable diameter, snow thickness and cable initial strain are assumed to be 0.0041 m, 0.0469 m and 0.000219, respectively. Table 4.3 shows the correspondence between the excitation period, motor speed level and time step in the numerical model. The slowest motor speed (longest excitation period) is simulated using a time step of 0.0165 s, which results in average acceleration at 220 m/s^2 and a 5.9% rate of shedding. Increasing the motor speed in the experiments is corresponding to decreasing the time step in the simulations. Figure 4.15 shows the shedding sequence for the four cases shown in Table 4.3, where snow shed for periods 1.039, 0.9072, 0.7812, 0.6741s by a rate of 5.9, 35.8, 86 and 100%, respectively. Snow sheds by unzipping way starting from the suspension-point, then partially similarly to what was observed in experiments. This sequence of fallen elements is identical for all the observed cases(Hefny et al., 2013).

Table 4.3 Correspondence between period of excitation, motor speed level and time step.

Motor speed level	Period of excitation (s)	Time step (s)
2 (Case1)	1.039	0.0165
3 (Case2)	0.9072	0.0144
4 (Case3)	0.7812	0.0124
5 (Case4)	0.6741	0.0107

(a)

(b)

(c)

(d)

Figure 4.15 Snow shedding scenarios: (a) 5.9% shedding, (b) 35.8% shedding, (c) 86% shedding and (d) 100 % shedding(Hefny et al., 2013).

Figure 4.16 compares time histories of cable acceleration at node 2 (1 cm from the suspension-point) calculated by the numerical model and that obtained experimentally for Case 1(1.039s). That figure serves only as an illustration for validation between modeling and experiments. This comparison demonstrates some high oscillations in the acceleration time history graph obtained numerically. The numerically-generated high amplitude content of the response is partly filtered out by the numerical integration (Bathe composite) method used. However, high-amplitude oscillations are still present, the reason behind this result is that the fundamental axial vibration of the snow-covered cable. The reason of such peak difference is unknown, but could be attributed to the difference in the load position between model and experimental study.

It can be observed that the increase of acceleration average peaks affects the mid-point cable jump and rate of shedding as well. Once the acceleration peaks jump is found at around 415 m/s^2, a 35.8% shedding scenario occurred for Case 2. The peak at 465 m/s^2 is assigned to the time step of 0.0124s, resulting in a rate of shedding of 86%. The load generates a transverse wave, where this wave transforms into a longer vibrating loop with a sufficient energy to de-ice longer parts of the sleeve. Figure 4.17 shows that the acceleration peaks decreased from the suspension-point to the mid-point by around 60%. The average of the acceleration peaks is around 90 m/s^2 at mid-point compared to 220 m/s^2 at the suspension-point, for Case 1.

Figure 4.16 Acceleration time history at 1 cm from the suspension-point (Node 2) (Hefny et al., 2013).

It is noteworthy that the acceleration peaks during a periodic motion with constant angular velocity is negligible compared to the accelerations (or to their right mean square) at the impacts. The following results demonstrate the agreement between the numerical results and the experimental ones. The comparison basis depends on the calculation of root mean squares of the impacts for both cases. The high impact values refer to impact forces, which may be elevated than the angular accelerations since it is a kind of impact. The impact for falling force is an example for how high the impact may reach (Appendix B).

Figure 4.17 Acceleration time history at the mid-point.

Figure 4.18 shows that the cable jump (peak to dip amplitude) at the mid-point increases by decreasing the excitation period or increasing the acceleration average peaks (Case 1 to Case 4). Moreover, it can be stated that cable jump decreases by moving far away from the suspension-point (cf. Figs 4.18 and 4.19). The cable jump at the mid-point is around 19 cm in the simulations compared to 16 cm experimentally, in which enhances good agreement between model and experiments (Figure 4.14, Table 4.4). This agreement ensures that the model may simulate the experimental conditions perfectly, therefore the validation is working well. The mid-point jump using the model is around 33 cm corresponding to 29.3 cm experimentally giving the rate of shedding of 80% and 86% in the experiments and the model, respectively. It may be concluded that the cable amplitude following partial shedding is proportional to the amount of snow removed. Moreover, acceleration magnitudes are generally higher for longer shedding length (Hefny et al., 2013).

Figure 4.18 Cable jump time history at L/4 from the suspension-point (Node 107).

Figure 4.19 Cable jump time history at mid-point (Hefny et al., 2013).

The numerical results reveal that the maximum cable jump at mid-point obtained for the instantaneous snow-shedding simulation (Case 4) is higher than propagating snow-shedding which occurs in Cases 1-3, as depicted in Figure 4.18. Partial shedding can take several seconds, whereas the time needed to achieve full-span shedding is significantly faster. Cable jump is about 39.5 cm numerically for instantaneous shedding, which corresponds to 39 cm experimentally (Table 4.4).

Table 4.4 Comparison of cable jump experimentally and numerically.

	Cable jump(cm)	
	Num.	Exp.
Case 1	6.5	0
Case 2	19	16
Case 3	33	29.3
Case 4	39.5	39

Num: Numerical study; Exp: Experimental study.

Table 4.5 presents a summary of the comparison between the experimental results and modeling results for the main case study. The cable jump at mid-point and rate of shedding seemed to be well predicted by the numerical model with a maximum of 10% discrepancy. High error percentage may be observed only in predicting cable jump for the acceleration loads with small impacts (Cases 1, 2 in Table 4.4).

Table 4.5 Rate of shedding of main case study.

Snow shedding scenarios	Motor speed level	Acc. peak Average (m/s^2)	RSS by ADINA (%)	RSS by Exp. (%)
1	2	220	5.9	0
2	3	415	35.8	40
3	4	465	86	80
4	5	540	100	100

RSS: rate of snow shedding in %.
Acc: Acceleration.

There are few explanations for the differences between the numerical simulations and the experimental results. The numerical simulations use the periodic-load (displacement) as the input, without considering there is some localized distribution of this displacement at the physical loading point (Mirchaefie, 2010). The model does not allowing study of this effect

since the cable mesh could only hold loads at nodal points. In the experimental study, both the snow deposit and the cable offer some bending stiffness to react to this localized effect.

Although the adhesion diminishes, snow maintains above the cable as a result of cohesion that does not consider in the modeling study. Moreover, there is a fundamental longitudinal (axial) vibration of snow-covered cable, where the effect of both of them creates the high-peak oscillations of the cable tension. A suggested solution should be stated to eliminate some spurious high peaks observed in the time history of cable end-tensions. It can be concluded that the average of tension peaks is decreased slightly by increasing rate of shedding after removing high spurious peaks; this is a logic aspect as a result of decreasing sag(Hefny et al., 2013)..

The fundamental longitudinal (axial) vibration of the snow deposit creates the high frequency oscillations of the cable tension; as mentioned before, thereby, the model shows over-estimation in tension peaks comparing with the experimental results. This overestimation is perhaps related in part to the bending stiffness of the cable, which was neglected in the numerical analysis (Mirshaiefie, 2010).

The periodic load is selected, since it causes severe repeatable damage compared with any regular oscillations. It is noteworthy that, the acceleration time histories studied in this chapter is a good reference for application in the real-scale transmission lines. By recognizing the effect of these forces on the snow shedding process and the cable response, the effect of any record of force/ acceleration spectrum, will be investigated as well. The current peaks and frequency results seem to be in the range of Aeolian vibrations type. Wind induced vibrations are stated in detail in Appendix B.

The static initial tension of the cable is measured at 218.5 N during the experimental study; however, the numerical model did not predict such a value. The problem is assumed to arise from the sensitivity of the numerical model to the flexibility of the cable-end supports of the experimental setup, which is not considered in the numerical model. An additional reason for this contradiction is the simplifying assumption used in modeling the tensional rigidity of the cable. As a conclusion, this model can not simulate accurately the cable tension and it is not used for that purpose. The effects of other parameters, such as LWC, excitation amplitude

and sleeve diameter will be discussed and compared to former experimental observations in next sections hereafter.

Two different approaches were used to obtain reliable tension results using ADINA software. The first approach was by using Rayleigh damping; however, its results were not applicable because the snow shedding rate was lower than experiments. The second approach was considering some kind of flexibility for the fixed-point by using a horizontal spring, which was connected between the fixed end-point of the cable and the precedent point. This horizontal spring has only stiffness of 8e16 N/m, but neither mass nor damping. Thus, the results indicate that cable tension high peaks rather decreased compared to the main tension results (before amelioration), but it still higher than experimental measurements. It may be stated that, this model could not perfectly simulate the cable tension because of the former illustrated reasons.

4.4.2.2 Effect of Snow LWC Values

The effect of LWC may be considered, i.e., the rate of shedding increases as the LWC of snow decreases (Table 4.6). An adhesion force of 4 N is used to simulate the low and high LWC for 10-15% and 35-40%, respectively, for cable sag of 25 cm. For these low/high ranges of LWC, snow persists a short time on the cable, where the whole sleeve sheds at motor speed level-3 showing a good agreement with the experiments.

It can be observed that the rate of shedding is 47% (versus 35% experimentally) at adhesion force of 4 N and motor speed level-2. While, there is a complete shedding at speed level-3 (Figures 4.20, 4.21). The acceleration peaks, which are calculated at motor speed level-3 (period of 0.9072 s) are lower than the main case study because of sag decrease. When LWC is low, the snow density and the cable sag are accordingly small; thereby, the driving system needs lower force than the main case study to raise the snow sleeve up. Moreover, the snow sleeve drops slowly resulting in small impact values.

LWC in the range of 15 to 18% is simulated by adhesion force of 5N. At this stage, snow continues on the cable up to motor speed level-4. The rate of shedding is 13.9% at motor speed level-2, then it increases to 64.7% at motor speed level-3, followed by a complete shedding at speed level-4 (period of 0.7812s). The numerical results predict the same experiments' acceleration obtained pattern. The acceleration peak at shedding for 5 N is

400 m/s^2 numerically versus 465 m/s^2 in the experimental study for middle LWC (Sec.4.3.2.1). Snow is detached in a mixed way (unzipping followed by partial shedding) in the two former cases presenting a good agreement with the experimental tests. The transverse wave has sufficient energy to de-ice the cable until its mid-span, causing only partial snow shedding at motor speed level-2 for force 4 N; and also, at motor speed level-3 for force 5 N. It should be stated that the cable jump at mid point for low LWC is lower than the main case study for middle range by around 20%.

Table 4.6 Rate of shedding by changing adhesion force corresponding to specific ranges LWC.

Adhesion Force (N)	LWC (%)	Case 1		Case2		Case 3		Case 4	
		RSS (%)		RSS (%)		RSS (%)		RSS (%)	
		Num	Exp	Num	Exp	Num	Exp	Num	Exp
4	10-15	47	35	100	100	100	-	100	-
5	15-18	13.9	26	64.7	74.5	100	100	100	-
6	18-20	11.9	5	51.2	44	100	100	100	-
7	20-22	6.5	2	39.3	42.5	91.5	87.4	100	100
8.7	22-30	5.9	0	35.8	40	86	80	100	100

Num: Numerical study, Exp: Experimental study, RSS: Rate of snow shedding.
-These data were unobtainable.

(a)   (b)

Figure 4.20   Snow shedding scenarios at (a) 47% shedding and (b) 100% shedding.
Conditions: Periods 1.039 s and 0.9072 s; Motor speed levels 2 and 3; and LWC 10-15%.

A summary of the results of the numerical simulations is presented in Table 4.6, which lists the rate of snow shedding (RSS), *i.e.,* the fraction of the snow shed in the span in %. It may be noted that the difference between the numerical model rate of shedding and what is obtained experimentally, is due to the fact that cohesion is not considered in the model, which results in less shedding during experimental tests.

Figures 4.21 and 4.22 present comparisons between the time history of cable acceleration calculated by the numerical model and that obtained experimentally for the first 6

s after the periodic-load is applied to the cable at t = 1.0 s. Upward accelerations reach a maximum peak of 240 m/s^2 for 47% shedding and 360 m/s^2 for the 100% shedding, showing a good agreement with experiments. The shedding scenarios of 47% and 100% correspond to 1.039 s and 0.9072 s (motor speed levels of 2 and 3), respectively occur at LWC of 10-15%.

It should be indicated that the average acceleration peaks seem to be in a good agreement with the experiments as shown in Figures 4.21, 4.22 and 4.23. Implementing smaller time steps in the initial phase of the response may have beneficial effects leading to smoother plots and less spurious high frequencies, also the reason behind this result is the parameter selected for Bathe Composite method.

Figure 4.21 Acceleration time history at suspension-point.
Conditions: Period 1.039 s, Motor speed level-2 and LWC 10-15%.

Examination of the results reveals that the mid-point accelerations are around 50% of the suspension-point accelerations. There is slight disagreement on the time scale (the numerical model is advanced in time) compared to that obtained experimentally after the first three impacts, although time step is the same. This might occurred because it is rather difficult

to adjust perfectly experimental conditions, as there is frequently a large horizontal movement caused by the setup system.

Concerning cable jump at the mid-point, it revealed that the model is compatible with the experimental study for complete shedding, but there is some difference appeared in case of motor speed level-2 (Fig. 4.24, Table 4.6). This point enhances that the cohesion is very high at low motor speed level and it cannot exceed the load strength. This mid-span jump is dominated by low-frequency (evaluated at about 1 or 1.25Hz) oscillations. The shedding of thick snow accretion from the cable generates additional cable displacement in the numerical model (47% shedding), while the remaining snow accretion stiffened the cable causing rather small jump, as shown in Figure 4.24.

Figure 4.22 Acceleration time history at suspension-point.
Conditions: Period 0.9072 s, Motor speed level-3 and LWC 10-15%.

Figure 4.23 Acceleration time history comparison at suspension-point.
Conditions: Periods 1.039 s and 0.9072 s, Motor speed levels 2 and 3 and LWC 10-15%.

Figure 4.24 Cable jump time history at mid-point.

Conditions: Periods 1.039 s and 0.9072 s, Motor speed levels 2 and 3 and LWC 10-15%.

(a)   (b)

(c)

Figure 4.25 Snow Shedding Scenarios at (a) 13.9% shedding, (b) 64.7% shedding and (c) 100 % shedding.
Conditions: Periods 1.039 s, 0.9072 s and 0.7812 s; Motor speed levels 2, 3 and 4; and LWC 15-18%.

Regarding LWC in the range of 15 to 18%, upward acceleration peaks at a maximum of 245 m/s^2, 435 m/s^2 and 458 m/s^2 are assigned to 13.9 %, 64.7% and 100% shedding rate, respectively (Figures 4.25- 4.28). There is a rather disagreement (discrepancy of less than 15%) concerning motor speed level-2 by comparing the numerical and experimental results (Table 4.6).

Figures 4.26 to 4.28 show the measured vertical periodic-loads applied to the cable during the experimental study comparing to the numerical model accelerations, in which the average values show a good agreement. Accelerations for the mid-point give peaks at 80, 180 and 280 m/s^2 for motor speed levels of 2, 3 and 4, respectively, as depicted in Figure 4.29.

Figure 4.26 Acceleration time history at suspension-point.
Conditions: Period 1.039 s, Motor speed level-2 and LWC 15-18%.

Figure 4.27 Acceleration time history at suspension-point.
Conditions: Period 0.9072 s, Motor speed level-3 and LWC 15-18%.

Figure 4.28 Acceleration time history at suspension-point.
Conditions: Period 0.7812 s, Motor speed level-4 and LWC 15-18%.

Figure 4.29 Acceleration time history at mid-point.
Conditions: Periods 1.039 s, 0.9072 s and 0.7812 s; Motor speed levels 2, 3 and 4; and LWC 15-18%.

The cable oscillated vertically around the equilibrium static profile and has a cable jump (peak to peak amplitude) of about 32 cm for complete shedding versus 15 cm and 19 cm for 13.9% and 64.7% shedding, respectively, as shown in Figure 4.30.

Concerning the cable jump at the mid-point, for LWC ranged from 15 to 18%, it should be noted that the model has lower shedding by around 30% for complete shedding than experimental investigation. For the case of complete shedding, it was observed that the effect of some horizontal movement of suspension-point, and cable high stiffness may cause this great jump in the experimental study, as seen in Figure 4.28.The model shows a rate of 13.9% shedding, which is lower than the experimental results. This contradiction arises from the fact that the snow sleeve at low LWC is very fragile resulting in fast shedding comparable to modeling, where it depends only on failure criteria (Figure 4.26).

Figure 4.30 Cable jump time history at mid-point.
Conditions: Periods 1.039 s, 0.9072 s and 0.7812 s; Motor speed levels 2, 3 and 4; and LWC 15-18%.

4.4.2.3 Effect of Excitation Amplitude

In order to investigate the effect of excitation amplitude, different amplitudes were examined, where 155, 170 and 185 mm are corresponded to low, middle and high amplitudes, respectively. In this section, the time step is assigned to 0.0144 s, which simulates motor speed level-3 in the previous main case study (sec.4.3.2.1). Adhesion forces vary from 4 N to 8.7 N which correspond to low and middle-ranges of LWC, respectively. The rate of snow shedding is 20.4% using low amplitude (155 mm peak) compared to 35.8% for main case study using middle amplitude (170 mm peak) (Table 4.7). Generally, when the acceleration input peak decreases (from middle to low amplitude) the rate of shedding decreases as well. The maximum cable jump at the mid-point for low amplitude is 8 cm comparing to 12 cm for middle amplitude; found in the experimental study (Table 4.4).

Using high-excitation input (185 mm peak) with the same period (0.9072 s), the resultant is higher rate of shedding compared to the case of middle amplitude (Table 4.7). The sleeve is completely unloaded at this stage, which ensures that high-amplitude excitation input affects snow shedding to a great extent causing a very high jump; around 29 cm compared to 8 cm for low amplitude, as illustrated in Figure 4.31. Small acceleration peaks lead to slightly small cable jump amplitudes due to the great number of snow elements staying on the cable. The model presents a cable jump at the mid-point of around 28, 13 and 7 cm for 42.9, 23.4 and 21.9% shedding, respectively, as shown in Figure 4.32. The simulation results show good agreement with the experimental study. Wherever, for the low excitation amplitude, snow persists on the cable up to motor speed level-8 for the case of low LWC. However, for high amplitude, snow can shed completely at motor speed level-3. Moreover, when LWC (and consequently, the adhesion force) decreases gradually from its mid-range value, the rate of shedding increases as a consequence (Tables 4.7). The periodic-load applied for adhesion forces of 7, 6 and 5 N results in a rate of snow shedding of 21.9%, 23.4% and 42.9%, respectively, which in turn corresponds to 0%, 9.5% and 45.5% experimentally (Figures 4.32-4.36, Table 4.8). It noteworthy that the 7, 6, 5N simulate LWC of (20- 22%), (18-20%), (15-18%), correspondingly.

Table 4.7 Rate of shedding for different adhesion forces as a function of different excitation amplitudes.

Excitation amplitude Adhesion force (N)	Low	Middle	High
4	100%	100%	100%
5	42.9%	64.7%	100%
6	23.4%	51.2%	100%
7	21.9%	39.3%	100%
8.7	20.4%	35.8%	100%

Figure 4.31 Cable jump time history at mid-point.
Conditions: Period of 0.9072 s; Motor speed level-3; LWC 20-22%; F7 (21.9%), 18-20%; F6 (23.4%) and 15-18% ; F5 (42.9%).

Table 4.8 Shedding rate and cable jump for low and high excitation amplitude.

Excitation amplitude type	Low amplitude						High amplitude	
Motor speed level	3		3		3		3	
Adhesion force(N)	7		6		5		7	
Results	Num	Exp	Num	Exp	Num	Exp	Num	Exp
Shedding Rate (%)	21.9	0	23.4	9.5	42.9	45.5	100	100
Cable jump(cm)	8	0	13	4	28	20	35.8	37

Figure 4.32 Snow shedding scenarios at (a) 42.9% shedding, (b)23.4% shedding.
Conditions: Period 0.9072 s, Motor speed level-3 and LWC 15-18%, 18-20%.

For LWC values in the range between 20 to 22%, snow may shed with a high degree
of shedding; reaching 21.9%. On the other hand, for the experimental tests there is no
shedding as a result of snow cohesion between particles (Figure 4.34). On the other hand, for
high-amplitude movement, the snow-shedding rate using modeling at motor speed level-3 is
apparently similar to experimental results presenting a complete shedding, as shown in Figure
4.36. It may be concluded that the acceleration values at the suspension-point are assumed to
be spurious and not realistic; although, the inertia forces resulting from these unrealistic
accelerations force snow shedding (Figures 4.33-4.36).

Acceleration magnitudes are generally high for long shedding length and also they are
proportional to the shedding length. Upward accelerations reach a maximum peak at 300 m/s^2
for 21.9 % shedding, 320 m/s^2 for the 23.4 % scenario and 400 m/s^2 for 42.9 % shedding,
successively (Figure 4.33). Fig.4.36 shows an acceleration peak located at 355 m/s^2, in which
this peak is assigned to high amplitude. The cable at the mid-point oscillates around the
equilibrium static profile and has peaks at 320 m/s^2, 248 m/s^2, 200 m/s^2 for 42.9%, 23.4%
and 21.9% shedding scenario, respectively (decrease of around 60% between suspension-
point and mid-point), as shown in Figure 4.36.

Figure 4.33 Acceleration time history at suspension-point.
Conditions: Period 0.9072 s; Motor speed level-3; LWC 20-22%; F7 (21.9%), 18-20%; F6 (23.4%) and 15-18% ; F5 (42.9%).

Figure 4.34 Acceleration time history at suspension-point.
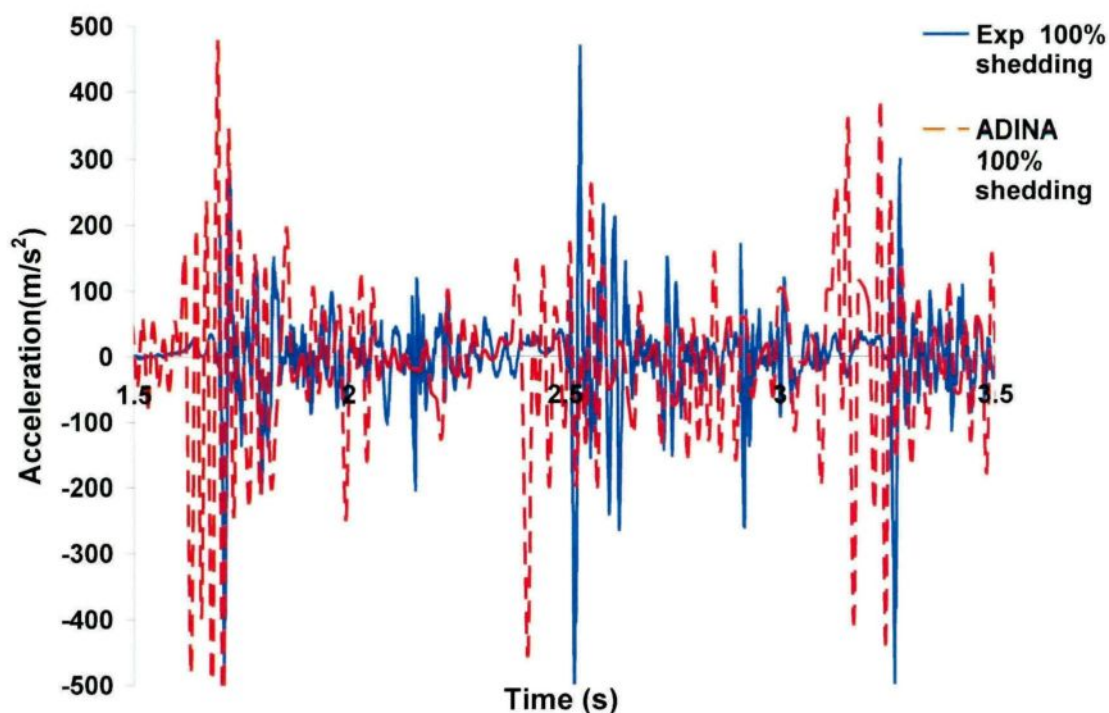Conditions: Period 0.9072 s, Motor speed level-3 and LWC 20-22%.

Figure 4.35 Acceleration time history at suspension-point.
Conditions: Period 0.9072 s, Motor speed level-3 and LWC 20-22%.

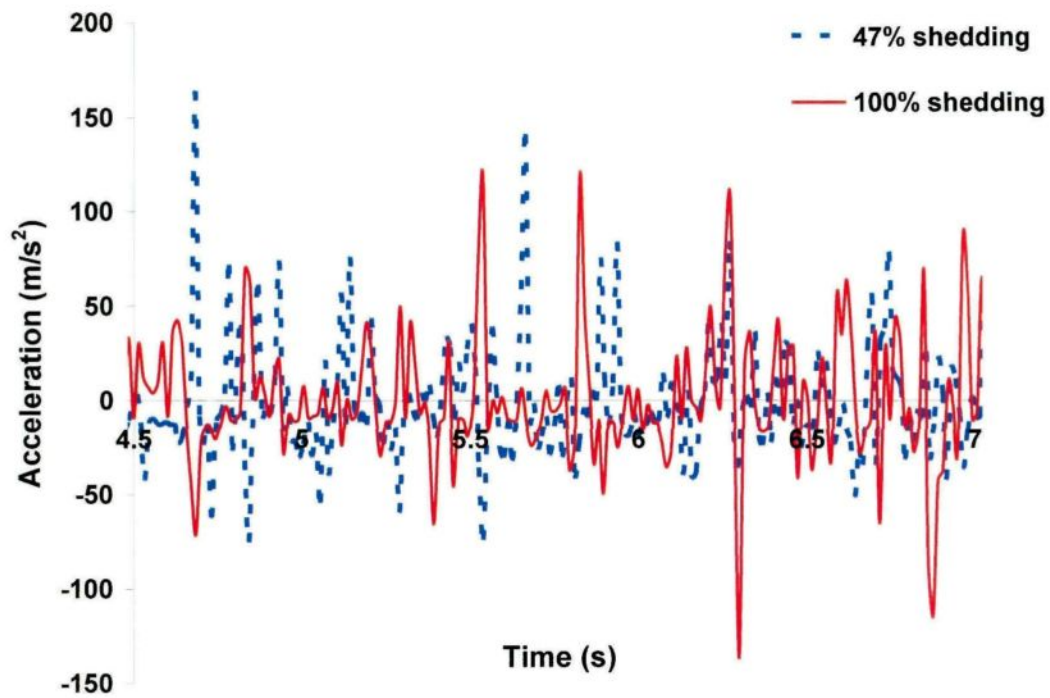Figure 4.36 Acceleration time history at mid-point.
Conditions: Period 0.9072 s; Motor speed level-3; LWC 20-22%; F7 (21.9%), 18-20%; F6 (23.4%) and 15-18% ; F5 (42.9%).

4.4.2.4 Effect of Snow Sleeve Diameter

Sleeve diameter of 0.051 m, sag to span ratio of 3.6%, snow thickness of 0.0235 m and cable initial strain of 973e-7 were used to investigate the effect of periodic load on the cable using the small snow sleeve model diameter. The model takes rather the same trend (snow stays up to motor speed level-5, *i.e.*, up to excitation period of 0.6741 s) using the small sleeve and middle amplitude, such as the large sleeve diameter. Shedding occurs partially, which is consistent with the experimental tests. There is some discrepancy between experiments and modeling, as snow persists only up to motor speed level-4 in the experimental study (LWC 25%, amplitude 170mm), Chapter 3.

The cable mid-span displacement tends to increase by about 16% compared with the experimental results (Tables 4.9 and 4.10). The small sleeve gives lower acceleration peaks compared with the large sleeve for the main case study and the same excitation period, because of decreasing cable sag and snow mass (Sections 4.3.2.1, 4.3.2.4). Moreover, the snow shedding sequence is depicted in Figure 4.38 demonstrates 11.5, 19, 100% for excitation period of 0.907, 0.7812, 0.6741s, respectively. Once the acceleration peak changed, the rate of shedding altered. Snow shed completely at acceleration peak of 380 m/s^2, which is in a good accord with the experiments (Figure 4.38).

Table 4.9 Rate of shedding using ADINA for different time steps and adhesion forces.

Time step (s)	0.0165	0.0144	0.0124	0.0107
Adhesion force(N)	(1.039 s)	(0.907 s)	(0.7812 s)	(0.6741 s)
4	22 %	43.8%	100%	100%
5	19%	33.6%	100%	100%
6	7%	27.9%	87%	100%
7	0%	19%	64%	100%
8.7	0%	11.5%	19%	100%

(Excitation period is in parentheses).

Table 4.10 Comparison between experimental and numerical model results.

Small sleeve (Case of middle amplitude and middle range of LWC)							
Motor speed level	2		3		4		5
Results	Num	Exp	Num	Exp	Num	Exp	Num
Shedding Rate (%)	0	35.8	11.5	87	19	100	100
Cable jump (cm)	0	5	11	9	19	16	27
Acceleration-end (m/s^2)	200	120	220	250	300	310	380
Acceleration-mid (m/s^2)	160	-	180	-	250	-	300

-These data were unobtainable.

(a) (b) (c)

Figure 4.37 Snow shedding scenarios at (a) 11.5% shedding, (b) 19% shedding, (c) 100% shedding.
Conditions: Period 0.907 s, 0.7812 s and 0.6741 s; Motor speed levels 3, 4 and 5; and LWC 25%.

Figure 4.38 Acceleration time history at suspension-point.
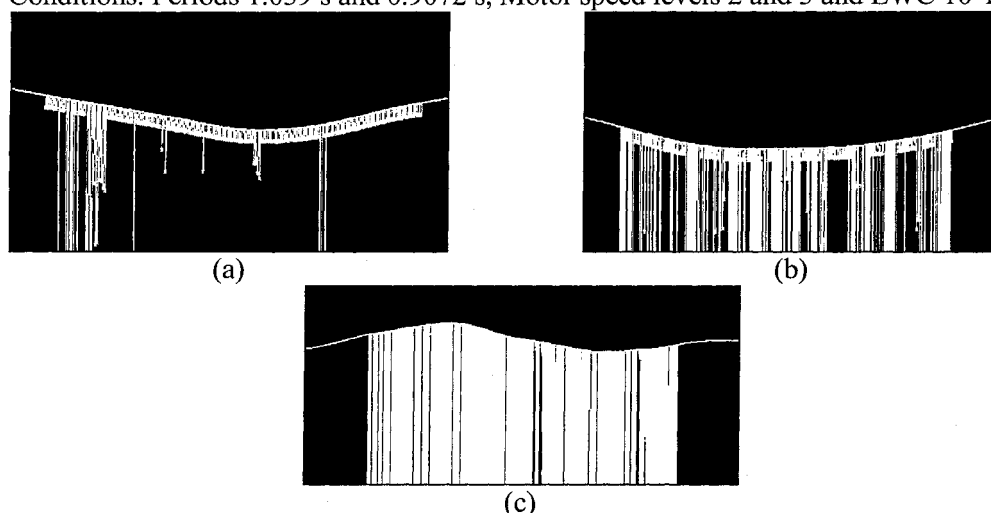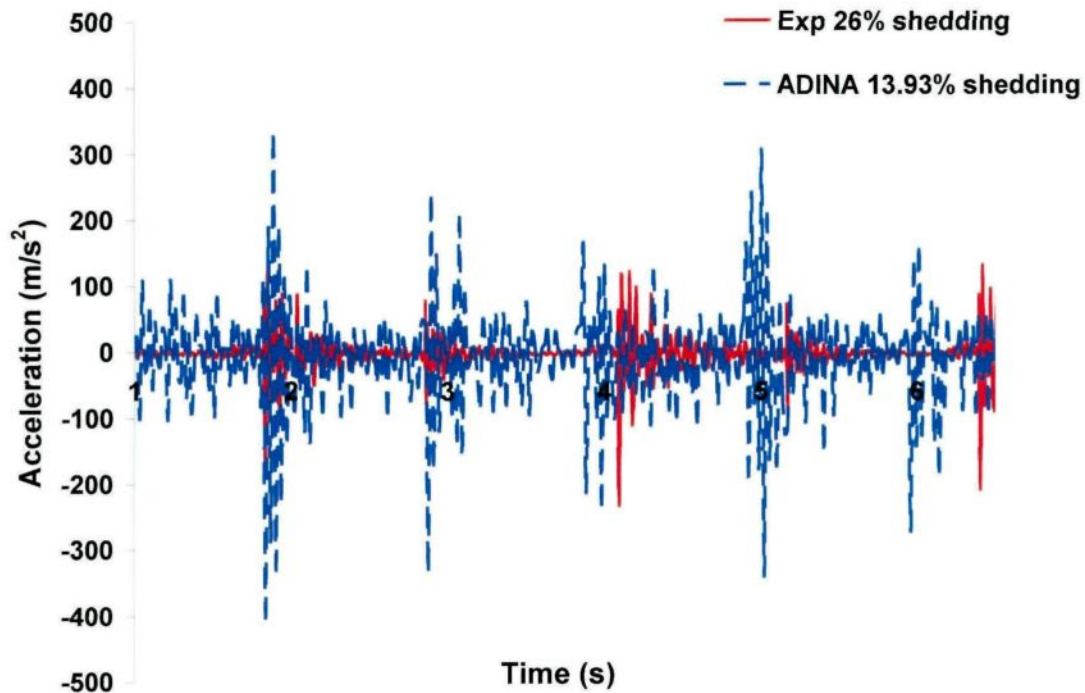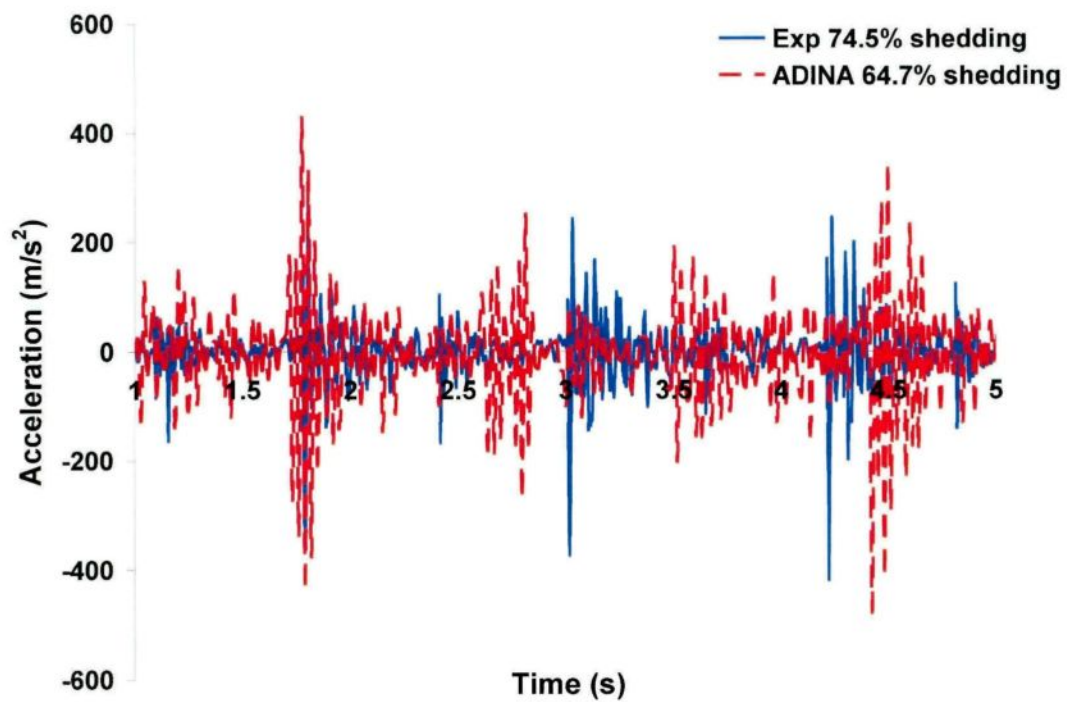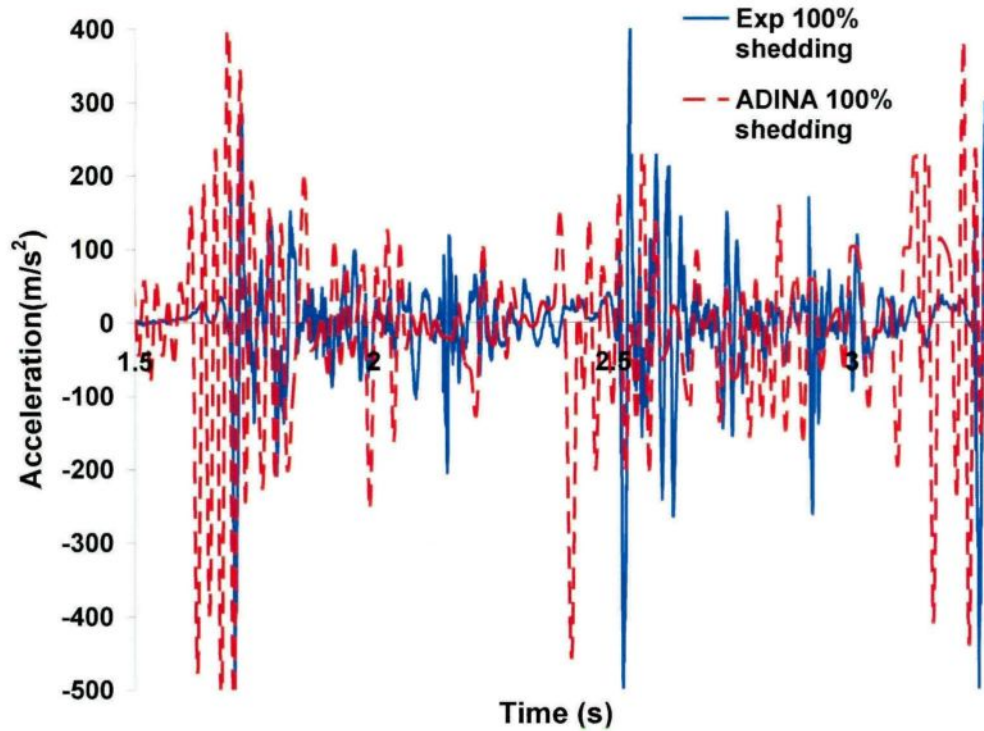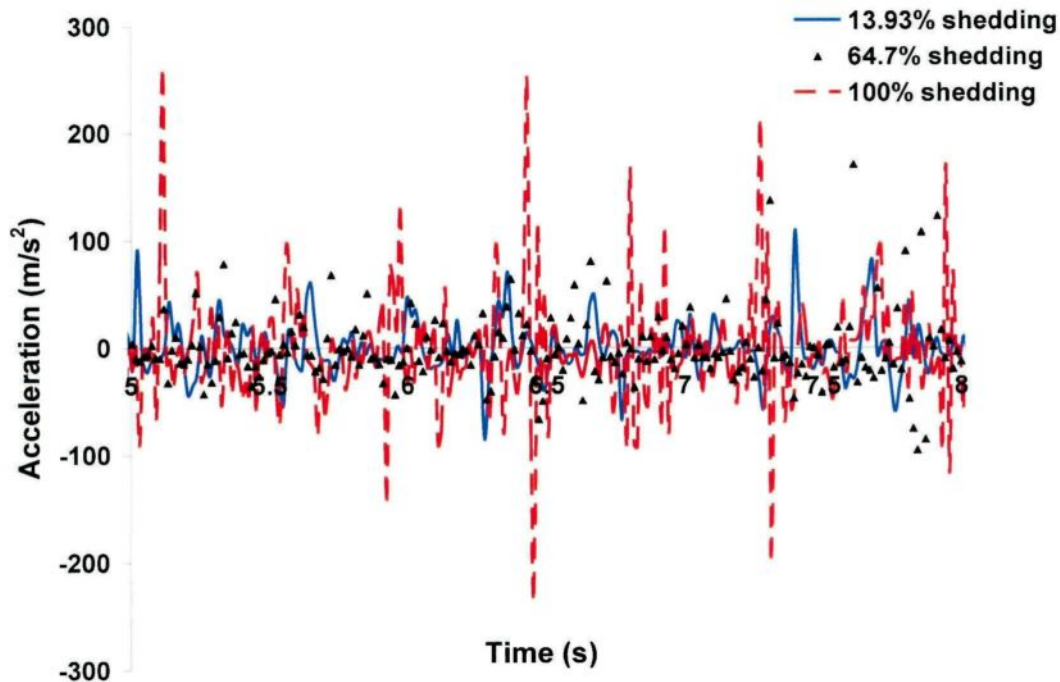Conditions: Period 0.6741 s; Motor speed level-5; and LWC 25%.

Upward accelerations peaks reach a maximum of 220 m/s^2 for 11.5 % shedding rate and 380 m/s^2 for 100% shedding scenario (Table 4.10). Snow stays long time on the cable

during modeling analysis because the acceleration failure condition is not sufficient to shed snow earlier. Acceleration peaks for the small sleeve model are higher than the corresponding peaks in the experimental study. The same time steps for large sleeve which are used in numerical simulations in large sleeve seem rather small, resulting high acceleration peaks. The snow load using the small sleeve diameter is small compared to the large sleeve and it takes more time between two successive impacts, as depicted in Figures 4.39-4.41 and Table 4.10. Concerning the mid-point acceleration, it is around 80% of the acceleration at the suspension-point, since the load is decreased by moving far away from its effect point, as shown in Figure 4.40. The cable jump for motor speed level-3 (excitation period of 0.9072 s) is about 11 cm showing a good agreement with experiments (9 cm). Whereas, in the case of complete shedding (excitation period of 0.6741 s), the jump is around 27 cm (Figures 4.39-4.41 and Table 4.10).

The model gives higher cable jump, but smaller rate of shedding than what observed in experimental results, the reason of such inverse behavior is unknown; hereafter, there are some possible explanations. A contradiction arises from the result that small sleeve is very fragile in the experimental tests, thereby any impact load may shed it easily; otherwise, the snow rate of shedding is small during simulations. This ensured that the snow shedding happened numerically according to adhesion failure condition only, once it fulfills snow detaches from the cable, as shown in Figures 4.39-4.40 and Table 4.10. The cable jump obtained experimentally is smaller than the numerical results; this discrepancy occurs since the suspension-point in the experimental study moves upward causing a small impact, where there is a small snow load. However, by using ADINA, the interrelated relations between cable sag, snow load and cable tension causes high jump.

Figure 4.39 Acceleration time history at suspension-point.
Conditions: Periods 1.039 s, 0.907 s, 0.7812 s and 0.6741 s; Motor speed levels 2, 3, 4 and 5; and LWC 25%.

Figure 4.40 Acceleration time history at mid-point.
Conditions: Periods 1.039 s, 0.907 s, 0.7812 s and 0.6741 s; Motor speed levels 2, 3, 4 and 5; and LWC 25%.

Figure 4.41 Cable jump time history at mid-point.
Conditions: Periods 1.039 s, 0.907 s, 0.7812 s and 0.6741s; Motor speed levels 2, 3, 4 and 5; and LWC 25%.

4.4.2.5. Effect of changing Snow LWC for Small Sleeve

4.4.2.5.1. Partial Shedding at Adhesion Force of 4 N

Changing adhesion force to lower forces than 8.7 N, reveals the increase of the rate of shedding gradually. This section studies the effect of excitation period at low LWC (low adhesion force) on the dynamic response. Rate of shedding is found to be about 22%, 43.8% and 100% for motor speed levels of 2, 3 and 4, respectively; using LWC 10-15% and adhesion force of 4 N (Figure 4.42).

For adhesion forces of 4 N and 5 N (LWC 10-15%, 15-18%) snow persists some time on the cable up to motor speed level-4; however, for high adhesion forces snow stays longer than the case of low LWC; up to motor speed level-5 (time step of 0.0107 s). It is noteworthy that there is a remarkable effect of LWC decrease on snow adhesive strength and rate of shedding, successively (Sec.4.3.2.2). A summary of the results of the numerical simulations is tabulated in Table 4.11, which lists the rate of snow shedding (RSS).

Figure 4.42 Snow shedding scenarios at (a) 22% shedding, (b) 43.8% shedding, (c) 100% shedding.
Conditions: Periods 1.039 s, 0.907 s and 0.7812 s; Motor speed levels 2, 3 and 4; and LWC 10-15%.

Table 4.11 Comparison between experiments and model analysis.

Small sleeve (Case of low LWC (4N))						
Motor speed level	2		3		4	
Results	Num	Exp	Num	Exp	Num	Exp
Shedding Rate (%)	22	29.3	43.8	92.7	100	100
Cable jump (cm)	9	4	20	13	26	14.6
Acceleration-end (m/s^2)	220	170	290	210	350	255
Acceleration-mid (m/s^2)	125	-	180	-	220	-

- These data were unobtainable

Upward accelerations reach a maximum at 290 m/s^2 and 350 m/s^2, which belong to the 43.8% and 100% shedding scenario, respectively, as shown in Figures 4.43-4.45. The acceleration peaks are found at 220 m/s^2 versus 170 m/s^2 experimentally for motor speed level-2 and at 350 m/s^2 versus 255 m/s^2 for motor speed level-4. Generally, the analysis of the numerical results shows that the acceleration peaks are high compared with the experimental

results. The cable jump at the mid-point is 14.6 cm experimentally, which corresponds to 26 cm using modeling, Table 4.11.

Figure 4.46 shows that the mid-point acceleration for rate of shedding of 22%, 43.8%, 100%, results in peaks at 125, 180 and 270 m/s^2, respectively (around 56% to 77% of the suspension-point acceleration). These observations substantiate the conclusions that the rate of shedding for numerical simulations is relatively lower than experiments for small sleeve and low LWC. It is important to know that the snow sleeve is brittle for low LWC and can shed more easily in the experiments; whereas, the numerical model considers only the failure criterion condition; as mentioned in previous sections. The cable mid-point displacement tends to increase by increasing shedding rate, as 9, 20, 26 cm corresponds to 4, 13, 14.6 cm in the experimental work (Figure 4.46 and Table 4.11).

Figure 4.43 Acceleration time history at suspension-point.
Conditions: Period 1.039 s, Motor speed level-2 and LWC 10-15%.
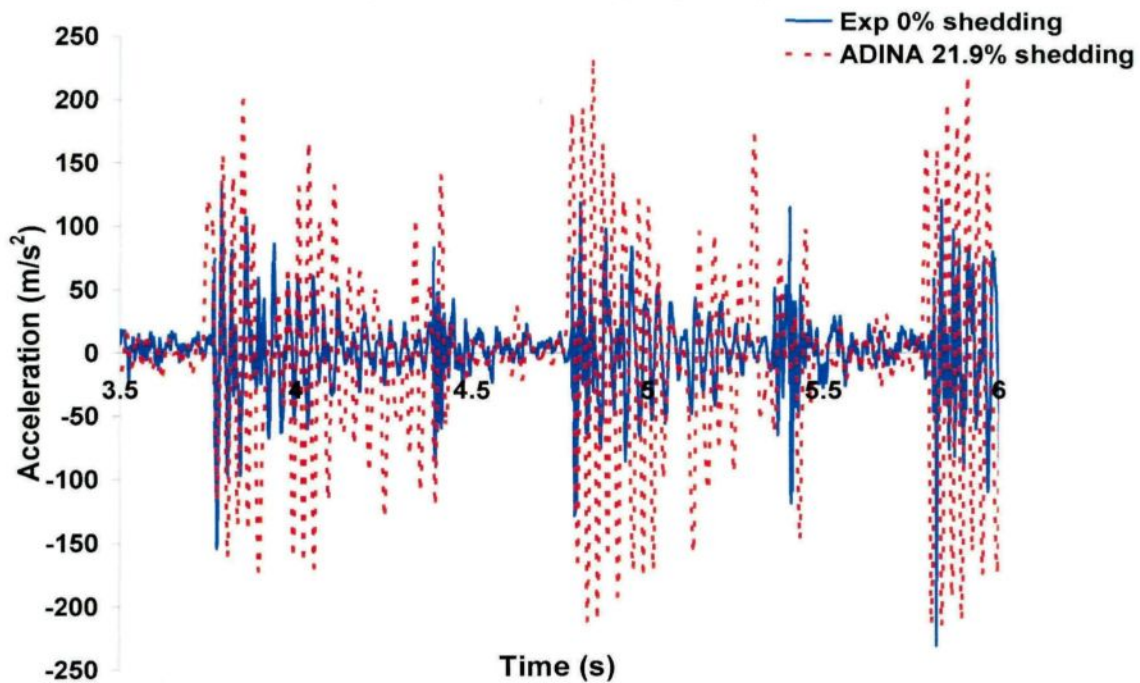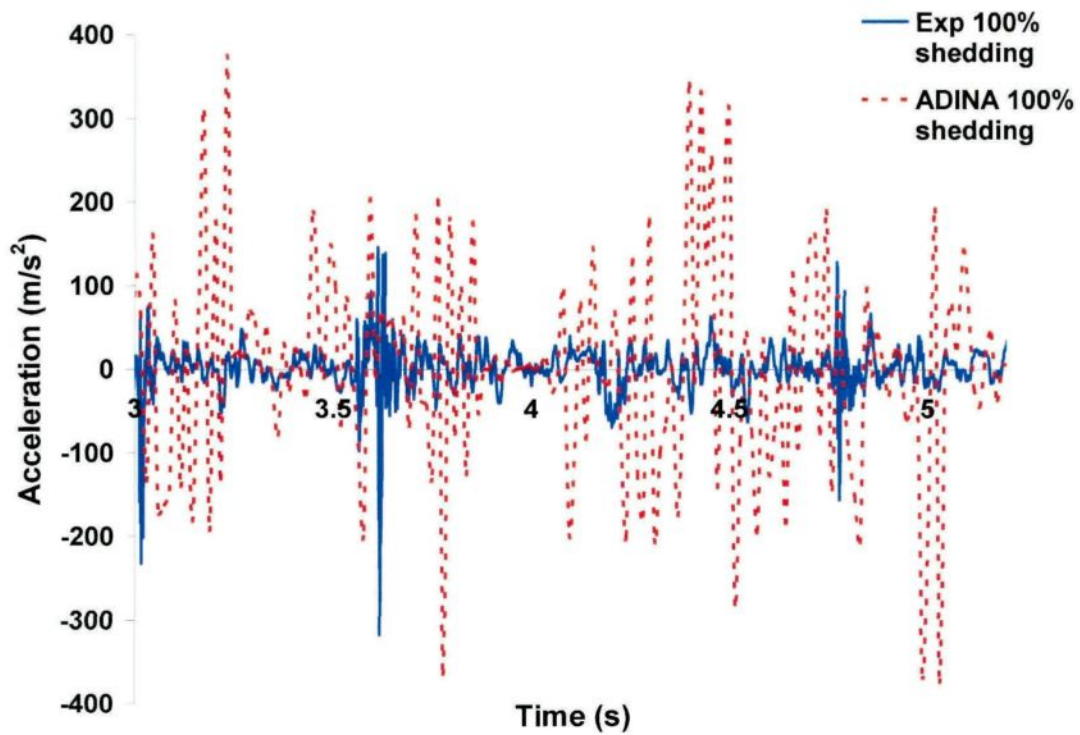
Figure 4.44 Acceleration time history at suspension-point.
Conditions: Period 0.7812 s, Motor speed level-4 and LWC 10-15%.

Figure 4.45 Acceleration time history at mid-point.
Conditions: Periods 1.039 s, 0.907 s and 0.7812 s; Motor speed levels 2, 3 and 4;
and LWC 10-15%.

Figure 4.46 Cable jump time history at mid-point.
Conditions: Periods 1.039 s, 0.907 s and 0.7812 s; Motor speed levels 2, 3 and 4; and LWC 10-15%.

4.4.2.5.2. Partial Shedding at Adhesion Force of 6 N

An outline of the results of the current numerical simulations is presented in Table 4.12, which lists the rate of snow shedding, acceleration and cable jump. Figure 4.47 shows the sequence of different snow shedding scenarios of 7, 27.9, 87 and 100%.

Figure 4.47 Snow shedding scenarios at (a) 7% shedding, (b) 27.9% shedding, (c) 87% shedding, (d) 100% shedding. Conditions: Periods 1.039 s, 0.907 s, 0.7812 s and 0.6741 s; Motor speed levels 2, 3, 4 and 5; and LWC 18-20%.

Upward accelerations reach a maximum peak at 275 m/s^2 for 7% shedding and 440 m/s^2 for the 87% shedding scenario, as shown in Figure 4.48 and Table 4.12. Acceleration peak at mid-point decreases by around 55% compared to the suspension-point; in which equals 70 m/s^2 for 7% shedding and 120m/s^2 for 87% shedding, as shown in Figure 4.49. Cable jump at the mid-point for 7% shedding rate is around 11 cm (peak to peak amplitude), which belongs to acceleration peak at 100 m/s^2, whereas cable jump is 28 cm for complete shedding, corresponding to peak at 400 m/s^2 (Fig.4.50 and Table 4.12).

Figure 4.48 Acceleration time history at suspension-point.
Conditions: Periods 1.039 s, 0.907 s, 0.7812 s and 0.6741 s; Motor speed levels 2, 3, 4 and 5 and LWC 18-20%.

Figure 4.49 Acceleration time history at mid-point.
Conditions: Periods 1.039 s, 0.907 s, 0.7812 s and 0.6741 s; Motor speed levels 2, 3, 4 and 5; and LWC 18-20%.

Figure 4.50 Cable jump time history comparison at mid-point.
Conditions: Periods 1.039 s, 0.907 s, 0.7812 s and 0.6741 s; Motor speed levels 2, 3, 4 and 5; and LWC 18-20%.

Table 4.12 Model results for partial shedding at Low LWC.

Small sleeve (Case of low LWC (6N))				
RSS (%)	7	27.9	87	100
Cable Jump (cm)	11	20	24	28
Acceleration end-point (m/s^2)	100	220	350	400
Acceleration mid-point (m/s^2)	70	100	120	150

4.4.2.6 Effect of Excitation Amplitude for Small Sleeve

The effect of excitation amplitude on cable response was examined using small sleeve diameter. Snow persists on the cable for long time using low-excitation amplitude compared to middle-excitation amplitude. Hence, the acceleration peaks for low-amplitude are lower than for middle-amplitude, for small sleeve (Sec.4.3.2.4). Whereas, the acceleration peaks increase using high-excitation amplitude and consequently the shedding rate. For example, for adhesion force of 6 N, snow remains on the cable at low-amplitude up to motor speed level-8, resulting in around 11.4% shedding and this is consistent with the experiments. However, for high-amplitude, snow shed completely at motor speed level-3 (Tables 4.13, 4.14).

Table 4.13 Rate of shedding for different adhesion forces as a function of excitation amplitude.

Excitation amplitude	Low	Middle	High
Adhesion force(N)			
4	100%	43.8%	100%
5	25.7%	33.6%	100%
6	11.4%	27.9%	100%
7	5.8%	19%	100%
8.7	0%	11.5%	100%

Table 4.14 Comparison between experiments and modeling using low and high excitation amplitudes.

Results	Low amplitude						High amplitude	
	Num (7 N)	Exp	Num (6N)	Exp	Num (5N)	Exp	Num (6 N)	Exp
RSS (%)	5.8	-	11.4	9.8	25.7	-	100	100
Cable Jump (cm)	10	-	14	2	30	-	37	11
Acceleration - end (m/s^2)	-	-	140	120	-	-	400	380
Acceleration - mid (m/s^2)	40	-	160	-	75	-	100	100

-These data were unobtainable.

Table 4.13 reveals that the rate of shedding decreases for the same adhesive force by using low-excitation amplitude, while it increases using high one. In addition, there is an increase of the rate of shedding by decreasing adhesion force (LWC) (Figure 4.51). It is believed that high acceleration peaks lead to high cable jump amplitudes due to a considerable number of snow elements that detach from the cable. The numerical observations reveal also the effect of using high-excitation amplitude, which it gives acceleration peak of around 400 m/s^2 versus 380 m/s^2 in the experimental study. The cable peak to peak amplitude is found 37cm using ADINA corresponding to only 11 cm experimentally (Chapter 3, Table 4.14). Acceleration at mid-point is around 45% of suspension-point acceleration for low-excitation amplitude and high-excitation amplitude as well (Figure 4.52, Table 4.14). Concerning the cable jump is appeared to be around 10, 14 and 30 cm for 5, 6 and 7 N, respectively, Figure 4.53.

There is an accord between experimental and numerical results since upward accelerations reach a maximum peak at 140 m/s^2 for 11.4% shedding rate numerically corresponding to 120 m/s^2 for 9.8% shedding rate resulted in the experimental tests (Figure 4.54). However, there is a complete shedding using high-amplitude for the same adhesion force (6N); experimentally and numerically, as shown in Figure 4.55.

(a)   (b)   (c)   (d)

Figure 4.51 Snow shedding scenarios at (a) 5.8% shedding, (b) 11.4% shedding, (c) 25.7% shedding, (d) 100% shedding.
Conditions: Period 0.907 s; Motor speed level-3; and LWC 10-15%, 15-18%, 18-20% and 20-22%.

Figure 4.52 Acceleration time history at mid-point (low amplitude).
Conditions: Period 0.907 s; Motor speed level-3; and LWC 15-18%, 18-20% and 20-22%.

Figure 4.53 Cable jump time history at mid-point (low amplitude).
Conditions: Period 0.907 s; Motor speed level-3; and LWC 15-18%, 18-20% and 20-22%.

Figure 4.54 Acceleration time history at suspension-point (low amplitude).
Conditions: Period 0.907 s; Motor speed level-3; and LWC 18-20%.

Figure 4.55 Acceleration time history at suspension-point (high amplitude).
Conditions: Period 0.907 s, Motor speed level-3, and LWC 18-20%.

4.5 Conclusion

A numerical model was developed using ADINA to simulate the effects of periodic loads on snow shedding process from transmission line cables and to predict the acceleration peaks and cable jump. This model demonstrated a reliable method to relate the properties of snow, in particular snow LWC, to its response when subjected to a given load, which is important for both small-scale and real lines. Comparison of numerical and experimental results showed that the numerical model well calculated the dynamic response of snow-covered cables subjected to periodic loads. The conclusions concerning the model may be stated as follows:

1. This study has shown that it is feasible to model the effects of snow shedding induced by a periodic load on single-span overhead cables where the snow deposit is considered. The finite element model presented may serve as a basis to study failure criteria of wet snow in terms of tensile adhesion strength.

2. Simulation results indicate that the energy content of the periodic load, which is capable of removing the accreted snow from the cable, is an important design issue. The larger the snow thickness, the larger is the energy content of the periodic load necessary to shed the snow. It is noteworthy that, while the transverse wave travels along the span, snow accumulated on the cable breaks up into small fragments and shed without any cracks. This snow-breaking action absorbs energy from the traveling wave but the wave continued; as long as the load is affected, i.e., the wave did not die out.

3. It may be concluded that the small-scale model has a high degree of sensitivity to the flexibility of the cable end.

4. The modeling approach accurately estimates the snow-shedding rate. For predicting snow shedding using ADINA, it is necessary to consider the adhesive strength of the fractured snow deposits remaining attached to the cable. Although, there is some overestimation less than 15% of shedding rate because the model did not consider the cohesion attraction among snow particles. Although snow adhesion diminishes, snow persists on the cable since the cohesion between snow and cable is still high, keeping snow particles connect to each other in the experimental study. Damping which is simulated by spring elements gives results better than Rayleigh damping. Rayleigh damping underestimates the ratio of shedding comparing to experimental results. It is remarkable that when the dynamic response (cable jump and acceleration) increase, the rate of shedding increases as well.

CHAPTER 5

APPLICATION OF THE NUMERICAL MODEL

TO REAL-SCALE OVERHEAD CONDUCTORS

CHAPTER 5

APPLICATION OF THE NUMERICAL MODEL TO REAL-SCALE OVERHEAD CONDUCTORS

5.1. Introduction

The numerical model, which was validated using a level single-span reduced-scale experimental model (Chapter 4) is applied to real-scale overhead ground wires. The effect of several parameters of snow-covered cable; such as span length, periodic-load, LWC, damping ratio, load position and snow-length characteristics on the dynamic response was investigated. The model is applied to a level single-span of a classical stranded steel ground wire (OHGW), where it is a conductor suspended usually above the line conductor to provide protection against lightning discharges.

5.2. Modeling overview

A total of 57 different shedding scenarios are studied including line parameters such as the span length of 470 m and 200 m, LWC, damping ratio and load position. The parameters of the line section with a span length of 470 m and 200 m are adopted from EDF (Roberge, 2006). In addition, Hydro-Quebec cable (Kalman, 2007) of 200 m is studied and its properties are mentioned in details. Moreover, a parametric study including the effect of adhesion force, load position and damping ratio for 200 m and 470 m of EDF cable is investigated.

It should be noted that this extended study on real scale lines can serve only as an illustration due to the lack of characterizing parameters of the real-scale test, such as the characteristics of the periodic load, in particular. In addition, the available real-scale experimental results are scarce, since snow shed very rapidly and it is subjected to fast metamorphism resulting in considerable change in its properties.

5.3. EDF Overhead Conductor 470-m

5.3.1 Main Case Study

Using the EDF cable properties (Table 5.1) and snow sleeve deposit of half span results in a partial shedding with a ratio depends on time step. The density, thickness and mass of snow, spring mass used are 600 kg/m^3, 0.0042 m and 9.05 kg, 0.045 kg, respectively. The excitation amplitude is around 11 cm, cable damping adopted to be equivalent of 2%; sleeve length is estimated to be 227m (same ratio of snow length to cable length used in experiments) (Hefny et al., 2012 c, d).

Mass spring elements are used to represent the snow load deposit accreted on the cable, with the same failure criteria aforementioned is applied to the real scale single span. The rupture of the snow deposit is defined in terms of adhesion force critical limit. Whenever this maximum adhesion force is fulfilled at any integration point of the snow element, the snow element detaches from the cable for the remainder of the analysis.

The time function of periodic load serves as input to the numerical model, defined by a displacement time history at the suspension-point (Chapter 4). The shape of the displacement time function is the same in each simulation, as shown in Figure 4.16 in Chapter 4. When the period of excitation decreases, the length of time steps, dt, is changed correspondingly, but the number of time steps in one cycle is kept constant. Shorter time steps result in a faster drop of the excitation point and greater peak impact values. The period varies from 0.586 s to 0.284 s by setting *dt* between 0.0093 s and 0.0045 s (Table 5.2). The time step during the calculation is set to be the same as prescribed in the time function. It may be noticed that the time steps used in reduced scale model (Chapter 4) have no appreciable effect on the real-scale results since the cable in this case is longer and the snow sleeve is half the span only. The period between each impact and the successive one should be decreased in order to increase impact peaks. Rates of shedding for various time steps such as 0.0093, 0.008, 0.0069 and 0.0045 are 0%, 29%, 73% and 100%, respectively, as depicted in Figure 5.1. The longer the duration (time-step) of the periodic-load; which is characterized by smaller acceleration peaks, the smaller is the initial amplitude of the transverse wave and the smaller the rate of shedding as well(Hefny et al., 2012 c, d).

Initial sag-to-span ratio is set to be around 2.5%. The 201 elements (same number of elements used for small-scale model) are selected to define the appropriate mesh size (mesh size of around 1.135 m). Incremental equilibrium for initial static analysis takes 100 steps completed in 1s, while the dynamic analysis is started at time of t = 1 s continuing for different durations.

When more energy is added to the system due to loading, thereby the cable vibrations increase. Once these vibrations reach the natural frequency of the cable, the cable is at resonance. Shedding happens as soon as a resonance criterion achieves. Natural variability in snow sleeve uniformity (particles size, snow density and snow LWC) on a span of few hundreds of meters prevented the sleeve from reaching a critical LWC (which causes shedding) along its entire span at the same instant, this is the reason of rather different rate of shedding between the numerical results and the actual results which will be obtained in the field (Eshiemogie, 2011).

The acceleration at the suspension-point for the main case study shows an increase in the acceleration impacts with decreasing period and also increase of rate of shedding from 0% to 100%. The acceleration peaks vary between 900 m/s^2 for 0% shedding and 2900 m/s^2 for complete shedding and in between-values for 39% and 73% shedding scenarios. The high oscillations are investigated in Figure 5.2 which refer to the finite element spurious oscillations (Chapter 4) are due to the use of numerical filtration integration parameters.

Table 5.1 EDF cable properties of 470-m long (Roberge, 2006).

Shield wire - EDF	
Name	Almelec–steel
Type	Steel strand
Cable length (m)	470
Sag (m)	11.8
Diameter (mm)	12.6
Area (mm^2)	94.1
Modulus of elasticity (GPa)	112
Mass per unit length(kg/m)	0.481
Density(kg/m^3)	5111
Initial strain	0.0015
Initial horizontal tension (kN)	11.042
Rated tensile strength (kN)	80.35

Table 5.2 Rate of shedding for different time steps(Hefny et al., 2012 c, d).

Time step (s)	Period (s)	Rate of shedding (%)
0.0093	0.586	0
0.008	0.504	29
0.0069	0.435	73
0.0045	0.284	100

(a)

(b)

(c)

(d)

Figure 5.1 Snow shedding scenarios at: (a) 0% , (b) 29%, (c) 73% , and (d) 100%.
Conditions: Periods 0.586 s, 0.504 s, 0.435 s, 0.284 s; Amplitude 170 mm and LWC 20-
30%(Hefny et al., 2012 c, d).

Figure 5.2 Acceleration time history comparison at the suspension-point.
Conditions: Periods 0.586 s, 0.504 s, 0.435 s, 0.284 s; Amplitude 170 mm and LWC 20-30%(Hefny et al., 2012 c, d).

The acceleration at the mid-point of the cable shows a different behavior comparing to small-scale cable of 4.14 m mentioned in Chapter 4; as it gives an equivalent of around 6% of the acceleration at the suspension-point. Since the cable is long, so the effect of the periodic-load is rather negligible and it is logic to be reduced at 235 m. The acceleration impacts vary between 60 m/s^2 to 100 m/s^2 for 0% and 100% shedding, respectively, as seen in Figure 5.3.

The cable jump at the mid-point gives values of 19 cm, 22 cm, 28 cm and 37 cm for 0%, 29%, 73% and 100% shedding, respectively. It should be mentioned that the cable jump is not much high comparing to the cable sag, which is 11.84 m, since the load is comparable to a length of 470 m. The cable at the 0% shedding scenario is observed oscillating around the equilibrium position during the vibration period. However, for the 29% and 73% shedding rate, the cable oscillates around the equilibrium position until 4 s followed by rather high jump. On the contrary, the complete shedding causes high oscillations far away from the equilibrium position, as depicted in Figure 5.4(Hefny et al., 2012 c, d).   .

Cohesion is the intermolecular forces between snow particles, although snow adhesion in the small-scale cable diminishes, snow still on the cable, which ensures that snow cohesion is higher than adhesion. Therefore, in the real- scale cables, cohesion will affect by a degree of extent. The author expects lower shedding rate (than what obtained by the model) due to cohesion, which was not considered in the current modeling study. However, it is difficult to say if the difference quantitatively is the same as in the small-scale model.

Figure 5.3 Acceleration time history comparison at the mid-point.
Conditions: Periods 0.586 s, 0.504 s, 0.435 s, 0.284 s; Amplitude 170 mm and LWC 20-30%(Hefny et al., 2012 c, d).

Figure 5.4 Cable jump time history comparison at the mid-point.
Conditions: Periods 0.586 s, 0.504s, 0.435s , 0.284s; Amplitude 170mm and LWC 20-30%
(Hefny et al., 2012 c, d).

Concerning the tension results, it may be observed that the average tension values are rather different comparing the suspension-point and the fixed end-point. Tension values are found 84850, 84870, 84890 and 84750 N for 0, 29, 73 and 100% shedding, respectively. These results enhance that tension values increase, although when there is a complete shedding the average tension decreases because there is no load on the cable, as seen in Figure 5.5. Results of the cable tension at the fixed end-point are a little higher than the tension values in the case of the suspension-point, in which are 84900 N, 84910 N, 84950 N and 84850 N for 0%, 29%, 73% and 100% shedding, respectively (Figure 5.6). Any change in tension will affect the system's material properties such as the system's stiffness and density and this ultimately influences the speed at which the wave travels through the system(Hefny et al., 2012 c, d).

Figure 5.5 Cable tension time history comparison at the suspension-point.
Conditions: Periods 0.586 s, 0.504 s, 0.435 s and 0.284 s, Amplitude 170 mm; and LWC 20-30%%(Hefny et al., 2012 c, d).

Figure 5.6 Cable tension time history comparison at the fixed end-point.
Conditions: Periods 0.586 s, 0.504 s, 0.435 s and 0.284 s; Amplitude 170 mm; and LWC 20-30%.

5.3.2. Effect of Adhesion Force

The variation of the adhesion force between 6 and 8.7 N has a significant effect on the rate of shedding. The force of 6 N results in a complete shedding, but any other forces higher than the critical force (the critical force is 8.7 N) gives zero shedding scenario. This model with these properties is very sensitive to any change in the adhesive force. It is believed that obtaining partial shedding such as the case of reduced scale model (Chapter 4) by changing adhesion force other than the critical force (8.7 N) is complicated to some extent (Table 5.3).

Table 5.3 Rate of shedding for different LWCs and time steps.

Force (N)	6 (LWC 18-20%)	8.7 (LWC 20-30%)
Time step (s)		
0.0093	100%	0%
0.008	100%	29%
0.0069	100%	73%
0.0045	100%	100%

5.3.3 Effect of Load Position

In order to investigate the effect of periodic-load position along the cable span on the dynamic response, the periodic-load is activated at 117.5 m away from the cable suspension-point. These numerical results indicate that the location of the periodic load along the span contributes to the increase of the rate of snow shedding (Table 5.4).

Changing the load position from the suspension-point to the quarter- span point causes a complete shedding, where LWCs and adhesion force are 20-30% and 8.7 N, respectively. This modeling result ensures that the location of the periodic load greatly affects the shedding rate and the cable response as well. The reason behind that result is that the snow length is short (half of the cable span). Moreover, the load is actuated just beside the end of the sleeve. However, the cable response will be different if the snow sleeve is a continuous section on the whole cable length, see hereafter in section 5.3(Hefny et al., 2012 c, d).

Table 5.4 Relation between time step and rate of snow shedding.

Time step (s)	Rate of snow shedding RSS (%)
0.0093	100
0.008	100
0.0069	100
0.0045	100

5.3.4. Effect of Damping Ratio

By increasing damping ratio from 1 to 10%, the rate of shedding decreases, while it increases with decreasing time step (period) (Table 5.5). Figure 5.7 shows snow shedding scenarios for different damping ratio for time step 0.008 s(Hefny et al., 2012 c, d).

Table 5.5 Rate of shedding for different damping ratios and time steps.

Time step (s) Damping ratio (%)	0.0093	0.008	0.0069	0.0045
1	1%	75.9%	90%	100%
5	0%	29%	73%	100%
10	0%	6.5%	8%	100%

(a)

(b)

(c)

Figure 5.7 Snow shedding scenarios at: (a) 6.5%, (b) 29% and (c) 75.9%.
Conditions: Period 0.504 s , Amplitude 170 mm and LWC 20-30%.

5.4. EDF Overhead Conductor 200-m

5.4.1. Main Case Study

For LWC ranged from 20 to 30% and excitation periods of 2.079 s, 1.512 s, 1.323 s and 1.134 s using the EDF cable with the properties mentioned in Table 5.6 results in a partial shedding for the snow sleeve on the whole cable (snow length is 198m). The cable of 200 m has smaller sag (5.038 m), lower tension and lower initial strain compared with the cable of

470m (Section 5.3) (cf.Tables 5.1, 5.6). It may be concluded that snow sleeve on the whole cable can shed partially if the sag and tension are small; however, snow can shed completely if the cable sag and tension are high. Figure 5.8 shows that the rate of shedding occurs at 0.25%, 1.75%, 5.38% and 100% for time steps 0.033, 0.024, 0.021 and 0.018, respectively (Table 5.7).

Table 5.6 Cable properties for EDF of 200-m long (Roberge, 2006).

Shield wire-EDF	
Name	Almelec -steel
Type	Steel strand
Cable length (m)	200
Sag (m)	5.038
Diameter (mm)	12.6
Area (mm^2)	94.1
Modulus of elasticity (GPa)	112
Mass per unit length (kg/m)	0.481
Density(kg/m^3)	5111
Initial strain	4.44^e-4
Initial horizontal tension (kN)	4.68

(a)　(b)　(c)　(d)

Figure 5.8 Snow shedding scenario at: (a) 0.3 %, (b) 1.8 %, (c) 5.4 % and (d) 100 %. Conditions: Periods 2.079 s, 1.512 s, 1.323 s, 1.134 s; Amplitude 170 mm , LWC 20-30%.

The damping constant is set to represent an equivalent viscous damping of 10% critical (Lapointe, 2003). This amount of damping is deemed to represent the effect of fractured-snow deposits and likely exceeds the amount of internal cable damping that exists in the reality. However, as the damping ratio of 10% gives the best and fast convergence of the dynamic analysis, it is used in this part of study.

Table 5.7 Rate of shedding for different time steps.

Time step (s)	0.033	0.024	0.021	0.018
Period (s)	2.079	1.512	1.323	1.134
RSS (%)	0.3	1.8	5.4	100

RSS (%): Rate of shedding

5.4.2. Effect of Adhesion Force

It should be enhanced that the rate of shedding increases with the decreasing of time step between two successive impacts (aforementioned), while the rate of shedding increases with decreasing the adhesion force. When the time step decreases, the excitation period reduces as well, thereby the impact increases causing higher rate of shedding. However, the increase of adhesive force affects the bonding between the cable and snow sleeve results in a great difficulty for the snow to detach from the cable. The numerical analysis is very sensitive to any change in time step because rate of shedding increased from 2.4% to 100% for 0.033 s and 0.024 s, respectively (Table 5.8).

Table 5.8 Rate of shedding for different LWCS and time steps.

Force (N) Time step (s)	6 (LWC 18-20%)	8.7 (LWC20-30%)
0.033	2.4%	0.3%
0.024	100%	1.8%
0.021	100%	5.4%
0.018	100%	100%

5.4.3. Effect of Load Position

Changing the load position from the suspension-point to L/4 from suspension increases the rate of shedding. The rates of shedding are 0.25, 1.75, 5.38 and 100% for 0.033, 0.024, 0.021 and 0.018 s, respectively, for the load locating at the suspension-point. Then the

rate becomes 16%, 100%, 100% and 100% by changing load to quarter of the span length (cf. Tables 5.7, 5.9).

Table 5.9 Rate of shedding for different time steps.

Time step (s)	Rate of snow shedding RSS (%)
0.1	23.3
0.033	16
0.024	100
0.021	100
0.018	100

Figure 5.9 Snow shedding scenario (16% shedding).
Conditions: Period 2.079 s, Amplitude 170 mm and LWC 20-30%.

For 16% shedding (load at L/4), snow chunks shed down widespread all over the cable, *i.e.*, focus at the area of the suspension-point, the area of load location (L/4) and the mid-span area. Whereas for 0.25% shedding (load at suspension-point), snow shedding occurs only at the center of the cable (cf. Figs. 5.8 and 5.9).

5.4.4. Effect of Damping Ratio

The cable response is not appreciably affected by the change of damping ratio, since the rate of shedding decreases by small ratio. Although logically with increasing the damping ratio, the cable vibrates slowly resulting in low rate of shedding. Moreover, the rate of shedding increases with time step decrease (excitation period) between two successive impacts (Table 5.10).

Table 5.10 Rate of shedding for different damping ratios.

Time step(s) Damping ratio (%)	0.033	0.024	0.021	0.018
1	0.4 %	2 %	5.5 %	100%
10	0.3 %	1.8 %	5.4 %	100%

5.5. Hydro-Quebec Overhead Conductor 200-m

Using the cable properties presented in Table 5.11 with cable length of 200 m and LWC of ranged from 20 to 30% (cf. Tables 5.6 and 5.11) results in a complete shedding, where the snow sleeve is along the whole cable. This complete shedding occurs as a result of using a different cable used by Hydro-Quebec with larger area, larger density and with higher Young's modulus than EDF cable (Sec.5.4). This Hydro Quebec cable can be considered as more weighted, more stiff and tensioned, but less deflected compared to EDF cable of 200 m. All these factors caused the complete shedding, although a high damping ratio, a small snow load and long period (0.1 s) are examined.

Table 5.11 Cable properties for Hydro Quebec of 200 m long (Kalman, 2007).

Shield wire- Hydro-Quebec	
Name	½ inch Galvanized
Type	Steel strand
Cable length (m)	200
Sag (m)	1.49
Diameter (mm)	12.7
Area (mm^2)	96.5
Modulus of elasticity (GPa)	172.4
Mass per unit length (kg/m)	0.759
Density(kg/m^3)	7865.29
Initial strain	0.0015
Initial horizontal tension (kN)	25.019

5.6. Conclusion

This study showed the feasibility of implementing the new snow-shedding criterion based on adhesion in overhead transmission line-section models. Numerical studies had enhanced that it is practical to model the effects of periodic-load induced snow shedding on single-span real-scale overhead line. The larger the span length is, the smaller is the energy content of the periodic load, which would shed the snow. However, the increase of the energy content of the periodic load is limited by the period between successive impacts of displacement input profile. It is believed that snow shedding observed in the model is due to

large accelerations in the snow elements and resultant high inertia forces. The numerical model used in Chapter 4 is extended to be applied for real scale overhead conductor for different types and spans like EDF of 470 m, EDF of 200 m and Hydro-Quebec of 200 m. Many factors are considered in the snow-shedding simulating analysis. These parameters include the cable length, the snow length, adhesion force, load position, damping ratio and cable properties. The flexibility of the end-point did not model in the small-scale model. Nevertheless, it is observed that no such degree of sensitivity characterized a real-scale line. Some conclusions may be drawn from this study:

5.6.1. EDF cable of 470-m Long

a- Using EDF of 470 m and snow sleeve on the mid-span of the cable with weight of around 9 kg, cable damping of 2% results in a partial shedding using different time steps. These time steps differ from that used in the numerical model for reduced scale cable, where the cable cannot be influenced by the acceleration impact used in the small scale cable, since the cable is rather long.

b- It may be concluded that decreasing the adhesive force causes the rate of shedding increase.

c- The observations reveal the significant effect of changing the load position, since rate of shedding increases by changing position to L/4 span length.

d-The raise of damping ratio causes reduction in the snow shedding rate, where it changed from 6.49% to 75.9% for 10% and 1%, respectively.

5.6.2. EDF cable of 200-m Long

a- It should be stated that using EDF cable of 200 m long with a long snow sleeve on the whole cable causes a partial shedding, because of the cable small sag and the low tension.

b- Excitation periods used for EDF cable of 200-m with complete snow sleeve are higher than EDF cable of 470-m with mid-span snow sleeve, which concluded that it is not rather easy for snow to be detached from mid-span on long overhead ground wires.

5.6.3. Hydro-Quebec cable of 200-m Long

There is a complete shedding using snow sleeve along the whole cable. This complete shedding is as a result of large cable area, density and also high Young's modulus. Using high damping ratio, small snow load, high adhesion force and long time-step does not have a considerable effect neither on shedding rate nor on cable response.

CHAPTER 6

CONCLUSIONS AND FUTURE WORK

CHAPTER 6

CONCLUSIONS AND FUTURE WORK

6.1. Introduction

A failure criterion for wet snow deposits on transmission line cables was examined, where this failure criterion depends on tensile adhesion varying with snow LWC. The measurements of tensile and shear adhesion strengths were performed, experimentally at CIGELE Laboratory of University of Quebec at Chicoutimi and applied into a numerical model. The dynamic experiments consist of three main stages: firstly, accumulating snow on a reduced-scale (4.14-m) single span of flexible cable, then monitoring its response to the application of a periodic load and finally, observing the resulting snow-shedding process. The numerical modeling approach was developed using the finite element commercial software ADINA, following the successful application of the snow failure criterion on the reduced scale model, then it was validated by comparing to experimental results. The same modeling approach was applied to a single-span of 200 m and 470 m of real overhead conductor, which considered as an application.

The reduced-scale models possess a high degree of sensitivity to the flexibility of the reduced scale cable end point, which is different from the real-scale line conductors. Unfortunately, no experimental results are available from full-scale tests to verify cable acceleration predictions following periodic loads. The time histories of acceleration have spurious high amplitudes and are over-predicted.

6.2. General conclusions

The following conclusions may be drawn for experimental study, numerical modeling and real-scale model approach as follows:

6.2.1. Experimental study

1. The shear and tensile strengths of snow augments as LWC increases, reaching its maximum value at certain limit of LWC for all surfaces. For high values of LWC, the shear and tensile strengths decrease with LWC.

2. The greater the surface roughness, the higher the shear adhesion would be, whereas, the opposite happens for the tensile adhesive strength.

3. Tensile strength for smooth surfaces is greater by a factor of about 1.9 than stranded surfaces, but it is slightly closer to rough surfaces. Relation between tensile strength and LWC of the present study is in a good agreement with the results of Wakahama (1979), although the maximum strength achieves at different LWC since the procedure is different (Chapter 3).

4. Concerning the dynamic tests, snow shed from cable by unzipping then by partial shedding for any sleeve diameter, although the length of shedding parts decreases by minimizing the snow diameter. Acceleration peaks at the suspension-point augments with decreasing excitation period between two impacts causing raise of rate of shedding. In the design analysis, the case of large snow sleeve with smallest excitation period can be considered as the worst case that should be avoided.

5. For small sleeve diameter, the acceleration peaks are lower than large sleeve diameter.

6. Tension increases slightly with excitation frequency raise, while it decreases after shedding. In addition, there is no effect of LWC change on cable tension to cable.

7. The effects of cohesion are experimentally observed, even if snow adhesion is diminished, snow remains connected to the cable. This conclusion proved that snow cohesion is higher than snow adhesion to cable.

8. For middle excitation amplitude: snow persists rather long time on the cable without detachment up to high excitation frequencies, whereas it remains on the cable for more/less time for low/high excitation amplitude, respectively, compared to middle excitation. For designing aspects, it is believed that using high excitation amplitude as input causes high jump and rapid snow shedding.

6.2.2. Numerical Model investigation

For reliable accuracy in predicting snow shedding, it is necessary to consider the tensile adhesive strength of the fractured snow deposits and its dependence on LWC. Snow shedding observed in the model, is due to large accelerations and resulting inertia forces in the snow elements. This research studies the numerical modelling of snow shedding phenomena for overhead transmission lines, when snow deposits on conductors are detached from the cable following a periodic load applied locally using a motor setup. The general conclusions obtained from the numerical results are stated as follows:

9. Numerical analysis of the reduced-scale line indicated that the periodic-load applied to the cable generates a transverse wave in the cable. It may be stated that while the transverse wave travels along the span, snow breaks up into small fragments then detach away, the wave does not die with time since it is always provided by more energy from the load and also the snow does not absorb any energy from the wave, demonstrating the same amplitude throughout the process. Therefore, the numerical model presented could accurately model the dynamic effects of periodic-load-induced snow shedding on overhead lines.

10. Total unzipping of a wet snow deposit progresses at the same speed as a transverse wave evolves leading to cable jump which is around 2% of the span length. It should be illustrated that cable jump decreases by moving far away from the suspension-point. The vertical accelerations generated by partial shedding should be sufficient to trigger more shedding. The larger the snow thickness is, the larger is the energy content of the periodic load necessary to shed the snow. Thereby, the small sleeve diameter should be considered during design since it has high rate of shedding. Moreover, it is recommended to increase time between two successive impacts to decrease the rate of shedding for both large sleeve and small one.

11. Both the experimental and numerical analyses indicate that the most severe dynamic loads, *i.e.*, the maximum cable tensions and cable jump occur during ten impacts of the load application to the cable, since there is no further shedding after that.

12. Comparisons of numerical and experimental results indicate that the numerical model accurately calculates the dynamic response of snow-covered cables subjected to periodic loads. However, it is also observed that the reduced-scale model has a high degree of sensitivity to the flexibility of the cable used. Nevertheless, it is believed that no such degree of sensitivity characterized a real-scale line. On the other hand, numerical analyses of the effects of system flexibility of the reduced-scale conductor model show that the model is not applicable for studying cable tension.

13. For a given load, the longer the duration (time–step) of the periodic-load is; which is characterized by smaller acceleration peaks, the smaller the initial amplitude of the transverse wave and the percentage of snow shedding will be.

14. Sensitivity studies of the reduced-scale numerical model reveals that the most accurate predictions of the cable response including acceleration, cable jump, or cable tension are obtained from the 415-element mesh model. The 415-element numerical model is used in the remaining analyses of snow-covered cables. In addition, the reliable results are

found by using 5%-axial damping, whereas 1%-axial damping gives high response and more severe shedding. Concerning Rayleigh damping, it causes low rate of shedding which results in its exclusion from the current modeling study.

15. For mid-values of LWC and middle excitation amplitude, snow shed only at high excitation frequencies; however, for low and high LWC, snow shed at low excitation frequencies.

16. At high-excitation amplitude, snow shed easily with a very fast sequence whereas at low amplitudes snow stays on the cable for longer time.

17. Acceleration values found for small sleeve are high because the same time steps for large sleeve are used. Since the snow load is small using the small sleeve, it needs long time between two successive impacts resulting in small impact.

18. Small sleeve is very fragile and may be shed easily in the experimental tests comparing with numerical modeling which considered only the failure condition achievement.

6.2.3. Real-Scale Model approach

19. The larger the cable span length and cable sag are, the smaller is the energy content of the periodic load necessary to shed the snow. It is desirable to remove snow from the cable, but the author would recommend avoiding conditions leading to the shedding of very high mass, because it may cause problems or even line damage; like using long cables with large sag.

20. Using EDF cable of 470 m long: accreted snow sleeve on the mid-span of the cable (weight of 9 kg, damping 2%) results in partial shedding using different time steps. It may be stated that when the damping ratio is small and load position is further from the suspension point, besides the LWC is low, the shedding rate is higher.

21. Using EDF cable of 200 m long: there is a partial shedding since the cable has small cable sag and small tension. Snow shedding for that cable results in lower acceleration impacts compared with 470 m cable with mid-span sleeve.

22. Using Hydro-Quebec cable of 200 m: accreted snow sleeve on whole span sheds completely as a result of large area, high density and high Young's modulus. Thus, the model is not applicable to simulate snow sleeve along the whole cable using these cable's properties (Table 5.11). The author would recommend avoiding conditions leading to the shedding of very high mass, because it may cause problems or even line damage.

6.3. Recommendations for Future Study

6.3.1. Modeling the Structures and Their Foundations (3-D Model)

In this study, a simple 2-D level single-span model was demonstrated which proposed that a one-end point is fixed to a rigid support, thus the flexibility of the towers and their foundations is neglected. However, improvements of the numerical model to account for the effects of towers, foundations and interfaces can easily be implemented, since the 3-D model may serve to overcome the main drawbacks of a 2-D model. Adding the influence of these components is expected to decrease the maximum load tension at the support and the magnitude of the displacement calculated which is preferable to decrease the line damage.

6.3.2. Application to Multiple Spans

Snow shedding generates cable tension oscillations, where on a real conductor these oscillations have an effect on adjacent spans. The numerical model may be used to study the effect of total and partial shedding on multiple spans.

6.3.3. Studying the Effect of Cohesion

The present suggested model used only the adhesion failure criterion, although the experimental study showed that snow adhesion can be diminished, but snow remained connecting to the cable, due to the cohesion between snow particles. It is recommended that the cohesion criterion can be added to the adhesion criterion for a new model by using horizontal springs.

6.3.4. Improvement of the Failure Criterion of Wet Snow

In this study, the failure criterion was defined for the snow in terms of adhesion. It is recommended that the failure criterion of snow can be improved by considering the axial, bending stresses together with the adhesive strength of snow. The development of a novelty snow model considering its material properties as mentioned in Chapter 4 is essential, but it may be difficult to apply in the 2D model. Thus, it is suggested that a 3D model element may be used in the future studies to apply this mechanical criterion.

6.3.5. Application to Different Conductors and Ground Wires

This study may be extended not only to conductors, but also to optical ground wires and long span lines which cross rivers, in order to obtain more investigation for the case study.

6.3.6. Investigation of Other Snow Properties

It is recommended that the effect of changing snow properties as grain size, shape (under metamorphism) and the ambient temperature may be investigated as it modifies the dynamic response of snow-covered cable when subjected to a given load.

6.3.7. Utilization of Diverse Cable Cross-Sections

The current model studied only the cable of circular section, but it may be interesting to extend this model to rectangular/square or ellipse or any other cross-section, to study the effect of the cable section shape on the cable response.

6.3.8. Studying the Effects of Shedding Scenarios on Line Parts

It is recommended to study the effects of shedding conditions/scenarios on power transmission lines. Since these shedding scenarios may cause damage to different parts of the line.

REFERENCES

ADINA R&D Inc. ADINA Theory and Modeling Guide, Watertown, MA, USA, September 2004.

Admirat P., Sakamoto Y., Lapeyre J.L., MacCagnan M., Quantitative Results and Proposed Mechanisms on Wet Snow Accretion in the Ishiuchi Wind Tunnel Facilities, Proceedings of the 3rd International Workshop on Atmospheric Icing of Structures, 1986;155-160.

Admirat P., Sakamoto Y., Wet Snow on Overhead Lines: State-of-Art, Proceedings of the 4th International Workshop on Atmospheric Icing Of Structures, 1988; 7-13.

Admirat P., Lapeyre J.L., Dalle B., Synthesis of Field Observations and Practical Results of the 1983-1990 " Wet Snow" Programme of Électricité de France, Proceedings of the 5th International Workshop on Atmospheric Icing Of Structures,1990;B6-2(1) – B6-2(5).

Archer P., Gupta V, Measurement and Control of Ice Adhesion to Aluminium 6061 Alloy, Journal Mech. Phys. Solids, 1998; 46(10):945-971.

Asch G. Les Capteurs en Instrumentation Industrielle, 5e édition, Paris, France: Dunod, 1999.

Bader H., Haefeli R., Bucher E., Neher J., Eckel O., Thams C., Niggli P., Der Schnee und Seine Metamorphose, USA Snow, Ice and Permafrost Research Establishment, Translation 14, 1954.

Ballard H., Feldt E.D., A Theoretical Consideration of the Strength of Snow, Journal of Glaciology, 1965; 6(43):159-170.

Bathe K.J., Finite Element Procedures, Upper Saddle River, NJ, USA: Prentice Hall, 1996.

Colbeck S.C., Grain Clusters in Wet Snow, Journal of Colloid and Interface Science, 1979;72(3):371-384.

Colbeck S.C., Overview of Seasonal Snow Metamorphism, Reviews of Geophysics and Space Physics, 1982; 20(1):45-61.

Colbeck S.C., Ackley S.F., Mechanism for Ice Boding in Wet Snow Accretions on Power Lines, Proceedings of the 1st International Workshop on Atmospheric Icing Of Structures, 1982;25-30.

Colbeck S.C., Akitaya E., Armstrong R., Gubler, Lafeuille J., Lied K., McClung D., Morris E., The International Classification for Seasonal Snow on the Ground, Issued by The International Commission on Snow and Ice of the International Association of Scientific Hydrology, 1990,23p.

Dalle B. Aspects Macro et Microphysiques de l'Accrétion de Neige Collante sur les Conducteurs des Lignes Aériennes. Journée SEE, Gif-sur-Yvette, 1984; 43-49.

Dalle B. Admirat P., Wet Snow Accretion on Overhead Lines with French Report of experience, Cold Regions Science and Technology, 2011;65:43-51.

Data Translation Inc., DT Measure Foundry, Marlboro, MA, USA, 2005.

Denoth A., The Pendular–funicular liquid transition in Snow, Journal of Glaciology, 25 (91) 1980; 25(9):93-97.

Denoth A, The Pendular-Funicular Liquid Transition and Snow Metamorphism, J. Glaciology, 1982; 28(99):768-364.

Elisson A.J., Thorsteins E., Field Measurements of Wet Snow Icing Accumulation, Proceedings of the 9th International Workshop on Atmospheric Icing of Structures, 2000; 8p.

Eshiemogie O.E., Dynamic Characteristics of Bare Conductors, Master Thesis, Faculty of Engineering, University of KwaZulu-Natal, Durban, South Africa, 2011.

Farzaneh M., Atmospheric Icing of Power Networks, Springer, Berlin, 2008; 381p.

Fonyo A., Experimental Study of Wet-Snow Shedding from Sagged Cables, Master Thesis, Department of Applied Mechanics, Budapest University of Technology and Economics, Budapest, Hungary, 2008.

Fukue M., Mechanical Performance of Snow under Loading, Ph.D. Thesis. Department of civil engineering and applied mechanics, McGill University, Quebec, Canada, 1977; 253p.

Gibson L.J., Ashby M.F., Cellular solids, 2nd edition, 1997.

Gland H., Admirat P., Meteorological Conditions for Wet Snow Occurrence in France: Calculated and Measured Results in a Recent Case Study on March 5th 1985, Proceedings of the 3rd International Workshop on Atmospheric Icing of Structures, Vancouver, Canada, 1986; 91-96.

Grenier J.C., Admirat P., MacCagnan M., Theoretical Study of the Heat Balance During the Growth of Wet Snow Sleeves on Electrical Conductors, Proceeding of the 3rd International Workshop on Atmospheric Icing Of Structures, 1986;125-129.

Gurung C.B., Yamaguchi H., Yukino T., Identification of Large Amplitude Wind Induced Vibration of Ice-Accreted Transmission Lines Based on Field Observed Data, Engineering Structures, 2002; 24:99-188.

Hefny R., Kollar L., Farzaneh M., Peyrard C., Adhesion of Wet Snow to Different Cable Surfaces Conductors, Proceedings of The 13th International Workshop on Atmospheric Icing of Structures, Suisse, Poster session, 2009; 7p.

Hefny R, Kollar L., Farzaneh M., « Influence of Dynamic Forces on Wet Snow Shedding from Overhead Cables ». Proceedings of the International Conference on Mechanical Engineering and Mechatronics, Ottawa, Canada, Paper 208, August 2012a.

Hefny R, Kollar L., Farzaneh M., « Experimental Investigation of Dynamic Force on the Performance of Wet Snow Shedding ». International Journal of Mechanical Engineering and Mechatronics, Vol. 1, Issue 1, 2012b, pp. 72-79.

Hefny R, Farzaneh M., Kollar L., « Simulation of snow adhesion on power transmission cables ». Proceedings of the International Conference on Mechanical Engineering and Mechatronics, Ottawa, Canada, Paper 79, August 2012c.

Hefny R, Kollar L., Farzaneh M., « Simulation of Snow Adhesion on Real-Scale Lines ». International Journal of Mechanical Engineering and Mechatronics, Vol. 1, Issue 1, 2012d, pp. 102-108.

Hefny R.M.H, Kollár L. E., Farzaneh M., "Modelling the influence of periodic loads on snow detachment from suspended cables," Cold Regions Science and Technology, accepted and in press for June 2013.

Irvine, H.M, Cughey, T.K, The linear theory of free vibrations of a suspended cable, Proc.R.Soc.Lond.A.341, 1974, pp.299-315.

Irvine H.M., Cable Structures, Cambridge, MA, USA: MIT Press, 1981.
Jamaleddine A., McClure G., Rousselet J., Beauchemin R., Simulation of Ice Shedding on Electrical Transmission Lines Using ADINA, Computers and Structures, 1993; 47 (4/5):523-536.

Javan-Mashmool M., Volat C. , Farzaneh M., A Theoretical Model for Measuring Stress Induced by a Vibrating Load at Ice/Material Interface, Proceedings of The 11th International Workshop on Atmospheric Icing of Structures, Montreal, June 2005.

Javan-Mashmool M., Theoretical and Experimental Investigations for Measuring Interfacial Bonding Strength Between Ice and Substrate, Master Thesis, Université de Québec à Chicoutimi, Chicoutimi, Québec, Canada, 2005.

Kalman T, Farzaneh M., McClure G., Leblond A., Dynamic Behavior of Iced Overhead Cables Subjected to Mechanical Shocks, Sixth International Symposium on cable dynamics , Charleston, Sep. 2005.

Kalman T., Farzaneh M., McClure G., Leblond A., De-Icing of Overhead Cables by Mechanical Shocks: Numerical and Experimental Analyses, Proceedings of The 12th International Workshop on Atmospheric Icing of Structures, Yokohama, October 2007; 9-13.

Kalman T., Farzaneh M., McClure G., Numerical Analysis of the Dynamic Effects of Shock-Load-Induced Ice Shedding on Overhead Ground Wires. Computers and Structures, 2007; 85:375-384.

Keeler C.M., Weeks W.F., Investigations Into the Mechanical Properties of Alpine Snowpacks, Journal of Glaciology, 1968;7(50):253-271.

Kollár L.E., Farzaneh M., Modeling the Dynamics of Overhead Cable with Ice, Proceedings of the 11th International Workshop on Atmospheric Icing of Structures, Montreal, Canada, 12-16 June 2005;309-314.

Laforte J.L., Allaire M.A., Laflamme J., State of the Art on Power Line De-icing, Atmospheric Research, 1998;46:143-158.

Laforte C., Beisswenger A., Icephobic Material Centrifuge Adhesion Test, Proceedings of the 6th International Workshop on Atmospheric Icing of Structures, Montreal, June2005.

Langham E.J. Chapter on "physics and Properties of Snowcover" Handbook of Snow: Principles, Processes, Management & Use, Edited by Gray D.M., Male D.H., Pergamon Press Canada, Willowdale, ON, Canada, 776p.

Lapointe M., Dynamic Analysis of a Power Line subjected to Longitudinal Loads, M. Eng. Thesis, Department of Civil Engineering and Applied Mechanics, McGill University, Montreal, Canada, 2003.

Loredo-Souza A.M., Davenport A.G., The Effects of High Winds on Transmission Lines, Journal of Wind Engineering and Industrial Aerodynamics, 1998; 74-76:987-994.

Matsuura M., Matsumato H., Maeda Y., Oata Y., The Study of Ice Shedding Phenomena on Transmission Lines, Proceedings of the International Symposium on Cable Dynamics, AIM, Liege, Belgium,19-21;October 1995:181-188.

McClung D.M., In Situ Estimates of the Tensile Strength of Snow Using Large Sample Sizes, Journal of Glaciology,1979;22(87):321-329.

McClung D.M., In-Situ Estimates of the Tensile Strength of Snow Utilizing Large Sample Sizes, Journal of Glaciology, 1979;22(87).

McClung D.M., Failure Characteristics of Alpine Snow in Slow Deformation, Mechanics of Structured Media, Ottawa, Canada, May 1981;Part A:409-418.

McClure G., Tinawi R., Mathematical Modeling of the Transient Response of Electric Transmission Lines due to Conductor Breakage, Computers and Structures, 1987;26 (1/2):41-56.

McClure G., Lapointe M., Modeling the Structural Dynamic Response of Overhead Transmission Lines, Computers and Structures 2003; 81: 825-834.

Mellor M., A Review of Snow Mechanics, Proc. Int. Symp. Snow Mechanics, Grindelwald, 1141AHS PUBL. London 1975; 251-291.

Mirshafiei F., Modelling the Dynamic Response of Overhead Line Conductors Subjected to Shock-Induced Ice Shedding, Master Thesis, McGill University, Montreal, Canada, 2010.

Momomura Y., Harukawa H., Okamura T., Hongo E., Ohkuma T., Full-Scale Measurements of Wind-Induced Vibration of a Transmission Line System in a Mountainous Area, Journal of Wind Engineering and Industrial Aerodynamics, 1997;72:241-252.

Morgan V.T, Swift D.A, Jump Height of Overhead Line Conductors after the Sudden Release of Ice Loads, Proceedings of IEE 1964; 111(10):936-946.

Narita H., Mechanical Behavior and Structure of Snow under Uniaxial Tensile Stress, Journal of Glaciology, 1980; 26(94):275-282.

Oberg E., Jones F.D., Horton H.L., Machinery's Handbook, New York, Industrial Press Inc.1976; 2482p.

Olqma O., Critères de Déclenchement du Délestage de la Neige Collante de Câbles Aériens, M. Eng. Thesis, Université de Québec à Chicoutimi, Chicoutimi, Québec, Canada, 2009.

Peabody A.B., Applying Shock Damping to the Problem of Transmission Line Cascades, Ph.D. Thesis, Department of Civil Engineering and Applied Mechanics, McGill University, Montreal, Canada, 2004.

Petrovic J.J., Review Mechanical Properties of Ice and Snow, Journal of Materials Science 2003; 38:1-6.

Podolny, W., Scalzi, J.B, Construction and design of cable-stayed bridges, 1976.
Poots G., Skelton P.L.I., Simple Models for Wet-Snow Accretion on Transmission lines: Snow Load and Liquid Water Content, International Journal of Heat and Fluid Flow, 1994; 15(5):411–417.

Poots G., Ice and Snow Accretion on Structures, Research Studies Press (England) and John Whiley and Sons Inc., New York, USA, 1996; 330p.

Rimai D., DeMejo L.P., Mittal K.L., Fundamentals of Adhesion and Interfaces, American Chemical Society, Utrecht, Netherlands, 1995.

Roberge M., Study of Wet Snow Shedding from an Overhead Cable, Master Thesis, McGill University, Canada, 2006.

Roberge M., Farzaneh M., McClure G., Peyrard C., Wet Snow Shedding from an Overhead Cable, part1: Experimental Study, Proceedings of the 12th International Workshop on Atmospheric Icing of Structures, Yokohama, October 2007.

Roberge M., McClure G., Farzaneh M., Pellet L., Wet Snow Shedding from an Overhead Cable, Part2: Evaluating the Dynamic Response of a Cable Subjected to Wet Snow Shedding, Proceedings of the 12th International Workshop on Atmospheric Icing of Structures, Yokohama, October 2007.

Roshan Fekr.M., Dynamic Response of Overhead Transmission Lines to Ice Shedding, Master Thesis, Department of Civil Engineering and Applied Mechanics, McGill University, Montreal, Canada, 1995.

Roshan Fekr.M., McClure G., Numerical Modeling of the Dynamic Response of Ice Shedding on Electrical Transmission Lines, Atmospheric Research 1998; 46:1-11.

Sakamoto Y., Admirat P., Lapeyre J.L., MacCagnan M., Thermodynamic Simulation of Wet Snow Accretion under Wind Tunnel Conditions, 1988.

Sakamoto Y., Admirat P., Lapeyre J.L., MacCagnan M., Thermodynamic Simulation of Wet Snow Accretion under Wind Tunnel Conditions, Proc. Fourth Int. Conf. on Atmospheric Icing of Structures, Paris, 1988;180-185.

Sakamoto Y., Snow Accretion on Overhead Wires, Philosophical Transactions of the Royal Society, 2000; 358(976):2941-2970.

Sakamoto Y, Tachizaki S., Sudo N., Snow Accretion on Overhead Wires, Proceedings of the 11th International Workshop on Atmospheric Icing of Structures, Montreal 2005;3-9.

Sommerfeld R.A., A Weibull Prediction of the Tensile Strength Volume Relationship in Snow. Journal of Geophysical Research, 1974;79(23):3353-56.

Upadhyay A., Joshi S.K., Chandel C., Tensile Strength of Snow Using Centrifugal Technique, Defense Science Journal, November 2007; 57(6):787-795.

Volât C, Farzaneh M and Leblond A. De-Icing/Anti-Icing Techniques for Power Lines: Current Methods and Future Direction, Proceedings of the 11th International Workshop on Atmospheric Icing of Structures, Montreal, Canada, 12-16 June 2005; 323-333.

Wagner, T., Modelling of Wind Borne Ice Accretion on Power Transmission Lines, Department of Architecture, Civil Engineering and Environmental Sciences, University of Braunschweig, Institute of Technology and the Faculty of Engineering, University of Florence, 2010.

Wakahama G., Metamorphosis of Wet Snow, Institute of Low Temperature Sciences, A23, 51-66, Hokkaido, 1977.

Wakahama G., Kuroiwa D., Goto D., Snow Accretion on Electrical Wires and Its Prevention, Journal of Glaciology, 1977;19(81):479-487.

Wakahama G., Mizuno Y., Studies on Tensile Strength of Wet Snow, Institute of Low Temperature Science, Hokkaido University, 1979.

Zhang C., Farzaneh M., Kiss L., A Numerical Study of Forced Convection around a Snow Sleeve in a Cross-flow of Air. Proceedings of the 13th International Workshop on Atmospheric Icing of Structures, Andermatt, Suisse, September 2009; 6p.

Web sites

http://www.adhesives.org/StructuralDesign/AdhesionCohesionTheory.aspx.

http://www.thisblogrules.com/2011/01/the-ten-worst-snowstorms-in-world-history.html.

http://www.uama.org/Abrasives101/101Standards.html.

http://en.wikipedia.org/wiki/Blizzard.

http://photos.nj.com/star-ledger/2011/01/5_phga0128snow_murray.html.

http://knowledge.allianz.com/energy/?697/blackouts.

Reports

Admirat P., Grenier J.C., Observations du Caractère «Collant» des Chutes de Neige Naturelles sur un Conducteur éprouvette, Hiver 83-84. EDF/DER/ERMEL/INAG m72/1B 5912, N.4, 24, 1984.

Admirat P., MacCagnan M., Observations de Neige Collante sur les Lignes Electriques, EDF-DER HM/72-5287, 1985, 41p.

Admirat P., Lapeyre J.L., Observations d'Accumulation de Neige Collante a' la Station de Bagnres de Lauchon les 6 ,7 Avril 1986: Effet Préventif des Contrepoids Anti-torsion», EDF-DER HM/72-5335,1986; 26p.
Colbeck S.C., Theory of Metamorphism of Wet Snow, US Army Corps of Engineers, Cold Regions Research and Engineering Laboratory, Hanover, N.h., Research report, N313, Dec 1973:17.

Colbeck S.C., A Review of Sintering in Seasonal Snowpack, US Army Corps of Engineers, Cold Regions Research and Engineering Laboratory, Hanover, N.h., CRREL Report 97-10, Dec 1977:11p.

Colbeck S.C, A Review of Sintering in Seasonal Snow, USA army corps of engineers, Cold Regions Research and Engineering Laboratory, CRREL Report 97-10, Dec 1997.

Colbeck S.C., Theory of Metamorphism of Wet Snow, Guidelines for Meteorological Icing Models, Statistical Methods and Topographical Effects, Working Group B2.16, Task Force 03,April 2006.

Guidelines for Meteorological Icing Models, Statistical Methods and Topographical Effects, Draft Report of Task Force 3 on Icing, March 2004.

Kovacs A., Michitti F., Kalafut J., Unconfined Compression Tests on Snow, A Comparative Study, Cold Regions Research and Engineering Laboratory, Hanover, New Hampshire, Tech. Rep. 1977; 77-20.

Shapiro L.H., Jerome B., Saturm M., Blaisdell G.L., Snow Mechanics, Review of the State of Knowledge and Applications, CRREL report, August 1997.

Sommerfeld R.A., Statistical Problems in snow Mechanics, U.S. Dept. of Agriculture. Forest Service, General Technical Report, RM-3, 1973; 29-36.

Stallabrass J.R., Price R.D., On the Adhesion of Ice to Various Materials, National Research Laboratories, Division of Mechanical Engineering, Low Temperature Laboratory, Report LR-350, 1962; 14p.

Systems for prediction and monitoring of ice shedding, anti-icing and de-icing for power line conductors and ground wires, Working Group B2.29, 2010; 100p.

APPENDIX

APPENDIX A

A.1 Diagrams for the experimental study

The following figure shows the connection between the signal conditioner and accelerometer.

Figure A.1 Signal conditioner- accelerometer connection.

A.2 Descriptions for devices used during the experimental study

(1) The load cell has a rated output of 2 mV/V nominal, a nonlinearity of $\pm 0.1\%$ of the rated output, an operating temperature of -50°C to 93°C, and deflection of 0.05 mm to 0.13 mm nominal.

(2) The signal conditioner amplifier for the load cell has a built-in regulated bridge excitation source that requires a power supply at the range of 12 to 24VDC. It provides a voltage output of ± 10 VDC at ± 2 mV/V.

(3) ICP accelerometer incorporates a built-in microelectronic amplifier that serves to convert the high-impedance charge output into a low-impedance voltage signal for analysis or recording. This sensor has a measuring capacity of ± 4900 m/s^2 pk. It has a sensitivity of 1.02 mV/(m/s^2), an operating temperature range from -54°C to +121°C and an upper frequency limit of 10 kHz. It provides an output bias voltage of 7 to 12 VDC.

(4) The signal conditioner for the accelerometer has frequency response as a trade-off between two restrictions; it should be not less than 0.1 Hz and not higher than 1000 kHz. It has excitation voltage around 25 to 27 VDC. The signal conditioner works in a temperature range from 0 to 50° C and also it can withstand DC power of 32 to 38 VDC and 0.12 amps. The constant current excitation provides to sensor is 2 to 20 mA.

(5) Analog to digital conversion is provided by a USB function module manufactured by Data Translation Inc. (model: DT9804). This module offers 16 single-ended or 8 differential inputs with 16-bit resolution, up to 100 kS/s throughput, 16 digital I/O lines, 2 user counter/timers and optional 16-bit analog outputs. A bias return path for the five differential channels is provided through the software by adding a 10 kΩ of termination resistance from the low side of the channel to the isolated analog ground.

A.3   Calibration procedure

The calibration procedure in order to verify the reliability of the acceleromter results is examined. It may be procceded by measuring the resultant acceleration due to the movement. Afterwards, the obtained results will be compared with the calculations using the standard equations mentioned below. The comparison shows a good agrrement between the measurement and the calculation, which ensures that the accelerometer works well.

The motion of a non-offset piston connected to a crank through a connecting rod can be expressed through several mathematical equations, as follows:

(a) Accelerometer fixation   (b) Elevation of accelerometer on the rod

Figure A.2 Calibration instruments(to check the reliability of setup results).

Figur A.3 Geometry layout of piston pin, crank pin and crank center

Angular velocity

$$\omega = \frac{2\pi \cdot \text{RPM}}{60}$$

(A.1)

Position

$$x - r \cdot \cos A = \sqrt{l^2 - r^2 \sin^2 A}$$
$$x = r \cos A + \sqrt{l^2 - r^2 \sin^2 A}$$

(A.2)

Velocity

$$
\begin{aligned}
x' &= \frac{dx}{dA} \\
&= -r \sin A + \frac{(\frac{1}{2}).(-2).r^2 \sin A \cos A}{\sqrt{l^2 - r^2 \sin^2 A}} \\
&= -r \sin A - \frac{r^2 \sin A \cos A}{\sqrt{l^2 - r^2 \sin^2 A}}
\end{aligned}
$$

(A.3)

Acceleration

$$
\begin{aligned}
x'' &= \frac{d^2 x}{dA^2} \\
&= -r \cos A - \frac{r^2 \cos^2 A}{\sqrt{l^2 - r^2 \sin^2 A}} - \frac{-r^2 \sin^2 A}{\sqrt{l^2 - r^2 \sin^2 A}} - \frac{r^2 \sin A \cos A.(-\frac{1}{2}) \cdot (-2).r^2 \sin A \cos A}{\left(\sqrt{l^2 - r^2 \sin^2 A}\right)^3} \\
&= -r \cos A - \frac{r^2 (\cos^2 A - \sin^2 A)}{\sqrt{l^2 - r^2 \sin^2 A}} - \frac{r^4 \sin^2 A \cos^2 A}{\left(\sqrt{l^2 - r^2 \sin^2 A}\right)^3}
\end{aligned}
$$

(A.4)

APPENDIX B

B.1 Wind induced vibrations relations

This table explains the differences between wind induced vibrations, showing how the current study has peaks and frequencies in the range of Aeolian vibrations.

Table B.1 Comparison of different types of wind induced vibrations (Eshiemogie, 2011).

	Aeolian Vibration	Conductor Galloping	Wake-induced Oscillation
Types of Overhead Lines Affected	All	All	Limited to lines with bundled conductors
Approx. Frequency Range (Hz)	3 to 150	0.08 to 3	0.15 to 10
Approx. Range of Vibration Amplitudes (Peak-to-Peak) (Expressed in conductor diameters)	0.01 to 1	5 to 300	Rigid-Body Mode: 0.5 to 80 Sub span Mode: 0.5 to 20
Weather Conditions Favoring Conductor Motion			
Wind Character	Steady	Steady	Steady
Wind Velocity	1 to 7m/s (2 to 15mph)	7 to 18m/s (15 to 40mph)	4 to 18m/s (10 to 40mph)
Conductor Surface	Bare or uniformly iced (i.e. hoarfrost)	Asymmetrical ice deposit on conductor	Bare, dry
Design Conditions Affecting Conductor Motion	Line tension, conductor self-damping, use of dampers, armor rods	Ratio of vertical natural frequency to torsion natural frequency; sag ratio and support conditions	Subconductor separation, tilt of bundle, subconductor arrangement sub span staggering
Damage			
Approx. time required for severe damage to develop	3 months to 20 + years	1 to 48 hours	1 months to 8 + years
Direct causes of damage	Metal fatigue due to cyclic bending	High dynamic loads	Conductor clashing, accelerate ate wear in hardware
Line components most affected by damage	Conductor and shield wire strands	Conductor, all hardware, insulators, structures	Suspension hardware, spacers, dampers, conductor strands

B.2 Cable properties and modulus of elasticity

This is the measured modulus of elasticity of the cable but in the current study an approximate curve was used. This approximate cable stress strain cable used resulted in accurate results

Figure B.1 Stress strain relation for cable (Kalman, 2007).

Stainless steel cable parameters		
Name		Stainless steel wire rope
Type		RR-W-410D 301/302
Cable No. 1		
Overall diameter	mm	4.1
Total cross-sectional area	mm²	13.2
Mass per unit length	g/m	70
Number of strands		7
Diameter of strands	mm	1.04
Number of wires in a strand		19
Rated tensile strength	kN	10.7
Cable No. 2		
Overall diameter	mm	3.2
Total cross-sectional area	mm²	8
Mass per unit length	g/m	43
Number of strands		7
Diameter of strands	mm	0.67
Number of wires in a strand		19
Rated tensile strength	kN	7.8

Figure B.2 Properties of the stainless steel cable (Kalman, 2007).

B.3 Damping of the level single-span reduced-scale conductor model

This figure shows the time history for the displacement, the resultant damping is 3-5% (Kalman, 2007).

Figure B.3 Relation between displacement and time(Kalman , 2007).

B.4 Input files for the model

B.4.1 Points geometry using parabolic equation

Table B.2 demonstrates the coordinates of some points like the suspension point (1), point 208 where it is the middle of the cable, point 414 the end of the cable, points 108 and 308, where the snow starts and ends on the cable. Whereas 600 and 800 are the spring start and end points.

Table B.2 Cable coordinates.

Point	x1	x2	x3	system
1	0	0	-0.00401	0
108	0	1.07	-0.233	0
208	0	2.07	-0.319	0
308	0	3.07	-0.231	0
414	0	4.13	-0.00218	0
600	0	1.07	-0.282	0
700	0	2.07	-0.368	0
800	0	3.07	-0.28	0

B.4.2 Element nodes for vertical springs

In the numerical analysis, 201 spring elements were used, each of them connected two nodes (108-600, ..., 308-800) and the defined DOFs are DOF1: Z-Translation, DOF2: Ground, Table B.3 demonstrates the first and last two points for these spring elements.

Table B.3 Example of some nodes simulate stiffness springs.

Spring element	Node1	Node 2	DOF1	DOF2
1	108	600	Z-Translation	Ground
2	109	601	Z-Translation	Ground
200	307	799	Z-Translation	Ground
201	308	800	Z-Translation	Ground

B.4.3 Element nodes for mass springs

In the numerical analysis, 201 spring mass elements were used, each of them connected two nodes (600-0, ..., 800-0) and the defined DOFs are DOF1: Z-Translation, DOF2: Ground, Table B.4 demonstrates the first and last two points for these spring elements.

Table B.4 Example of mass springs.

Spring element	Node 1	Node2	DOF1	DOF2
1	600	0	Z-Translation	Ground
2	601	0	Z-Translation	Ground
200	799	0	Z-Translation	Ground
201	800	0	Z-Translation	Ground

B.4.4 Example of boundary conditions for some points

There is a small part of boundary conditions added in the numerical model.

Table B.5 Boundary conditions for main case study.

Node	X translation	Y trans	Z trans	X rot	Y rot	Z rot	fluid potential	ovalization	pipe warp	temperature	beam warp
2	Fixed	Free	Free	Fixed	Fixed	Fixed	Fixed	Fixed	Fixed	Free	Free
3	Fixed	Free	Free	Fixed	Fixed	Fixed	Fixed	Fixed	Fixed	Free	Free
4	Fixed	Free	Free	Fixed	Fixed	Fixed	Fixed	Fixed	Fixed	Free	Free
5	Fixed	Free	Free	Fixed	Fixed	Fixed	Fixed	Fixed	Fixed	Free	Free
6	Fixed	Free	Free	Fixed	Fixed	Fixed	Fixed	Fixed	Fixed	Free	Free

B.4.5 Solution process

Equation solver: sparse

Iteration scheme: full Newton method

Maximum no of iterations: 100

B.5 Main equations for the cable

Young's modulus:
$$E = \frac{\sigma}{\varepsilon} = \frac{F}{A} * \frac{L}{\Delta L} \tag{B.1}$$

where E is the elastic modulus, σ is the stress, ε is the strain, F is the force, L the cable length, A the cable area, ΔL is the increase in cable length

Damping constant:
$$C = 2\left(\zeta\sqrt{AEm}\right) \tag{B.2}$$

where C is the damping constant, A is the cable area, M is the cable mass, ζ is the damping ratio

Initial strain:
$$\zeta_i = \frac{F}{AE} \tag{B.3}$$

where ζ is the initial strain of the cable

Tension:
$$T = \frac{mgl^2}{8d} \tag{B.4}$$

where T is the cable tension, m is the cable mass, g is the acceleration, d is the cable sag.

B.6 Impact force from falling object
(http: //hyperphysics.phy-astr.gsu.edu/hbase/Flobi.html)

Even though the application of conservation of energy to a falling object allows us to predict its impact velocity and kinetic energy, we cannot predict its impact force without knowing how far it travels after impact.

$$PE = mgh$$

$$KE = 0$$

h

Impact velocity

$$v = \sqrt{2gh}$$

$$KE = \frac{1}{2}mv^2$$

$$PE = 0$$

Greater penetration implies smaller impact force.

Harder ground, less penetration, higher impact force.

If it bounces back, the impact force is even greater because of the greater change in momentum.

Figure B.4 Falling object

If an object of mass m= 1.5 kg is dropped from height
h = 1 m, then the velocity just before impact is
v = 4.4271 m/s. The kinetic energy just before impact is equal to
K.E. = 14700 J.

But this alone does not permit us to calculate the force of impact!

If in addition, we know that the distance traveled after impact is
d =0.1 m, then the impact force may be calculated using the work-energy principle to be
Average impact force = F = 147 N.

Note that the above calculation of impact force is accurate only if the height h **includes** the stopping distance, since the process of penetration is further decreasing its gravitational potential energy.

Note: 9kg causes 882 N impact force

APPENDIX C

MATLAB CODE

C.1 Catenary and parabolic profiles

1- Using parabolic equation as a guide to obtain H (horizontal component of cable tension); to work as a start point for H assumption for the catenary's procedure.

$$H = \frac{mgl^2}{8d} \tag{C.1}$$

2- Using Newton Raphson method to obtain a convergent value for H for the catenary's procedure, because of the hyperbolic cosine.

$$d = \frac{H}{mg}(\cosh \frac{mgl}{2H} - 1) \tag{C.2}$$

3- Using H value obtained by Newton Raphson to have cable profile by catenary's and comparing with cable profile by parabolic which the parabolic H value used, taking into account that the axes for catenary's at center but the parabolic axes at one end, also calculating the error difference between two profiles. Repeating the same analysis, but for large sag using another value for Newton Raphson.

$$y = \frac{H}{mg}(\cosh \frac{xmg}{H}) \text{ at center o' (catenary's)} \tag{C.3}$$

$$y = \frac{mgl^2}{2H}\left\{ \frac{x}{l} - \left(\frac{x}{l}\right)^2 \right\} \text{ (Parabolic)} \tag{C.4}$$

C.2 In-plane modes for Eigen-value analysis

C.2.1 For anti-symmetric in-plane modes

(i) Using the next equation to obtain natural frequencies for number of modes from 1 to 5.

$$\omega_n = \frac{2n\pi}{l}\sqrt{(\frac{H}{m})} \tag{C.5}$$

(ii) Calculating the natural frequencies again but for the case of snow accretion, by using equation (C.5) with just a change of horizontal force and cable mass.

(iii) Calculating the mode shapes for 5 cases by using this next equation:

$$\tilde{v}_n(x) = A_n \sin(2n\pi x / l) \qquad \text{(C.6)}$$

C.2.2 For symmetric in –plane modes

(i) Calculating λ^2 by next equation as follows:

$$\lambda^2 = \left(\frac{8d}{l}\right)^2 \left(\frac{l}{HL_e / E_C A_c}\right) \qquad \text{(C.7)}$$

(ii)Using Newton Raphson two times:

- With the main following equation: In order to find β

$$\text{Tan} \left((\frac{1}{2}\beta l) = (\frac{1}{2}\beta l) - (4/\lambda^2)(\frac{1}{2}\beta l)^3 \right) \qquad \text{(C.8)}$$

- Repeating Newton Raphson using this specific equation:

$$\text{Tan} \left(\left(\frac{1}{2}\beta l\right) = \frac{1}{2}\beta l \right) \qquad \text{(C.9)}$$

Which can be used for $\lambda^2 > 100$, in order to check β values.

(iii)

Using the roots of the case of $\lambda^2 > 100$ and then calculating natural frequency for 5 values of β using the equation mentioned later

$$\beta = \left(m\omega^2 / H\right)^{\frac{1}{2}} \qquad \text{(C.10)}$$

Repeating the natural frequencies for the case of snow accretion

(iv) Calculating the mode shapes using this equation:

$$\frac{\tilde{v}(x)}{8d} = \frac{\tilde{h}}{H} \frac{1}{(\beta l)^2} \left\{ 1 - \tan\left(\frac{1}{2}\beta l\right) \sin \beta x - \cos \beta x \right\} \qquad \text{(C.11)}$$

For each value of β, then repeating the mode shapes with change of H by adding additional horizontal force (Irvine, 1981, Podolny and Scalzi, 1976, Biran and M. Breiner,1995, Cughey and Irvine, 1974).

C.3 Program code

C.3.1 Part one: Catenary and parabolic profiles

Newton RAPHSON for catenary procedure

%Finding roots by Newton Raphson method:

%ITERMENU displays menu for interactive, iterative root finding

```
disp('please choose one of the following: ')
disp('to get a zoom of the plot enter......1')
disp('to choose an initial guess value and solve enter....2')
disp('to exit the program enter.......3')
```

%NEWTON finds the real zeros of the function y by an interactive Newton Raphson procedure

```
tol=.00001;
disp('Enter the equation to be solved ,y(H),and the derivative')
disp('of y with respect to H as strings variables ,for example: ')
disp('y =''(((H/mg)*cosh((mgL/2)/H))-(H/mg)-d)''')
y='(((H/mg)*cosh((mgL/2)/H))-(H/mg)-d)'
disp('dHdx=''(((1/mg)*cosh((mgL/2)/H))-(((mgL/2)/(H*mg))*sinh((mgL/2)/H))-H)''')
dydH='(((1/mg)*cosh((mgL/2)/H))-(((mgL/2)/(H*mg))*sinh((mgL/2)/H))-H)'
disp('when the program returns the prompt k enter the appropriate')
disp('escape command to exit keyboard mode and continue')
disp('the program.')
keyboard
disp('Enter now the range within which you want to plot.')
disp('Then,after viewing the graph press any key to continue')
Hmin=input('Hmin= ')
Hmax=input('Hmax= ')
HH=Hmin:(Hmax-Hmin)/100:Hmax;
z=zeros(1,100);
for k = 1:101
    H=HH(k);
    yy = eval(y);
    z(k) = yy;
end
plot(HH,z),
```

```
grid
title('plot of the equation to be solved')
xlabel('H')
ylabel('y(H)')
pause
real_zeros=[];      %%initialize array of real zeros
answer=input('Enter your choice')
while answer~=3
   if answer ==1
      Hmin=input('Hmin= ')
      Hmax=input('Hmax= ')
      Hstep=(Hmax-Hmin)/100;
      HH=Hmin:Hstep:Hmax;
      z=zeros(1,100);
      for k=1:101
         H=HH(k);
         yy=eval(y);
         z(k)=yy;
      end
      plot(HH,z)
      grid
      xlabel('H')
      ylabel('y')
      pause
      answer=input('Enter your choice')
   elseif answer==2
      disp('Enter initial guess')
      [H,yg]=ginput(1)
      for l=1:100
         H0=H;
         H=H0-eval(y)/eval(dydH)
         if abs(H-H0)<tol
            break
         end
```

```
        end
        if(l==100)&(abs(H-H0)>=tol)
            disp('procedure is not convergent')
        else
        real_zeros=[real_zeros H];
        end
        answer=input('Enter new choice')
    else
        if answer~=3
            disp('Incorrect answer ,please repeat')
            answer=input('Enter new choice')
        end
    end
end
%....conductor with span length L m,suspended at the end points at the same height.the
desired sag is ...% of the span length%
% l(span length)=L m, d(sag)=d m,mg(self weight of the cable)= mg N/m
%Catenary equations:%d(sag)=(H/mg)*(cosh(mg*l/2*H)-1)where  H  is  the  horizontal
component of cable tension
%y(cable profile)=(H/mg)*cosh(x*mg/H)
%Parabolic equations:%%%%%H=mg*l^2/(8*d)
%y(cable profile)=(mg*l^2/2*H)*((x/l)-(x/l)^2)
%(1)Catenary and parabolic comparison:
H = H ;cf=H/mg;
for x=-(L/2)+[(0:1:L)]';
    y=-(H/mg)-d+[cf*cosh(mg*x/H)]';
    plot(x,y,'r*');
end
Hp=(mg*L^2)/(8*d);
for i =1:(L/2+1);
f(i)=2*(i-1);
yp(i)=-(mg**L^2)/(2*Hp)*((f(i)/L)-(f(i)/L)^2);
s=plot(f,yp);d=plot(x,y);g=((d-s)/d)*100;
    plot(f,yp,'g*',x,y,'r*'),
```

```
legend('cable profile parabolic','cable profile');
xlabel('Cable length(m)');ylabel('Vertical component of cable profiles (m)');
end
jh=y(:,1);uh=yp(:,1);gd=((-jh+uh))*100,kg=y(:,(L/2+1));cg=yp(:,(L/2+1)/2);ga=((kg-cg)/kg)*100,
 H=H;
%(2)Catenary profile
H = H ;cf=H/mg;
for x=(0:1:(L/2))';
   y=[cf*cosh(MG*x/H)]';
   plot(x,y,'r*'),
   title('Cable profile');
   xlabel('Cable length(m)');
   ylabel('Vertical component of cable profile(m)');
end
```

C.3.2 Part two: symmetric in-plane modes

```
....Finding roots by Newton Raphson method for symmetric in plane modes:
%ITERMENU displays menu for interactive , iterative root finding
disp('please choose one of the following: ')
disp('to get a zoom of the plot enter......1')
disp('to choose an initial guess value and solve enter....2')
disp('to exit the program enter.......3')
NEWTON finds the real zeros of the function y by an interactive Newton Raphson procedure
tol=.00001;
disp('Enter the equation to be solved ,y(B),and the derivative')
disp('of y with respect to B as strings variables .for example: ')
disp('y ="(((L/2)*B)-(((4/Lamdasqr))*((L/2)*B)^3)-tan((L/2)*B))"')
y='(((L/2)*B)-(((4/Lamdasqr))*((L/2)*B)^3)-tan((L/2)*B))'
disp('dydB="((L/2)-(((3*L/2*4/Lamdasqr))*((L/2)*B)^2)-(L/2)*(sec((L/2)*B))^2)"')
dydB='((L/2)-(((3*L/2*4/Lamdasqr))*((L/2)*B)^2)-(L/2)*(sec((L/2)*B))^2)'
disp('when the program returns the prompt k enter the appropriate')
disp('escape command to exit keyboard mode and continue')
disp('the program.')
```

```
keyboard
disp('Enter now the range within which you want to plot.')
disp('Then,after viewing the graph press any key to continue')
Bmin=input('Bmin= ')
Bmax=input('Bmax= ')
BB=Bmin:(Bmax-Bmin)/100:Bmax;
z=zeros(1,100);
for k = 1:101
    B=BB(k);
    yy = eval(y);
    z(k) = yy;
end
plot(BB,z),
grid
title('plot of the equation to be solved')
xlabel('B')
ylabel('y(B)')
pause
real_zeros=[];     %%%initialize array of real zeros
answer=input('Enter your choice')
while answer~=3
  if answer ==1
    Bmin=input('Bmin= ')
    Bmax=input('Bmax= ')
    Bstep=(Bmax-Bmin)/100;
    BB=Bmin:Bstep:Bmax;
    z=zeros(1,100);
    for k=1:101
      B=BB(k);
      yy=eval(y);
      z(k)=yy;
    end
    plot(BB,z)
    grid
```

```
        xlabel('B')

        ylabel('y')

        pause

        answer=input('Enter your choice')

    elseif answer==2

        disp('Enter initial guess')

        [B,yg]=ginput(1)

        for l=1:100

            B0=B;

            B=B0-eval(y)/eval(dydB)

            if abs(B-B0)<tol

                break

            end

        end

        if(l==100)&(abs(B-B0)>=tol)

            disp('procedure is not convergent')

        else

        real_zeros=[real_zeros B];

        end

        answer=input('Enter new choice')

    else

        if answer~=3

            disp('Incorrect answer ,please repeat')

            answer=input('Enter new choice')

        end

    end

end
```

It can be noticed that Newton Raphson will be convergent only when

= .... N,so we will use this value = ...in our procedure

because it is the most convergent one.

A.2...Finding roots by Newton Raphson method:

%ITERMENU displays menu for interactive , iterative root finding%

disp('please choose one of the following: ')

disp('to get a zoom of the plot enter......1')

```
disp('to choose an initial guess value and solve enter....2')

disp('to exit the program enter.......3')

NEWTON finds the real zeros of the function y by an interactive Newton Raphson procedure

tol=.00001;

disp('Enter the equation to be solved ,y(B),and the derivative')

disp('of y with respect to B as strings variables ,for example: ')

disp('y ="(((L/2)*B)-tan((L/2)*B))"')

y='(((L/2)*B)-tan((L/2)*B))'

disp('dydB="((L/2)-(L/2)*(sec((L/2)*B))^2)"')

dydB='((L/2)-(L/2)*(sec((L/2)*B))^2)'

disp('when the program returns the prompt k enter the appropriate')

disp('escape command to exit keyboard mode and continue')

disp('the program.')

keyboard

disp('Enter now the range within which you want to plot.')

disp('Then,after viewing the graph press any key to continue')

Bmin=input('Bmin= ')

Bmax=input('Bmax= ')

BB=Bmin:(Bmax-Bmin)/100:Bmax;

z=zeros(1,100);

for k = 1:101

    B=BB(k);

    yy = eval(y);

    z(k) = yy;

end

plot(BB,z),

grid

title('plot of the equation to be solved')

xlabel('B')

ylabel('y(B)')

pause

real_zeros=[];      %%initialize array of real zeros

answer=input('Enter your choice')

while answer~=3
```

```
if answer ==1
    Bmin=input('Bmin= ')
    Bmax=input('Bmax= ')
    Bstep=(Bmax-Bmin)/100;
    BB=Bmin:Bstep:Bmax;
    z=zeros(1,100);
    for k=1:101
        B=BB(k);
        yy=eval(y);
        z(k)=yy;
    end
    plot(BB,z)
    grid
    xlabel('B')
    ylabel('y')
    pause
    answer=input('Enter your choice')
elseif answer==2
    disp('Enter initial guess')
    [B,yg]=ginput(1)
    for l=1:100
        B0=B;
        B=B0-eval(y)/eval(dydB)
        if abs(B-B0)<tol
            break
        end
    end
    if(l==100)&(abs(B-B0)>=tol)
        disp('procedure is not convergent')
    else
    real_zeros=[real_zeros B];
    end
    answer=input('Enter new choice')
else
```

```matlab
    if answer~=3
        disp('Incorrect answer ,please repeat')
        answer=input('Enter new choice')
    end
  end
end
%It can be noticed that Newton Raphson will be convergent only when
%B= ...., N,so we will use this value (  = ......,)in our procedure
%because it is the most convergent one.
%Antisymmetric in-plane modes
l=L;H=H;An=1;m=mg/9.8;m1= m+(mg/9.8); H1=h+H;
for j =1:5;
   n3(j)=j;
   w3(j)=((2*n3(j)*pi)/l)*sqrt(H/m),
   w33(j)=((2*n3(j)*pi)/l)*sqrt(H1/m1),
end
%The antisymmetric in-plane modes( wn values)
for kk=1:((L/2)+1);
   xxx(kk)=2*(kk-1);
   wn2(kk)=sin((5*2*pi*xxx(kk))/l);
   plot(xxx,wn2,'b-'),
   title('Fifth antisymmetric in-plane mode before and after snow loading');
   xlabel('Cable length(m)');
   ylabel('Vertical components of fifth antisymmetric in-plane mode(m)');
end
%Symmetric in-plane modes%
d=d;l=L;H=H;E=E;Ac=pi*(D*10^-3/2);Le=Le;m=mg/9.8;
Lamdasqr=(8*d/l)^2*((l)/(H*Le/E*Ac));
m=mg/9.8;H=H;
m1= m+(mg/9.8); H1=h+H;%%%where m1 is snow mass added to cable mass,H1 is cable hz
component added to additional one
for ii=3:5;
   n(ii)=(ii);
   B(ii)=((2*n(ii)+1)*pi)/L;B(1)=((2.86*pi)/L),B(2)=(4.92*pi)/L;
```

```
    w(ii)=sqrt((H*B(ii)^2)/m),
w(2)=sqrt((H*B(2)^2)/m),w(2)=sqrt((H*B(2)^2)/m),%%%%%where w is the natural frequency
w1(ii)=sqrt((H1*B(ii)^2)/m1),w1(1)=sqrt((H1*B(1)^2)/m1),w1(2)=sqrt((H1*B(2)^2)/m1),%
where w1 is the natural frequency after snow load added
end
for jj=1:((L/2)+1);
    x(jj)=2*(jj-1);
    v(jj)=(8*d)*(1/H)*(1/(B(1)*l)^2)*(1-(tan((L/2)*B(1))*sin(B(1)*x(jj)))-
cos(B(1)*x(jj)));%%%%where v is the vertical
    %symmetric components at different modes
    plot(x,v,'b-'),
    title('First symmetric in plane mode');
    xlabel('Cable length(m)');
    ylabel('Vertical component of first symmetric in plane mode(m)');
    yy(jj)=(8*d)*(1/H1)*(1/(B(5)*L)^2)*(1-(tan((L/2)*B(5))*sin(B(5)*x(jj)))-
cos(B(5)*x(jj)));%where yy is the
    %vertical symmetric components at different modes after snow load added
    plot(x,yy,'r-'),
    title('Fifth symmetric in plane mode after snow loading');
    xlabel('Cable length(m)');
    ylabel('Vertical component of fifth symmetric in plane mode(m)');end
```